CHARACTERISATION OF CTR-17 AND CTR-20, NOVEL CHALCONE DERIVATIVES THAT INHIBIT TUBULIN POLYMERISATION ACTIVITY

by

Indeewari Kalhari Silva Lindamulage

A thesis submitted in partial fulfillment
of the requirements for the degree of
Doctor of Philosophy (PhD.) in Biomolecular Sciences

The Faculty of Graduate Studies
Laurentian University
Sudbury, Ontario, Canada

THESIS DEFENCE COMMITTEE/COMITÉ DE SOUTENANCE DE THÈSE
Laurentian Université/Université Laurentienne
Faculty of Graduate Studies/Faculté des études supérieures

Title of Thesis Titre de la thèse	CHARACTERISATION OF CTR-17 AND CTR-20, NOVEL CHALCONE DERIVATIVES THAT INHIBIT TUBULIN POLYMERISATION ACTIVITY
Name of Candidate Nom du candidat	Lindamulage, Indeewari
Degree Diplôme	Doctor of Philosophy Science
Department/Program Département/Programme	Biomolecular Sciences
Date of Defence Date de la soutenance	December 17, 2015

APPROVED/APPROUVÉ

Thesis Examiners/Examinateurs de thèse:

Dr. Hoyun Lee
(Supervisor/Directeur(trice) de thèse)

Dr. Robert Lafrenie
(Committee member/Membre du comité)

Dr. Sabine Montaut
(Committee member/Membre du comité)

Approved for the Faculty of Graduate Studies
Approuvé pour la Faculté des études supérieures
Dr. David Lesbarrères
Monsieur David Lesbarrères

Dr. Paul Spagnuolo Acting Dean, Faculty of Graduate Studies
(External Examiner/Examinateur externe)

Doyen intérimaire, Faculté des études supérieures

Dr. Nelson Belzile
(Internal Examiner/Examinateur interne)

ACCESSIBILITY CLAUSE AND PERMISSION TO USE

I, **Indeewari Lindamulage**, hereby grant to Laurentian University and/or its agents the non-exclusive license to archive and make accessible my thesis, dissertation, or project report in whole or in part in all forms of media, now or for the duration of my copyright ownership. I retain all other ownership rights to the copyright of the thesis, dissertation or project report. I also reserve the right to use in future works (such as articles or books) all or part of this thesis, dissertation, or project report. I further agree that permission for copying of this thesis in any manner, in whole or in part, for scholarly purposes may be granted by the professor or professors who supervised my thesis work or, in their absence, by the Head of the Department in which my thesis work was done. It is understood that any copying or publication or use of this thesis or parts thereof for financial gain shall not be allowed without my written permission. It is also understood that this copy is being made available in this form by the authority of the copyright owner solely for the purpose of private study and research and may not be copied or reproduced except as permitted by the copyright laws without written authority from the copyright owner.

ABSTRACT

Agents targeting colchicine-binding sites are recognised as valuable lead compounds in the development of new anticancer drugs. Although colchicine can effectively inhibit cell proliferation, its use as an anticancer agent has not been approved by the FDA due to its inherent toxicity. To develop colchicine-binding site targeting agents with low or no toxicity, in collaboration with Rajiv Gandhi Technical University of India, several chalcone derivatives were created and examined. Preliminary studies at the Lee Lab identified CTR-17 and CTR-20 as promising leads. Their anti-proliferative activities using three human breast cancer cell lines (MDA-MB468, MDA-MB231 and MCF-7) and two matching non-cancer breast cell lines (184B5 and MCF10A) were initially determined. Subsequently, nine other cancer cell lines were used to assess the broad spectrum anti-proliferative effects of the CTR compounds. Data from this study showed that CTR-17 and CTR-20 preferentially kill cancer cells 10-25 times over non-cancer cells. Data obtained from flow cytometry, confocal microscopy and Western blotting showed that CTR-17 induced a prolonged mitotic arrest, leading to cancer cell death probably via apoptosis. I also found that both CTR-17 and CTR-20 inhibited tubulin polymerisation and bound to purified tubulin fibers with a dissociation constant of 4.58±0.95 μM and 5.09±0.49 μM, respectively. CTR-17 and CTR-20 competitively inhibited the binding of colchicine to tubulin with an inhibitory concentration of 5.68±0.35 μM and 1.05±0.39 μM, respectively, suggesting that the CTR compounds bind to tubulin at a site partially overlapping the colchicine-binding site. Molecular docking studies confirmed this binding to occur via two and one hydrogen bonds between tubulin and CTR-20 and CTR-

17, respectively. More interestingly, CTR compounds inhibit the proliferation of multi-drug resistant cell lines, which overexpress drug transporters involved in the efflux of clinically available microtubule targeting agents. In addition, the CTR compounds exhibit a synergistic relationship with paclitaxel in causing cytotoxicity to a P-glycoprotein overexpressing cell line. Therefore, these novel chalcone derivatives not only possess cancer-specific cell killing property but also the ability to exhibit similar cytotoxicity to both the multi-drug sensitive and resistant cells. Hence, CTR compounds possess substantial potential as safe and effective anticancer drugs.

ACKNOWLEDGMENTS

First and foremost, I would like to express my sincere gratitude to my supervisor, Dr. Hoyun Lee for recruiting me as a PhD student, from a country as far off as Sri Lanka. I would not have been able to successfully complete my graduate studies without your continuous support, guidance, encouragement and scientific enthusiasm. You have been my inspiration and I thank you very much for believing in me, especially when I underwent some rough periods during my journey to earn this PhD. I am very lucky to have pursued my doctoral studies under your guidance. Not only have I enhanced my ability to think independently as a scientist but I have also learnt several lessons to lead a happy life.

Most importantly, my heartfelt thanks go to my thesis committee members, Dr. Robert Lafrenie and Dr. Sabine Montaut. Your valuable suggestions and ideas allowed me to progress smoothly in my research program and eventually produce some exciting research to the scientific field. I would also like to convey a special thanks to Dr. Leslie Sutherland, who has been an extremely encouraging individual from the start of my career as a PhD student.

My sincere thanks go to all members of the Lee Lab. Certainly, the four years I spent at the Lee Lab would not have been memorable, without a team like you. Whenever experiments went wrong, there was nothing better than sitting with you and figuring out any wrong turns of the experiment, right from the start. I have learnt a lot from you and I will never forget the team at Lee Lab, ever in my life. Special thanks go to Vandana and James for the immense contribution in performing HPLC and training me with the X-ray machine respectively. Thanks to all personnel at AMRIC, especially Jane Vanderklift for organizing committee meetings and assistance with all aspects of administration. I was fortunate enough to be a recipient of the Ontario Trillium Scholarship from the Government of Ontario for four consecutive years. This scholarship was very much valuable to me and enabled me to dedicate my fullest efforts towards my studies. Special friends, including Arshi, Hiren and the Dube family brought me immense strength during various aspects of my study and will always be appreciated and immensely acknowledged.

Last but not the least, my dearest family, back at home. Your daily skype conversations are a part of my life now. Your enthusiasm in my studies is what drives me forward. Even though you are miles apart from me, your interest in my research makes me want to do better each day. Finally, the most important person in my life my dearest husband, Harish. You have been my never fading pillar of strength. I thank you deeply for supporting me and encouraging me in all my years at my studies. I have put you in much difficult situations especially, when I come home with a failed experiment, but you handled the situations wisely and tactfully and encouraged me in achieving my ultimate goal. Most importantly, your love, wisdom and our special friendship have taught me more about life and especially to be grateful, for which I am forever indebted to. Thank you!!!

TABLE OF CONTENTS

LIST OF ABBREVIATIONS

ΔF	Change in fluorescence intensity
ΔF_{max}	Maximum change in the fluorescence intensity
°C	Degree Celsius
µM	Micromolar
+TIPs	MT-plus-end-tracking proteins
2-ME	2-Methoxyestradiol
ACD	Abnormal chromosome division
AML	Acute myelogenous leukemia
APC/C	Anaphase promoting complex/cyclosome
ATCC	American type culture collection
BCA	Bicinchoninic acid
BCRP	Breast cancer resistant protein
BSA	Bovine serum albumin
Bub	Budding uninhibited by benzimidazoles
BubR1	Budding uninhibited by benzimidazole-related 1
C	Concentration
CAK	Cdk activating kinase
Cdc20	Cell division cycle 20
Cdk1	Cyclin-dependent kinase 1
Cenp	Centromere protein
CI	Combination Index
CLIPs	Cytoplasmic linker proteins
D	Dose of the drug
DCX	Doublecortin
D_m	Median effect dose
DME/F12	DMEM/Ham's Nutrient Mixture F-12
DMEM	Dulbecco's Modified Eagle Medium
DMSO	Dimethylsulfoxide
DT	Double thymidine
ECL	Enhanced chemiluminescence
EdU	5-ethynyl-2'-deoxyuridine
EGTA	Ethylene glycol-bis(2-aminoethylether)-*N,N,N′,N′*-tetraacetic acid
F	Fluorescence
F0	Fluorescence of the colchicine-tubulin complex
F_a	Fraction affected
FBS	Fetal bovine serum
FS	Forward scatter
GDP	Guanosine-5'-diphosphate
GTP	Guanosine-5'-triphosphate
h	Hour(s)
H	Hydrogen
hEGF	Human epidermal growth factor
HPLC	High performance liquid chromatography
HRP	Horse radish peroxidase
IC_{50}	50% inhibitory concentration
K_d	Dissociation constant
kDa	Kilo Dalton

Ki	Inhibition constant
m	Slope of the curve
Mad	Mitotic arrest deficient
MAPs	Microtubule-associated proteins
MCAK	Mitotic centromere-associated kinesin
MDDs	Microtubule destabilizing drugs
MDR	Multidrug resistance
MDS	Myelodisplastic syndrome
MGMT	O(6)-Methylguanine-DNA methyltransferase
min	Minute(s)
ml	Millilitre (s)
MOE	Molecular operating environment
MRP1	MDR-associated protein 1
MSDs	Microtubule stabilizing drugs
MTOC	Microtubule organizing centre
MTs	Microtubules
nm	Nanometer
nM	Nanomolar
NSCLC	Non-small cell lung cancer
Op18	Oncoprotein 18
PAGE	Polyacrylamide gel electrophoresis
PBS	Phosphate buffered saline
PBST	PBS with 0.1% Triton-X 100
Pgp	P-glycoprotein
PI	Propidium iodide
PIPES	Piperazine-*N,N′*-bis[2-ethanesulfonic acid] equisodium salt
PMSF	Phenylmethylsulfonyl fluoride
Pol	Polymerized
PTMs	Post-translational modifications
PVDF	Polyvinylidene fluoride
RMS	Rhabdomyosarcoma
RPMI	Roswell Park Memorial Institute
SAC	Spindle assembly checkpoint
SAR	Structure-activity relationship
SCLC	Small cell lung cancer
SDS	Sodium dodecyl sulphate
Ser	Serine
SS	Side scatter
Sol	Soluble
SRB	Sulforhodamine
STR	Short tandem repeat
TBS	Tris buffered saline
TBST	TBS with 0.05% Tween-20
TCA	Trichloroacetic acid
Thr	Threonine
Tyr	Tyrosine
TMZ	Temozolomide
WCE	Whole cell extract

LIST OF FIGURES

LIST OF TABLES

1.0 Introduction

1.1 Background

Chalcones are a group of compounds that are highly abundant in plants such as ferns (*Pityrogramma calomelanos* L.) and evergreen trees belonging to magnolia (*Fissistigma lanuginosum* Merr.), myrtle (*Calythropsis aurea* C.A. Gardner) and matico (*Piper aduncum* L.) families (Stanton et al. 2011). Chalcones are the precursor molecules to a wide variety of flavonoids and isoflavonoids and, chemically, they contain a three-carbon α, β unsaturated carbonyl system that joins two aromatic rings (Rahman 2011). Chalcones and their derivatives possess diverse pharmacological activities, including antioxidant, anti-inflammatory, antimicrobial, anti-HIV, antimalarial, anti-tubercular, anti-allergic and anticancer properties (Lawrence et al. 2006). Both synthetic and naturally occurring chalcones are investigated for their anti-proliferative ability, however their mechanism of action is vast and remains to be fully explored (Prabhakar et al. 2014). Chalcone-based compounds such as benzacetophenones contain a trimethoxyphenyl ring, similar to colchicine and podophyllotoxin, and have been reported to show potent cytotoxic properties by arresting cells in mitosis about 300 times more efficiently than colchicine (Smith et al. 1988). Certain chalcone derivatives, including MDL-27048 (*trans*-1-(2,5-dimethoxy)-3-[4-(dimethylamino) phenyl]-2-methyl-2-propen-1-one), competitively inhibits the binding of colchicine and podophyllotoxin to tubulin. Hence, they are recognised as colchicine-site binding agents that have been shown to interact with tubulin reversibly and more rapidly than colchicine (Peyrot et al. 1992).

Microtubule-targeting drugs bind to tubulin via three major binding sites: the taxane, vinca and colchicine-binding sites. While the taxanes and the vinca alkaloids have been recognised as clinically successful drugs, agents binding to the colchicine-binding site including podophyllotoxin have not been used as anticancer therapeutics due to their extreme toxicities to normal tissues (Lu et al. 2012).

Many of the currently available microtubule-targeting drugs suffer from several limitations including drug-resistance, dose-limiting toxicities, complexities in synthesis, complicated formulations, scarcity and reduced bioavailability. Therefore, the search for novel microtubule-targeting agents has remained the priority for a number of years (Schmidt & Bastians 2007).

Chalcones make an attractive drug scaffold because of their extremely simple skeleton and the ease of synthesis from acetophenones and substituted benzaldehydes (Lawrence et al. 2006). Structure-activity relationship (SAR) modifications and alterations can be performed easily on the chalcone structure (Prabhakar et al. 2014). The activity of this class of compounds is rendered mainly by the extended conjugation and high electrophilicity, while their potent antioxidant properties rely on the ability to completely delocalise the pi electrons (Awasthi et al. 2009; Cheng et al. 2000). Despite the identification of antimitotic chalcones in the 1980s, there are currently no chalcone derivatives that have reached the stage of human clinical trials as anticancer therapeutics. However,

preclinical studies hold promise, demonstrating minimal toxicities, rapid metabolism and effective inhibition of tumor growth and metastasis. In addition to the use of chalcones for other diseases such as ulcers, the abundance of chalcones in edible fruits suggest that they are well-tolerated by humans (Jandial et al. 2014). Several chalcone derivatives are currently in various developmental stages as promising anticancer drugs. In collaboration with Rajiv Gandhi Technical University of India, we synthesized several chalcone derivatives and examined for their anticancer property. Preliminary studies in our lab identified CTR-17 and CTR-20 as the promising leads and major part of my work was focussed on elucidating the molecular mechanism of CTR-17 and the target of the CTR compounds.

1.2 Objectives

The specific aims of this study were:

Aim 1: To evaluate the potential of CTR-17 as an effective and selective anticancer drug using a panel of cancer and non-cancer cell lines

Aim 2: To determine the functional mechanism of CTR-17

Aim 3: To determine the molecular target of CTR-17 and CTR-20

1.3 Microtubules as an anticancer drug target

Microtubules (MTs) are ubiquitous cytoskeleton polymers composed of two spherical proteins, the α and β-tubulins, each with a mass of 55kDa. Linear polymers of these tubulin heterodimers are bound head-to-tail to form the protofilaments, which are then arranged in a parallel configuration to form each microtubule (Nogales 2000). The self-assembly of thirteen protofilaments to form the MTs and their association with diverse cellular factors are governed by the sequence and structure of the tubulin protein itself (Jordan et al. 1998). MTs perform multiple roles within the cells, including the maintenance of cell shape and structure, cellular transportation, cellular motility, faithful segregation of chromosomes and cell division. These roles rely on the ability of the microtubules to interact with the microtubule-associated proteins (MAPs), the expression of tubulin isotypes and their post-translational modifications (PTMs). MTs are dynamic polymers that alternate stochastically between phases of growth and shortening with periods of undetectable activity or “paused” periods that intervene both *in vitro* and *in vivo*. This non-equilibrium and agitated behaviour is known as “dynamic instability.” Although energetically unfavourable, this dynamic instability of the MT is fundamental to their diverse intracellular roles including the construction of the highly elegant mitotic spindle during cell division (Stanton et al. 2011; Nogales 2000).

High concentrations of purified tubulin can be used to assemble MTs *in vitro*; however, the assembly of MTs *in vivo* is highly controlled and occurs via the centrosome, also known as the MT organization centre (MTOC) (Gould & Borisy

1977). During interphase, the MTs emanate from the centrally located centrosomes and projects towards the periphery of the cells. MTs are polar in nature due to the intrinsic heterogeneity of the MT ends. The plus (+) end of the MTs displaying the β-tubulin is responsible for the rapid growth. They may be located free in the cytoplasmic space or even reach the plasma membrane. On the other hand, the minus (-) end of the MTs displaying α-tubulin is more sluggish and usually embedded in the MTOC (Walker et al. 1988) (Figure 1).

MT polymerization occurs in two steps: a nucleation phase that involves the formation of a polymerization nucleus, followed by a growth phase that constitutes the reversible and non-covalent addition of the tubulin subunits (Jordan & Wilson 2004). For net MT growth, the association of the tubulin subunits to the polymer end is faster than disassembly, and the depolymerisation of the MTs is counterbalanced by the addition of αβ heterodimers during equilibrium (Nogales 2000; Valiron et al. 2001). Thus, MTs exhibit dynamic instability by alternating between episodes of shrinkage and growth, and this process is fueled by the binding and hydrolysis of GTP (Weisenberg et al. 1968).

Figure 1: Microtubules and their intrinsic heterogeneity
MTs contain about 13 protofilaments composed of αβ tubulin heterodimers, arranged to form a cylinder about 24 nm in diameter. Each protofilament comprises a plus-end that is fast growing and a minus-end which is slow in growth. γ- tubulin plays a role in the appropriate assembly of the MT. As the new dimer is added, guanosine-5'-triphosphate (GTP) at the E site of the β-subunit is hydrolysed to guanosine-5'-diphosphate (GDP). The figure was adopted from Conde & Cáceres (2009).

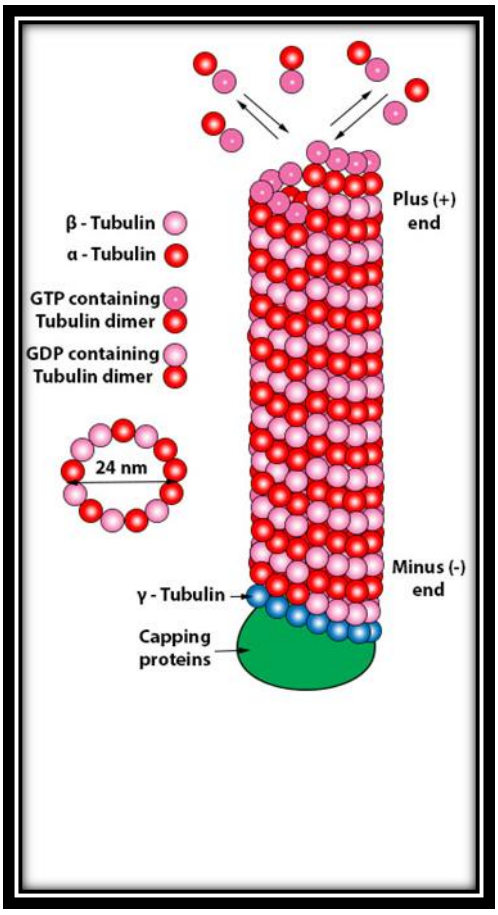
β - Tubulin
α - Tubulin
GTP containing Tubulin dimer
GDP containing Tubulin dimer
24 nm
Plus (+) end
Minus (-) end
γ - Tubulin
Capping proteins

Both α and β monomers bind to one molecule of GTP. The GTP molecule that binds to the α-tubulin subunit via the N-site is neither hydrolyzed nor exchanged; however, the β-tubulin subunit accommodates both GTP and GDP at the E-site in an exchangeable and hydrolysable fashion (Stanton et al. 2011). MT polymerization occurs when free tubulin heterodimers containing a GTP molecule at the E-site of β-tubulin subunit integrates into the MT structure. The GTP molecule then undergoes hydrolysis and the resultant GDP remains bound to tubulin. During rapid growth of the MTs, new GTP bound subunits are added on to the MT polymer before the GTP of the previously added subunit has undergone hydrolysis, eventually leading to the build-up of GTP-containing tubulin subunits at the MT tip resulting in a "GTP cap." However, during slow growth of MTs, there remains sufficient time for GTP to undergo the process of hydrolysis, which will then eventually lead to the exposure of a GDP-containing tubulin subunit at the tip of the MT. The hydrolysis of GTP reduces the binding ability of the neighbouring subunits, thus favouring the process of MT depolymerisation and a state of a curved configuration (Stanton et al. 2011). Therefore, straight protofilaments are acquired by GTP-containing tubulin, on the contrary to the curved protofilaments that are acquired by the GDP-containing ones (Warner & Satir 1973) (Figure 2). During "treadmilling," which is another form of dynamic instability, tubulin dimers are constantly added to the plus-ends of the MTs which are simultaneously dissociated from the minus-end (Margolis & Wilson 1998; Margolis & Wilson 1978).

Figure 2: Dynamic behaviour of MTs
MT polymerization occurs when tubulin heterodimers containing a GTP molecule at the E-site of β-tubulin subunit integrates into the MT structure. GTP molecule then hydrolyses and GDP remains bound to tubulin. The GTP molecule that binds to the α-tubulin subunit via the N-site is neither hydrolyzed nor exchanged. During rapid growth of the MTs, new GTP-bound subunits are added on to the MT polymer before the GTP of the previously added subunit has not yet undergone hydrolysis, leading to a "GTP cap." During slow growth of the MTs, GDP-containing tubulin subunit is exposed at the tip of the MT. This favours the process of MT depolymerisation and a state of a curved configuration. MTs are dynamic polymers that alternate between phases of growth and shortening with periods of undetectable activity or "paused" periods. This non-equilibrium and agitated behaviour is known as "dynamic instability." The figure was adopted from Conde & Cáceres (2009).

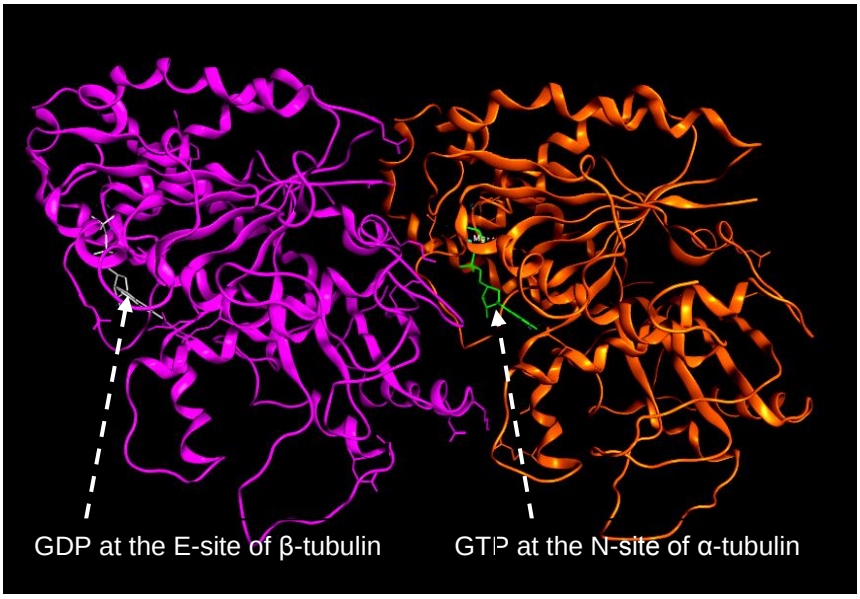
GDP at the E-site of β-tubulin
GTP at the N-site of α-tubulin

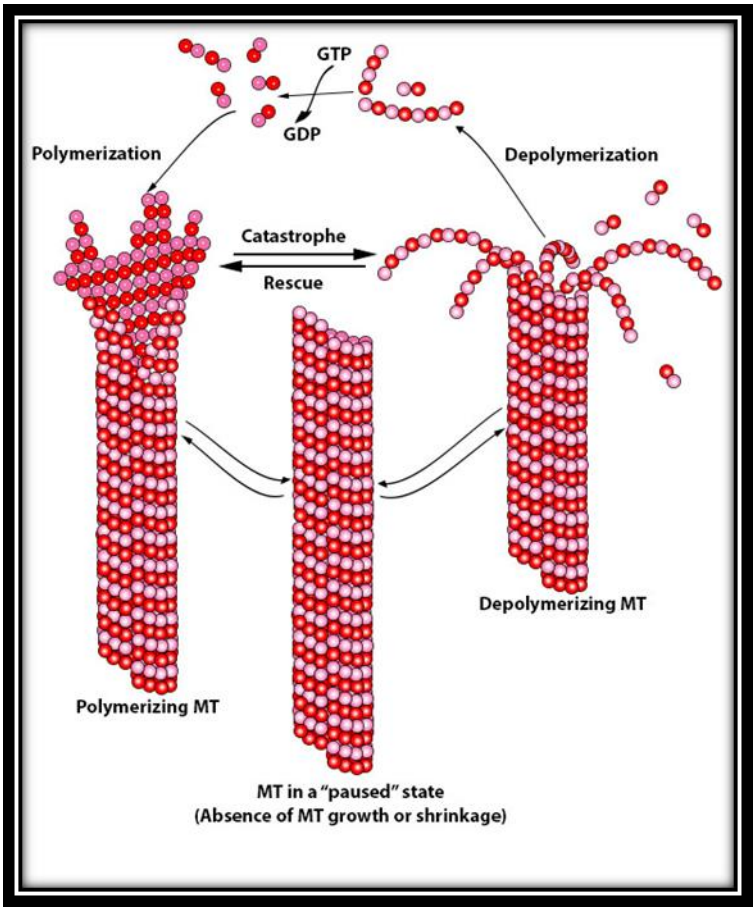
GTP
GDP
Polymerization
Depolymerization
Catastrophe
Rescue
Depolymerizing MT
Polymerizing MT
MT in a "paused" state
(Absence of MT growth or shrinkage)

This process occurs during metaphase and anaphase, playing an important role in maintaining a constant length of the polymer while ensuring a constant flux of tubulin heterodimers from the plus-end to the minus-end of the MTs (McIntosh et al. 2002). Both dynamic instability and treadmilling are displayed simultaneously in some MTs, whereas in others they display one form or the other. However, the degree to which each of these behaviours is displayed relies largely on the ability of MTs to interact with MAPs, the expression of tubulin isotypes and their PTMs, such as phosphorylation, acetylation, polyglutamylation, polyglycylation or tyrosination/detyrosination (Farrell et al. 1987). In humans, there are 6 genes for α-tubulin and 7 for β-tubulin, and these isotopic forms are expressed differentially in different cells and tissues. PTMs further divide these isotypes into various subtypes, leading to differential overall efficacy to anti-tubulin drugs (Lewis et al. 1985; Villasante et al. 1986; McKean et al. 2001).

1.4 Microtubules and their binding partners

MT dynamics are described by variables, such as the speed of MT growth and shortening and the rate of the transitions between “catastrophes” (rapid MT shrinkage) and “rescues” (switching back from shrinkage to growth). Regulation of these parameters occurs by the cellular expression of a group of modulating factors known as MAPs that fall into two major categories: MT-stabilizing and MT-destabilizing factors (Stanton et al. 2011). The stabilizing factors function by decreasing the speed of shortening, preventing catastrophes or by rescuing depolymerising MTs; on the contrary to the destabilizing factors enhance the speed of shortening and increase catastrophes.

Microtubule-stabilizing factors such as MAP1, MAP2, MAP4, tau and doublecortin (DCX) antagonises MT disassembly (Mollinedo & Gajate 2003; Drechsel et al. 1992). MAP4 is the most abundant and stabilizes MTs in non-neuronal cells by specifically enhancing the rescue of depolymerizing MTs (Mandelkow & Mandelkow 1995). Previous reports suggest that cdk1 phosphorylates MAP4 upon entry into mitosis, which causes a reduction of its binding efficiency to the microtubules and, hence, completely abrogates the MT stabilizing ability. This feature of MAP4 regulation suggests that this protein is specifically involved in stabilizing MTs at interphase. However, it is switched off during mitosis to ensure the dynamicity of MTs during the bipolar spindle formation (Vandré et al. 1991; Tombes et al. 1991). MT-plus-end-tracking proteins or +TIPs is a large group of MAPs that bind to the growing ends or the plus-ends of the MTs (Schuyler & Pellman 2001). Cytoplasmic linker proteins (CLIPs) are MT rescue factors that are found localized in the cytoplasm. The first member to be isolated was CLIP-170, which is localized to the plus-ends of the MTs in the form of small clusters (Rickard & Kreis 1990). CLIP-associated proteins, or the CLASPs, are dynamic MT stabilizing factors that are concentrated at different locations, such as the MT ends, the kinetochores or the centrosomes (Maiato et al. 2004). Their localization is also cell cycle dependent. For example, the CLASPs remain at the spindle midzone during anaphase and eventually migrate to the midbody matrix during telophase and cytokinesis, suggesting their role in the regulation of MT dynamics during mitosis (Lemos et al. 2000; Maiato et al. 2003). EB1 is another MT stabilizing factor that is involved

in overcoming MT catastrophe. Several reports suggest the involvement of EB1 in MT associated functions such as cell division, morphogenesis and cell migration by interacting with other +TIPs (Vaughan 2005; Akhmanova & Steinmetz 2008).

On the other hand, MT destabilizing factors induce MT depolymerisation and cause a reduction in their assembly by antagonising the activity of the stabilizing proteins (Maiato et al. 2004). Katanin, the first MT destabilizer to be discovered, causes MT severance by the energy liberated from MT-mediated ATPase activity (Vale 1991; McNally & Vale 1993; Hartman et al. 1998; Hartman & Vale 1999). Katanins are concentrated at the spindle poles and centrosomes in an MT-dependent manner and play an important role in detecting defects in the microtubular lattice (Davis et al. 2002). The kinesin-13 family members, including Kif2A, 2B and 2C (mitotic centromere associated kinesin or MCAK) are MT depolymerizers that perform dual roles. Firstly, they induce catastrophe of the MTs through ATP hydrolysis and secondly sequesters tubulin in an ATP-independent manner (Newton et al. 2004). Oncoprotein (Op) 18/stathmin is another MT destabilizing protein that is highly abundant in leukemic cells. Stathmin binds to tubulin via two binding sites to form a tubulin-stathmin complex, resulting in a kinked MT geometry. This induces a bent conformation in the MT lattice, thus, favouring MT disassembly and catastrophe (Jourdain et al. 1997). Stathmin is negatively regulated by cdk1 and polo-like kinase through phosphorylation. Hyper-phosphorylation and hence down-regulation of stathmin

was observed during mitosis to aid in the formation of the mitotic spindle (Marklund et al. 1996; Larsson et al. 1997).

Motor proteins belong to a different category of MAPs and play a vital role in many of the MT functions, including cell division, that allows the sliding of MTs past each other and the transport of secretory vesicles and membrane bound organelles such as mitochondria and golgi bodies (Goldstein & Yang 2000). Kinesins and dyneins are the two major classes of motor proteins that depend on the MT network. Kinesins transport molecules towards the plus-end of the MTs with the help of the motor domain that generates energy via ATP hydrolysis and the tail domain that determine the cargo specificity. They play essential roles during cell division, particularly during spindle assembly and segregation of chromosomes and are also involved in transport (Goldstein & Philp 1999). Dyneins, on the other hand, are minus-end directing motor molecules composed of two or three heavy chains, with many distinct intermediate and light chains. They are essential for the transport of secretory vesicles and membrane bound organelles (Goldstein & Yang 2000). Therefore, kinesins and dyneins transport vesicles and organelles in opposite directions in an MT-dependent manner and are responsible for bi-directional intracellular transport.

1.5 Mitosis

Mitosis is a fundamental event that occurs during the life cycle of any proliferating somatic cell. When cells progress into mitosis, the dynamicity of the MTs is enhanced by approximately 20-100 times, in combination with a 7-fold increase

in the MT nucleation at the centrosomes (Saxton et al. 1984). The half-life of tubulin that is undergoing polymerization is very short during this period and remains only about 10-30 seconds in duration. When cells enter prophase and prometaphase, MTs grow rapidly in length and subsequently shrink in search of the kinetochores that need to be attached to the spindle MTs. As a result, each kinetochore of a chromosome is captured by MTs emanating from the opposite pole of the cell, resulting in a tensile alignment of the chromosomes at the metaphase plate. Anaphase begins only with the proper alignment of chromosomes, which will then eventually trigger the separation of chromatids towards opposite poles of the cell (Hayden et al. 1990; Piehl et al. 2004). This requires the rapid shrinkage of MTs attached to the kinetochores in combination with the assistance provided by the MT-associated motor proteins in chromosome separation (Maiato et al. 2004). Finally, during telophase, the chromosomes undergo decondensation to form two separate nuclei which are then followed by cytokinesis that requires the activity of the contractile actin-myosin rings (Schmidt & Bastians 2007) (Figure 3). During the process of mitosis, proper chromosome alignment at the center plate is of utmost importance for the onset of anaphase and, hence, the faithful segregation of chromosomes to the newly formed two daughter cells. However, some cells fail to achieve the chromosome alignment and hence lead to chromosome instability and aneuploidy, which may eventually lead to cell death or tumorigenesis.

Figure 3: The role of the mitotic spindle in mitosis
During interphase, chromatin is not condensed and the MTs (green fibres) are distributed around the centrosome (orange circle) in a radial fashion. With the onset of prophase, chromosomes (blue) undergo condensation and duplicated centrosomes separate. The breakdown of nuclear envelope leads to prometaphase and the chromosomes are now not restrained in the nucleus (brown). Kinetochore MTs (dark green) connect the kinetochores (red dot joining the chromatids) to the spindle MTs. This facilitates the alignment of chromosomes at the equator of the cell, leading to metaphase. The (-) ends of the MTs face the centrosome and the (+) ends face towards the cell equator. The (+) ends of the astral MTs emanating from the centrosomes, face the cell cortex. Early anaphase involves the movement of chromosomes towards the opposite poles of the cell, which is then soon followed by the late anaphase, where the spindle poles move apart. During telophase, chromosomes decondense and nuclear envelope is reformed. At the spindle midzone, a central bundle of MTs are present which aid in the process of cytokinesis and the faithful completion of the mitotic cell cycle. The figure was adopted from Walczak, Cai, & Khodjakov (2010).

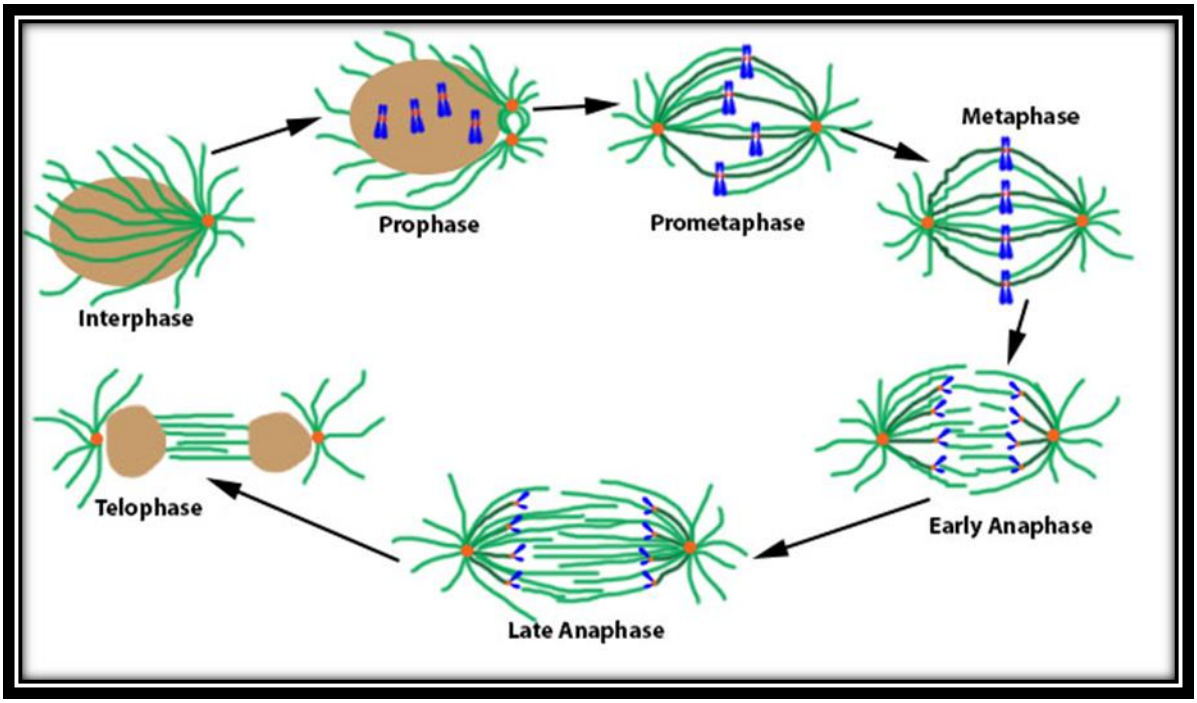
Interphase
Prophase
Prometaphase
Metaphase
Early Anaphase
Late Anaphase
Telophase

To circumvent this potential problem, cells adopt a spindle assembly checkpoint (SAC) that inhibits anaphase onset until all the kinetochores are under tensile attachment to the spindle MTs. Therefore, in the presence of spindle poisons that interfere with the MT dynamics, many kinetochores may not get tensile attachment. This may trigger the activation of SAC, and cells are prevented from entry into anaphase, leading to a prolonged mitotic arrest (Schmidt & Bastians 2007).

1.6 Spindle activation checkpoint (SAC)

Cells enter into mitosis with the activation of cyclin-dependent kinase 1 (cdk1) by its regulatory partner cyclin B. Once cells progress into metaphase, the exit of mitosis is governed by a SAC (Figure 4). During a normal mitotic cell division, SAC remains active only for a brief duration as the unattached kinetochores are rapidly picked up by the spindle MTs, correcting any improper attachments (Matson & Stukenberg 2011). When SAC is active, it inhibits the anaphase promoting complex or cyclosome (APC/C) activity, which is involved in the degradation of both cyclin B and securin (Clute & Pines 1999). This allows cdk1 to be active and protects cohesin from degradation, thus delaying the onset of anaphase. Cell division cycle 20 (Cdc20) is essential for the ubiquitin ligase activity of the APC/C complex. When the SAC is active, core proteins of the checkpoint complex, including mitotic arrest deficient (Mad) 1, Mad2, budding uninhibited by benzimidazoles (Bub) 1, budding uninhibited by benzimidazole-related 1 (BubR1) Bub3 and centromere protein (Cenp)-E interact with the kinetochores of the misaligned or unattached kinetochores.

Figure 4: The role of the SAC in safeguarding against aneuploidy
Bi-orientation of chromosomes ensures the accurate segregation of chromosomes to two daughter cells. Therefore, a tensile attachment between the kinetochores of the chromosomes and the MTs is essential to avoid missegregation and generation of aneuploidy. In the presence of an unattached kinetochore (for example: during prometaphase), SAC is activated and the onset of anaphase is delayed until all the chromosomes are properly attached. Proteins of the SAC core complex, including Mad, Bub and Cenp-E proteins interact with the unattached kinetochore and a signal is generated to inhibit Cdc20-mediated activation of the APC/C. Cohesin protein that holds the sister chromatids together, is cleaved by separase during anaphase. However, the activity of separase is governed by at least the following two mechanisms: (1) The binding of securin to separase; and (2) interaction of cyclinB-cdk1 complex in a phosphorylation-dependent manner to separase, inhibits both cdk1 and separase. When chromosomes are properly attached, SAC is terminated, leading to the ubiquitination and degradation of both cyclin B (inactivation of cdk1) and securin and the initiation of anaphase. The figure was adopted from Holland & Cleveland (2009).

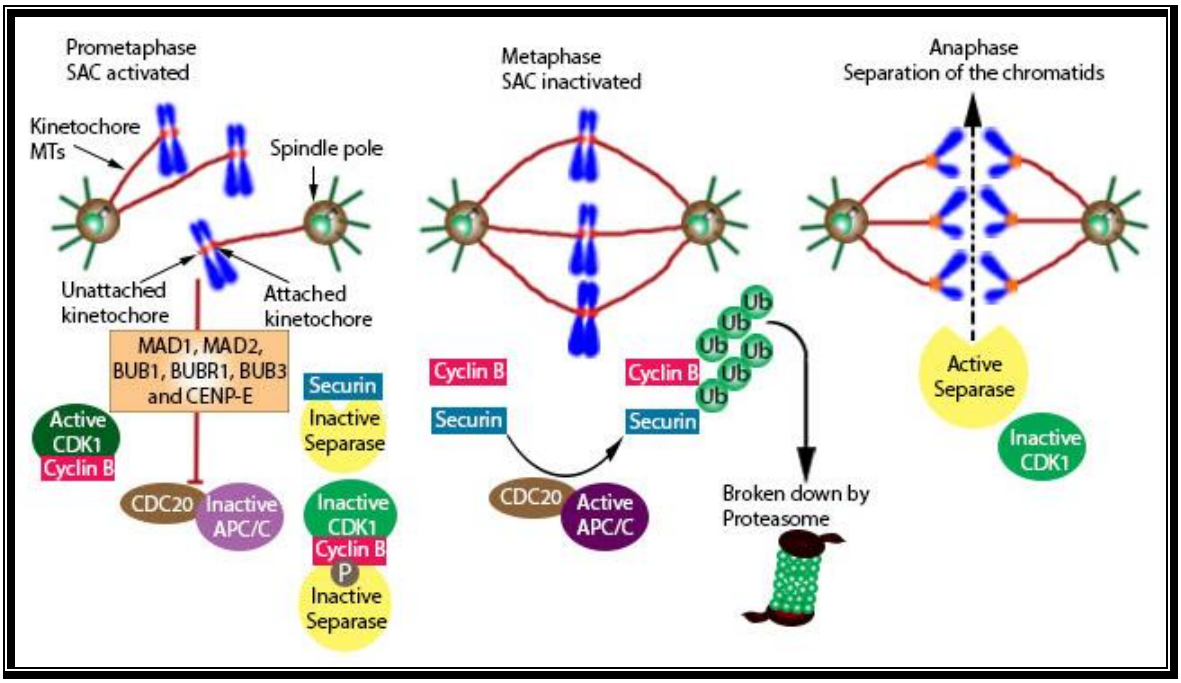
Prometaphase
SAC activated
Kinetochore
MTs
Spindle pole
Unattached
kinetochore
Attached
kinetochore
MAD1, MAD2,
BUB1, BUBR1, BUB3
and CENP-E
Active
CDK1
Cyclin B
CDC20
Inactive
APC/C
Securin
Inactive
Separase
Inactive
CDK1
Cyclin B
P
Inactive
Separase
Metaphase
SAC inactivated
Cyclin B
Securin
CDC20
Active
APC/C
Ub
Cyclin B
Securin
Broken down by
Proteasome
Anaphase
Separation of the chromatids
Active
Separase
Inactive
CDK1

This generates a signal that abrogates the Cdc20-mediated activation of the APC/C and inhibit its ubiquitin ligase activity. However, when all of the chromosomes are properly attached, SAC is inactive and Cdc20 is now freely available to activate the APC/C complex. This leads to the degradation of cyclin B and securin and the completion of mitosis in a timely manner (Peters 2006). In the presence of microtubule-targeting agents or spindle poisons, the chromosomes will never be able to undergo a tensile attachment therefore, the SAC remains active for a longer duration that often lasts for hours. As a result, the cells will either undergo cell death during mitosis or exit mitosis aberrantly, by a phenomenon known as mitotic slippage (Brito & Rieder 2006).

1.7 Microtubules as an epitome of anticancer targets

A number of essential cellular functions including cell division, migration and intracellular transportation rely on the activity of the MT network along with their association with MAPs. Hence, MTs are undoubtedly recognised as validated targets for anti-cancer therapy (Jordan & Wilson 2004). Most of the MT-targeting drugs are involved in either promoting the assembly or the disassembly of the MTs by binding to tubulin directly or by altering the post- translational modifications associated with the MTs. However, since the MTs are important entities for the normal functioning of non-cancerous tissues, anti-tubulin drugs have been reported to induce severe toxicities, including peripheral neuropathies, myelosuppression, immunosuppression and gastrointestinal toxicity. Therefore, continuous investigations are being carried out to establish novel drugs with a

better therapeutic index and minimal toxicities to surrounding non-cancerous tissues (Stanton et al. 2011).

Most of the MT-binding drugs are either MT stabilizing agents (eg: taxanes, epothilones) or destabilizing agents (eg: vinca alkaloids, colchicine). However, the boundary between these two categories are sometimes not very clear as both the classes interfere with the dynamicity of MTs at nanomolar concentrations and, thus, they are collectively referred to as agents that suppress the dynamic instability of MTs (Jordan & Wilson 2004; Yvon et al. 1999; Panda et al. 1996).

1.8 Microtubule Stabilizing Drugs (MSDs)

MSDs bind to polymerized MTs and prevent their depolymerisation into individual α/β tubulin heterodimers.

1.8.1 Agents binding to the taxane-binding site

This group of microtubule stabilizing agents binds within the lumen of polymerized MTs, specifically at the β-tubulin subunit bound with GDP, and eventually, converts into a more stable GTP-bound conformation (Elie-Caille et al. 2007). This increases the rate of tubulin polymerization and hence the equilibrium is shifted from the soluble form of tubulin towards the polymerized form (Rao et al. 1999). Analogues of paclitaxel (Taxol®) and docetaxel (Taxotere®) along with other similar molecules bind to tubulin via the taxane-binding site (Geney et al. 2005). The cytotoxic effects of these taxane-site

binding agents are attributed to their binding capacity to tubulin that leads to its stabilization and thus over-polymerization and, finally, leading to cell death by apoptosis (Morris & Fornier 2008).

Taxoids: Paclitaxel (Figure 5), being the prototype of this group of drugs, is still regarded as the gold standard in the treatment of solid tumors, such as the carcinomas of the breast, ovary, prostate and lung. In the 1960s, paclitaxel was initially isolated from the barks of the Pacific Yew tree (*Taxus brevifolia* Nutt), which was then eventually approved by the FDA in 1992 as an ovarian cancer therapeutic (Stanton et al. 2011). Docetaxel, which is semi-synthetically synthesized from a precursor isolated from the European Yew tree (*Taxus baccata* L) was introduced as a second generation taxane with better pharmacological properties than paclitaxel. Docetaxel exhibited better water solubility and more activity against the proliferation of cancer cells, making it more useful in chemotherapeutic regimens for the treatment of breast and prostate cancers (Schmidt & Bastians 2007; Stanton et al. 2011). Tubulin polymerization by paclitaxel is favoured during all reaction conditions. The presence of low tubulin concentrations, reduced temperatures and absence of GTP or MAPs does not hinder its stabilizing activity (Kumar 1981; Thompson et al. 1981). Moreover, the presence of MT bundles not originating from the MTOC suggests that paclitaxel also facilitates its nucleation (De Brabander et al. 1981).

Figure 5: Structures of Microtubule Stabilizing Drugs (MSDs)
MSDs bind to tubulin, usually close to the taxane-binding site. This leads to the stabilization of the MT lattice that prevents MT depolymerisation and, eventually, lead to cell death (Stanton et al. 2011; Gerth et al. 1996; Liu et al. 2007; Giannakakou & Fojo 2000).

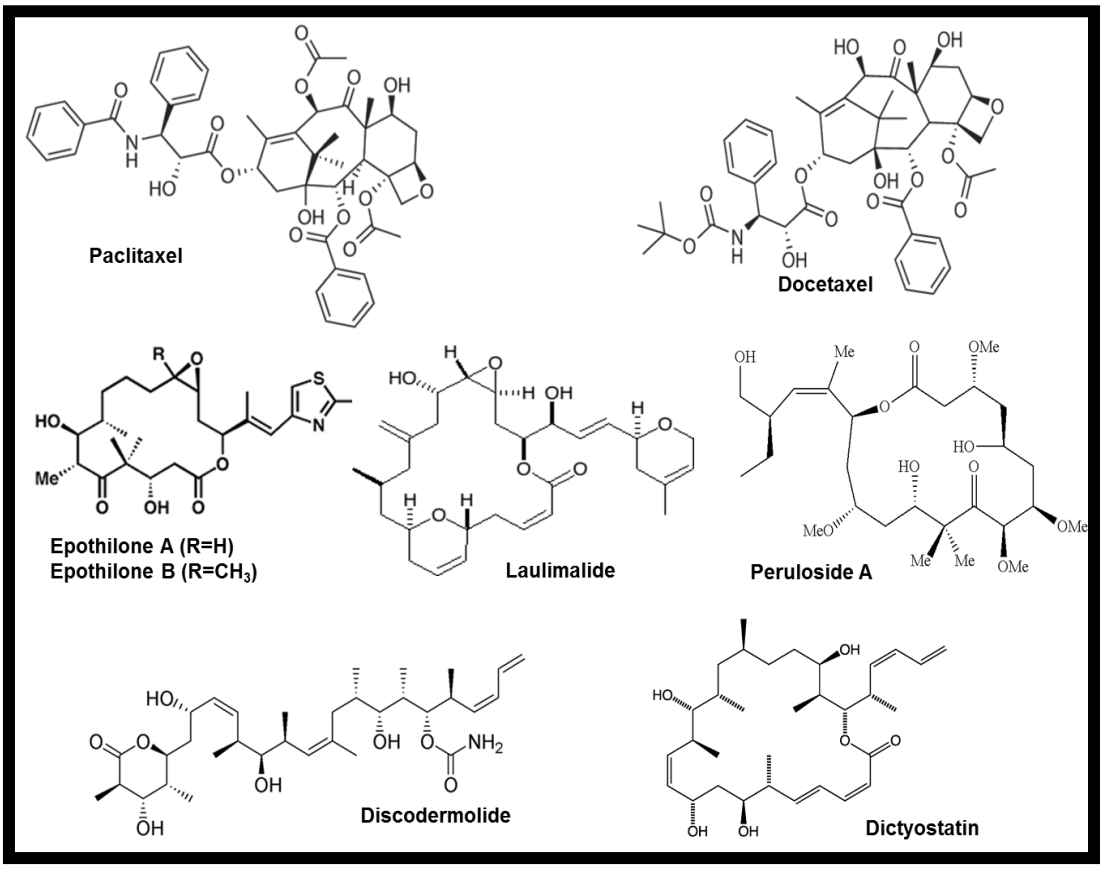
Paclitaxel
Docetaxel
Epothilone A (R=H)
Epothilone B (R=CH3)
Laulimalide
Peruloside A
Discodermolide
Dictyostatin

However, there are many factors that limit their use in a clinical setting, including acquired resistance, severe toxicities and hypersensitivity issues in the recipient patients (Stanton et al. 2011). Resistance to paclitaxel is acquired by at least two main causes. Firstly, the overexpression of P-glycoprotein (Pgp), which is responsible for the excessive efflux of paclitaxel from the tumor cells. Secondly, the overexpression of the βIII tubulin isoform that reduces paclitaxel's binding ability to tubulin (Morris & Fornier 2008; Sève & Dumontet 2008). Paclitaxel is also associated with several dose-limiting side effects such as peripheral neuropathies and myelosuppression, making it difficult to use for a long-term clinical treatment. In addition, the reduced water solubility of paclitaxel requires its formulation with agents such as cremophor or DMSO leading to hypersensitivity in some patients. This suggests the urgent need to synthesise and characterize drugs which are more specific but highly efficient towards cancerous tissues (Stanton et al. 2011).

Epothilones: Epothilones A and B (Figure 5) were originally produced using the myxobacterium, *Sorangium cellulosum* So ce90. These drugs belong to the family known as the macrolides (Gerth et al. 1996). These drugs bind close to the taxane-binding site as they were reported to show competitive binding with paclitaxel (Bollag et al. 1995). Since epothilones are generated using bacteria, they are easy to produce. Importantly, they are not transported via Pgp channels; hence, they can be used for the treatment of paclitaxel-resistant tumors (Kowalski et al. 1997). Two epothilones, patupilone and ixabepilone are currently

under development and clinical investigation, as they are more efficient and less toxic than paclitaxel. In addition, patupilone diffuse across the blood brain barrier whereas ixabepilone is effective against taxane-resistant tumors (Goodin et al. 2004; Lee et al. 2001).

1.8.2 Laulimalide and peloruside A

Isolated from marine sponges, laulimalide and peloruside A (Figure 5) are effective against taxane-resistant tumors, similar to the epothilones. However, their use is limited due to their low therapeutic specificity. Previous studies using NMR suggested that laulimalide and peloruside A bind to tubulin through the α-tubulin subunit. However, subsequent studies using mass spectrometry showed that these drugs bind to β-tubulin via a site adjacent to the taxane-binding site (Liu et al. 2007; Wilmes et al. 2007). Nevertheless, these drugs do not compete with paclitaxel in binding experiments and demonstrate synergistic behaviour with the taxanes, suggesting a combination regimen could be used to enhance their efficiency as chemotherapeutic agents (Hamel et al. 2006).

1.8.3 Discodermolide and dictyostatin

Both discodermolide and dictyostatin are similar to laulimalide and peloruside A, as they are derived from marine origin and exhibit synergistic effects with paclitaxel by binding to a different site on tubulin. Both of these agents are produced by marine sponges as a part of their defence mechanism and are involved in MT stabilization by increasing MT polymerization, and nucleation of

MT bundles, while decreasing MT depolymerisation (Madiraju et al. 2005; Giannakakou & Fojo 2000).

1.9 Microtubule Destabilizing Drugs (MDDs)

MDDs, at high concentrations lead to MT depolymerisation; however, both MSDs and MDDs are involved in disrupting the dynamicity of the MTs at low concentrations.

1.9.1 Vinca-site binding agents

Agents that compete with the binding of vinca alkaloids (eg: vinblastine, vincristine) to MTs are known as vinca-site binding agents (Chen et al. 2010). Vinca alkaloids, which were introduced into the clinics during the late 1950s and have proven to be successful. These agents are involved in MT destabilization by interfering with GTP hydrolysis and with nucleotide (GDP to GTP) exchange during the regeneration of GTP-bound tubulins (Risinger et al. 2009).

Vinca alkaloids: Isolated from *Catharanthus roseus* L commonly known as periwinkle, the vinca alkaloids (Figure 6) bind to the β-tubulin subunit close to the GTP-binding site. Hence, they interfere with the hydrolysis of GTP following tubulin polymerization and the nucleotide exchange of GDP with GTP (Cutts et al. 1960; Rai & Wolff 1996). This results in a curved or peeling conformation, unlike the straight or growing conformation that is preferred during MT growth and polymerization.

Figure 6: Structures of Microtubule Destabilizing Drugs (MDDs)
MDDs bind to tubulin and inhibit the polymerisation of the MTs at high concentrations and reduce the dynamic behaviour of the MTs at low concentrations. There are two main types of MDDs: (1) Vinca-site binding agents compete with the vinca alkaloids to bind to β-tubulin subunit, close to the GTP-binding site; and (2) Colchicine-site binding agents bind at the interface of α and β tubulin subunits, causing a conformational transition towards a curved tubulin geometry that favours MT depolymerisation.

1

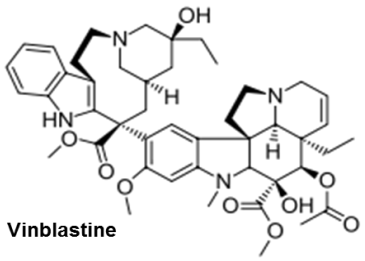

Vinblastine

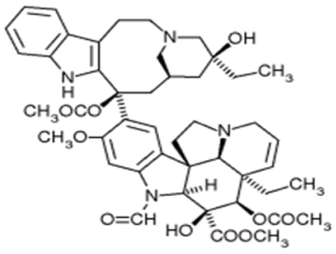

Vincristine

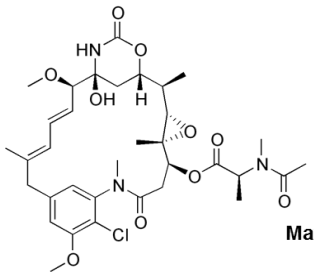

Maytansine

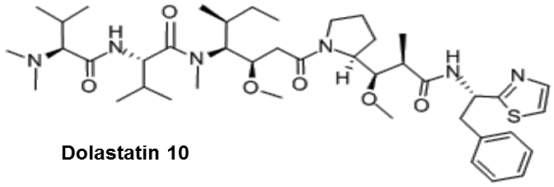

Dolastatin 10

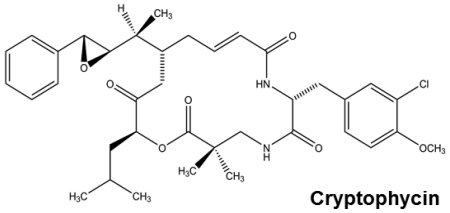

Cryptophycin

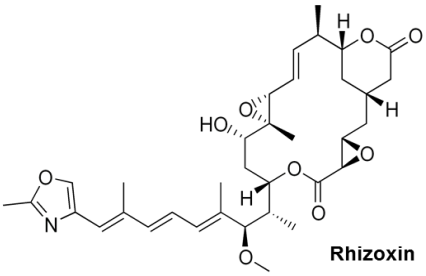

Rhizoxin

2

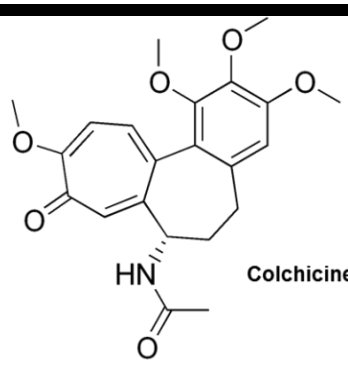

Colchicine

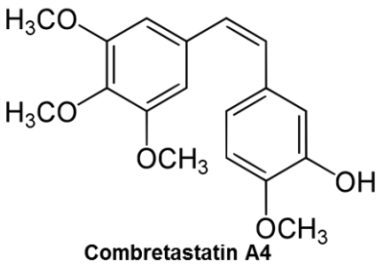

Combretastatin A4

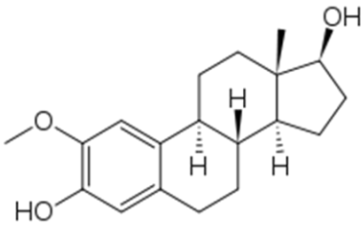

2-Methoxyestradiol

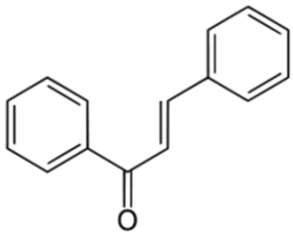

Chalcone

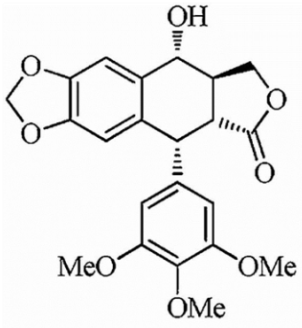

Podophyllotoxin

These agents are also known as end poisons, as they bind to one or a few tubulin molecules at the plus-end of the MTs, preventing their copolymerization into the tubular lattice (Chen et al. 2010). At higher concentrations, the vinca alkaloids promote paracrystals, tubules and spirals formation by binding to free tubulin heterodimers (Takanari et al. 1990; Wilson et al. 1982; Warfield & Bouck 1974). The first generation vinca alkaloids are vinblastine and vincristine; however, there are several semi-synthetic analogues including vinorelbine, vindesine and vinflunine (Risinger et al. 2009; Cutts et al. 1960) that are proven to be more effective than vinblastine. The parent compound and these agents are currently used for the treatment of lymphomas and leukemias (Kruczynski et al. 1998).

Maytansinoids: This group of compounds are found in plants and include maytansine (Figure 6) (isolated from *Maytenus ovatus* Loes). Derived from *Nocardia* species, ansamitocin is a structurally similar compound to maytansine and is shown to possess antiproliferative property (Hamel 1996). Maytansinoids have been reported to exhibit 100-1,000 times better cytotoxic properties than vincristine or vinblastine (Liu & Chari 1997). They inhibit the binding of vinca alkaloids, especially vincristine competitively; hence, they are thought to bind at least partially overlapping the vinblastine-binding site (Bai et al. 1993). However, dose-limiting side effects such as gastro and neuronal toxicities in combination with a low therapeutic value during the clinical trials discontinued further use as anticancer therapeutics (Cassady et al. 2004).

Vinca site-binding peptides: This group may include peptides, depsi-peptides, or cyclic or modified peptides that bind to tubulin at a site partially overlapping the binding site of the vinca alkaloids (Chen et al. 2010). Dolastatin analogues (from *Dolabella auricularia* Lightfoot) and cryptophycins (Figure 6) (from *Nostoc*, a cyanobacterium species) are well-characterized agents belonging to this group (Gupta & Bhattacharyya 2003; Hamel 1996). One of the most effective dolastatin analogues that binds to tubulin and causes a prominent mitotic arrest is dolastatin 10 (Figure 6). It inhibits the binding of vincristine, rhizoxin and phomopsin A to tubulin and also prevents GTP hydrolysis and nucleotide exchange (R Bai, G R Pettit, et al. 1990a; R Bai, George R. Pettit, et al. 1990b; Ludueña et al. 1992). In spite of being a substrate of Pgp, dolastatin 10 is efficiently retained within tumor cells, leading to stronger inhibition of tumor cell growth as compared to clinically successful drugs such as vinblastine (Toppmeyer et al. 1994). Cryptophycins, on the other hand, are not substrates of Pgp and show anticancer activity against multiple cancers (Smith et al. 1994). They inhibit vinblastine binding non-competitively and abrogate GTP hydrolysis (Smith & Zhang 1996). Cryptophycin-52 entered clinical trials but failed due to extreme toxicity profiles (Edelman 2003).

Other vinca domain binding agents: Rhizoxin (Figure 6), which is a macrocyclic lactone is derived from *Rhizopus chinensis* Saito (Iwasaki et al. 1984). It exhibits potent anticancer activity by binding at a site similar to maytansine, overlapping the vinblastine-binding site. Vinblastine, at high

concentrations promote the formation of tubulin aggregates, however this feature is not observed in the presence of rhizoxin (Takahashi et al. 1987; Gupta & Bhattacharyya 2003). Although rhizoxin is effective against human and murine cells along with their vincristine-resistant cell lines, clinical trial of rhizoxin was discontinued due to low efficacy (McLeod et al. 1996). Phomopsin A (from *Phomopsis leptostomiformis* Bubak) (Hamel 1996) and ustiloxins (from *Ustilaginoidea virens* Takahashi) (Koiso et al. 1994) arrest cells in mitosis by preventing the polymerization of MTs. In addition, similar to the vinca alkaloids, these two compounds also inhibit tubulin-dependent GTP hydrolysis, GDP-GTP nucleotide exchange and promote spiral aggregation of tubulin (R Bai, George R. Pettit, et al. 1990; Hamel 1996; Ludueña et al. 1990). However, they do not exhibit potent cytotoxic properties and require about 1,000 fold higher concentrations than paclitaxel and vinblastine to kill cells. Although the mechanism for this effect is not yet known, the permeability of the cell membrane and the rate of drug metabolism is thought to play a role (R Bai, G R Pettit, et al. 1990; Koiso et al. 1994; Li et al. 1995).

1.9.2 Colchicine-site binding agents

The colchicine-binding site is situated at the interface of the α- and β-tubulin subunits. When colchicine binds to tubulin, a conformational transition occurs to yield a curved tubulin geometry, followed by the inclusion of the colchicine-tubulin complex within the protofilament. The steric clash that arises during this process favours the process of MT depolymerisation (Downing & Nogales 1999; Downing & Nogales 1998; Garland 1978).

Colchicine: *Colchicum autumnale* L, commonly known as meadow saffron, was used first to extract colchicine (Figure 6), the first MT destabilizing agent to be discovered (Peterson & Mitchison 2002; Zhou & Giannakakou 2005). Colchicine was then used to investigate detailed properties of the MTs and its subunits (Stanton et al. 2011). Colchicine binds to tubulin via a two-step process. Firstly, colchicine associates with tubulin reversibly and with low affinity to form a pre-equilibrium complex, which then undergoes conformational changes that lead to the formation of a nearly irreversible tubulin-colchicine complex, favouring MT depolymerisation (Stanton et al. 2011). Similar to the vinca alkaloids, colchicine hinders the MT dynamics at low concentrations and reduces the MT polymer mass at high concentrations. Colchicine causes more toxicity in cancer cells due to their high rate of proliferation as compared to the normal cells; however, colchicine administration leads to severe dose-limiting side effects including neutropenia, myelosuppression, anemia and gastrointestinal toxicities that reduces its therapeutic value and limits its use as a safe anticancer agent (Lu et al. 2012).

Combretastatins: Isolated from *Combretum caffrum* Kuntze, commonly known as the South African tree (Hamel 1996), combretastatins inhibit the polymerization of MTs via binding to tubulin at the colchicine-binding site. This causes a severe mitotic arrest in the treated cells that leads to cell death through apoptosis (Zhou & Giannakakou 2005; Hamel 1996). In terms of both cytotoxic properties and binding capacity, the most effective combretastatin is

combretastatin A4 (Figure 6), which is administered as a phosphate salt due to its poor solubility. It, then undergoes dephosphorylation to form the active product, combretastatin A4 *in vivo* (Lu et al. 2012).

Combretastatins have been reported to block the vasculature within the core of the tumor by causing the endothelial cells that line the capillaries to swell up; however, the edge of the tumor remains unaffected, therefore, combinational regimens including drugs like paclitaxel are needed to kills cells at the tumor margins (Ahmed et al. 2003).

There are several clinical trials using combretastatin A4 for multiple cancers, including relapsed ovarian cancer, anaplastic thyroid cancer and lung cancer. High blood pressure, being the major side effect during the treatment is kept under control using medications, nevertheless there are currently no combretastatin drugs approved by the FDA (Rustin et al. 2010).

2-Methoxyestradiol (2-ME): It is an endogenous derivative of β-estradiol that is formed via a hydroxylation and a methylation reaction by enzymes, cytochrome P-450 and catechol *O*-methyl transferase, respectively. 2-ME (Figure 6) exhibits potent anti-proliferative ability and is known to inhibit tumor vasculature (Mabjeesh et al. 2003). In addition, 2-ME reduces the rate at which the MTs assemble by binding at the colchicine site (D'Amato et al. 1994). However, clinical studies show signs of several adverse effects including diarrhoea, fatigue,

nausea, neuropathy, dyspnea and edema (Matei et al. 2009). ENMD-1198 is a chemically derived analogue that exhibits better metabolic stability along with the ability to prevent proliferation of endothelial cells, migration, motility, morphogenesis and to damage the tumor vasculature within a short period of time (Bohlin & Rosén 1996; Pasquier et al. 2010).

Podophyllotoxin: Isolated from the roots of *Podophyllum peltatum* L, podophyllotoxin (Figure 6) and its analogues are used in the treatment of several ailments including tuberculosis, gout, syphilis, rheumatism, cirrhosis, constipation and cancer (Desbène & Giorgi-Renault 2002). Podophyllotoxin has been reported to inhibit tubulin polymerization by binding to tubulin via the colchicine-binding site, more rapidly and reversibly than colchicine (Lu et al. 2012; Stanton et al. 2011). Podophyllotoxin was employed as the lead compound to synthesize less toxic derivatives known as etoposide and teniposide. Both these compounds are used in combinatorial regimens where etoposide functions more effectively as a topoisomerase II inhibitor than a tubulin polymerization inhibitor (Desbène & Giorgi-Renault 2002; Hamel 1996).

1.10 Importance of agents binding to colchicine site

Tubulin binding chemotherapeutics such as the vinca alkaloids and taxanes have been immensely successful in the clinic, however colchicine-site binding agents have not yet entered a commercial phase. Although the use of colchicine as an anticancer agent is restrained due to its low therapeutic value, multiple efforts are undertaken to establish colchicine binding-site agents. As detailed above and in

a plethora of published data within the past few years, numerous agents that bind to the colchicine-binding site have been synthesized and characterized with the hope of developing a safe but efficient anticancer drug. Colchicine site-binding agents are particularly attractive due to several reasons. Firstly, they have the potential to serve as effective vascular disrupting agents and angiogenesis inhibitors. Secondly, their ability to overcome multidrug resistance (MDR) would enhance the intracellular drug concentrations. MDR arises due to the overexpression of the MDR1 gene that encodes Pgp and, as previously mentioned, both taxanes and vinca alkaloids are substrates of this drug efflux pump, leading to the reduction in cellular drug concentration and hence their cytotoxic potential. Apart from the overexpression of drug efflux pumps, resistance to drugs also arises due to mutations in tubulin that alters the binding sites of the drugs and secondly due to the overexpression of the βIII-tubulin isoform that leads to a considerable increase in MT dynamics (Lu et al. 2012). Previous reports suggest that the colchicine-site binding agents, including colchicine itself and 2-ME, are not affected by β-tubulin expression pattern (Mollinedo & Gajate 2003; Jordan et al. 1998). However, the major problems associated with this group of compounds are their reduced oral bioavailability and a reduced therapeutic index, apart from metabolic instabilities and poor pharmacokinetic profiles. Dose-limiting side effects, including peripheral neuropathies, myelosuppression and hypersensitivities discourage the use of these agents as main stream therapeutics. Therefore, research efforts are underway to establish novel colchicine-site binding agents with improved

therapeutic index. However, no agent binding to tubulin via the colchicine-binding site has thus far been approved as a valid anticancer therapeutic (Lu et al. 2012).

1.11 Colchicine-site binding agents in clinical trials

Colchicine has been employed in several clinical trials for the treatment of multiple diseases, including cancer; however, severe toxicities associated with the administration of colchicine forced to the discontinuation of its use as an anticancer therapeutic. ZD6126, a potent antiangiogenic and antineoplastic agent was examined for its potential in clinical trials for treating metastatic colorectal cancers; however, severe cardiotoxicity forced termination of the studies at the phase II stage (Goto et al. 2002; Lippert 2007). Zybrestat (combretastatin A4P), developed by OxiGene, is currently being evaluated for the treatment of recurrent ovarian cancer and neuroendocrine tumors. Multiple phase II clinical trials are either completed or ongoing for zebrestat for the treatment of solid tumors such as relapsing ovarian cancer, anaplastic thyroid cancer and non-small cell lung cancer (NSCLC) (Rustin et al. 2010). Oxi4503 (combretastatin A1 diphosphate) is employed mainly to target the tumor vasculature. However, currently, a phase I clinical trial is also being conducted for refractory acute myelogenous leukemia (AML) and myelodisplastic syndrome (MDS) (Lu et al. 2012). Ombrabulin 5 (AVE8062) is a more water soluble and orally bioavailable analogue of combretastatin A4 that exhibits better anticancer properties with reduced toxicities in the Colon 26 (murine) carcinoma model. The antitumor activity of ombrabulin 5 is due to its ability to disrupt the formation of new blood vessels in tumors, and it has been reported to be effective against taxane-resistant cells

(Tae et al. 2007). During a phase I clinical trial, ombrabulin 5 was administered in combination with docetaxel and was well-tolerated by patients (Eskens et al. 2014). Teniposide, asetoposide and etoposide phosphate are useful drugs that are synthesized from the lead compound podophyllotoxin (Bohlin & Rosén 1996). Both teniposide and etoposide are used in clinical settings to treat several types of cancers, including small cell lung cancer (SCLC), lymphomas and testicular cancer. Etoposide and teniposide were approved by the US FDA in 1983 and 1993, respectively. Thereafter, to enhance the tolerability in receiving patients, etoposide was approved in the form of gelatin capsules in 1987 (You 2005). Etoposide and teniposide are usually used as a combinational therapy for the treatment of lung cancers, leukemias and testicular cancers. Unfortunately, they show several side effects including myelosuppression, nausea, vomiting, hair loss and hypersensitivities, necessitating the development of safer drugs (You 2005). Nocodazole, a lead compound for the synthesis of novel colchicine-site binding agents, is a potent antimitotic drug that interferes with MT polymerization leading to a reversible and rapid mitotic arrest. However, the use of nocodazole in the clinic is limited due to the severe side effects, including myelosuppression, leukopenia, neutropenia and anemia. Nevertheless, nocodazole has been useful as a reference compound to explore the process of mitosis (Lu et al. 2012). T138067 inhibits the polymerization of MTs by covalently binding to the Cys239 residue of the β-tubulin subunit. It was shown to be effective against tumors with multi-drug resistance phenotype; hence, T138067 entered phase II clinical trials. Unfortunately, it also showed signs of gastrointestinal, hematological and

neurotoxicities (Shan et al. 1999). Similarly, there are several other colchicine binding-site agents that have reached the clinical trials stage, including ABT-751 (phase II), CI-980 (phase II), MN-029 (phase I). However, all of them are associated with several toxicities such as constipation, fatigue and abdominal pain for ABT-751(Hande et al. 2006), significant neurotoxicity for CI-980 (Thomas et al. 2002), and anorexia, diarrhoea, fatigue, nausea, vomiting and headache for MN-029 (Shi & Siemann 2005; Ricart et al. 2011). Therefore, despite their significant ability to arrest cell cycle progress and kill cancer cells through both mitotic and apoptotic pathways, severe dose-limiting side effects including neurotoxicity, thromboembolic and cardiovascular events warrant for continuous research on this group of agents to develop a safe and effective anticancer therapeutic in the near future.

1.12 Summary of work presented in this thesis

MTAs still remain one of the most successful antimitotics used for the treatment of cancer. Unfortunately, the inherent toxicities, hypersensitivities and acquired resistance to these drugs reduces their therapeutic index and, thus, warrants the development of better chemotherapeutic agents (Lu et al. 2012). This thesis provides evidence of novel chalcone derivatives that potentially fit this description. CTR compounds inhibit the proliferation of a broad range of cancer cells, at sub-micromolar concentration. I initially focussed on the characterization of CTR-17, and later I also studied the mechanism of action of CTR-20. The cytotoxic effects of CTR-17 and CTR-20 in cancer cells are 10-25 times more effective than non-cancer cells, which is a highly desirable property of anti-cancer

agents to achieve a better therapeutic index. When compared with colchicine that exerts only about 2.5 to 3.5 times better selectivity, for cancer cell killing over non-cancerous cells, CTR-17 and CTR-20 appear to be much more desirable drugs. CTR-17 arrests the cells in mitosis via the activation of the spindle checkpoint, thereby delaying mitotic exit by the inhibition of anaphase-promoting complex/cyclosome (APC/C) ubiquitin ligase activity. CTR-17 causes a prolonged mitotic arrest that lasts more than 20 hours in a variety of cell lines, including in HeLa, Hek293T, MDA-MB468 and MDA-MB231 cells. All these cells then eventually undergo cell death. However, in non-cancer cells (184B5 and MCF10A), only about 25% of cells undergo cell death and the remaining cells follow a normal cell cycle progression.

Data from immunofluorescence staining experiments revealed that CTR-17 leads to elongation and denser astral MTs, defects in chromosome alignments, short spindles and fragmentation of centrosomal materials. Most of these effects are attributable to the inhibition of MT dynamics during mitosis and reduction of the MT polymer mass. Therefore, the ability of the CTR compounds, to inhibit MT polymerization was analysed using purified tubulin and cell culture systems. Fluorescence microscopy and molecular docking studies identified that both of the CTR compounds bind directly to tubulin partially overlapping the colchicine-binding site. Importantly, both the CTR compounds were also effective against cells resistant to paclitaxel, vinblastine and colchicine.

In conclusion, data presented in this thesis suggests that novel chalcone derivatives, CTR-17 and CTR-20 have a broad range of anti-tumor activities via MT depolymerisation through its binding to tubulin at the colchicine-binding site. It is important to recognise that CTR-17 and CTR-20 exert lesser toxicity to normal tissues and are also active against cell lines resistant to drugs. These desirable properties identify CTR-17 and CTR-20 to be attractive lead compounds to design safer and more effective anticancer therapeutics.

2.0 Materials and Methods

2.1 Cell culture

All cancer cell lines were purchased from American Type Culture Collection (ATCC) (Manassas, VA) and cultured in Roswell Park Memorial Institute-1640 (RPMI-1640) medium supplemented with 10% v/v fetal bovine serum (FBS) and 1% v/v antibiotic antimycotic solution (100 units of penicillin, 100 µg of streptomycin, and 0.25 µg of amphotericin B per ml), purchased from Hyclone (South Logan, UT). 184B5 and MCF10A were cultured in Dulbecco's Modified Eagle's Medium/Ham's Nutrient Mixture F-12 (DME/F12) medium (HyClone) supplemented with 10% v/v FBS, 1% v/v antibiotic antimycotic solution, 0.5 µg/ml hydrocortisone, 10 ng/ml human epidermal growth factor (hEGF) and 5 µg/ml insulin (SingleQuots Kit, Clonetics, Burlington, ON, Canada).

KB-3-1, the parental wild-type human epidermal cervical carcinoma cell line and KB-C2 which is an ABCB1/Pgp-overexpressing drug-resistant cell line were kindly provided by Dr. Amit K Tiwari (University of Toledo, OH). The KB-C2 cell line was established in the presence of increasing concentrations of colchicine by Dr. Shin-ichi Akiyama, Kagoshima University, Japan. The MRP-overexpressing cell lines, H69AR and the parental wild-type small cell lung carcinoma H69, was purchased from ATCC. H69AR cells were established in the presence of increasing concentrations of adriamycin (doxorubicin) by Dr. Susan Cole (Queen’s University Cancer Research Institute, Kingston, Canada). H69 cells grow as large multi-cell aggregates; hence, accurate cell counts were difficult. Therefore, cytotoxicity results obtained from H69AR cells were compared to SW1271 cells which are another small cell lung carcinoma cell line, purchased

from ATCC. All cells were maintained in a humidified incubator at 37°C with 5% CO_2. Cell line authentication was performed through Genetica DNA Laboratories (Burlington, NC) using short tandem-repeat (STR) profiling (March 2015; July 2015).

2.2 Sulforhodamine B (SRB) assay

An optimum density of cells (40,000/ml) was seeded in each well of a 96-well plate and incubated for 16 h as described previously (Vichai & Kirtikara 2006; Skehan et al. 1990). The medium was then replaced with different concentrations of the drugs dissolved in DMSO (final concentration of DMSO was 0.1%). Sham-control wells contained only medium with DMSO (final concentration of DMSO was 0.1%). 100 µl of 10% trichloroacetic acid (TCA) was used as negative control (Thermo Fisher Scientific, Ottawa, ON, Canada). Incubation of cells with these agents was continued for an additional 72 h. The cells were subsequently fixed with cold 10% TCA for 1 h at 4ºC. TCA was then removed and cells were washed with cold tap water, and the plate was air-dried. Cells were then stained using 50 µl of 0.4% SRB (Sigma, Oakville, ON, Canada) in 1% acetic acid (Thermo Fisher Scientific) solution for 30 min. The unbound dye was washed off quickly with 1 % v/v acetic acid once followed by three washes with cold tap water. The plates were allowed to air dry and the bound SRB was then solubilised in 200 µl of 10 mM Tris Base, pH 10.5 (Thermo Fisher Scientific). Absorbance was measured at 540 nm using an automated plate reader (Synergy H4 Hybrid Multi-Mode Microplate Reader - Bio-Tek, Winooski, VT). Cell growth was calculated by the following formula:

% cells proliferation = [($A_{treated}$ – $A_{negative}$)/ (A_{sham} – $A_{negative}$)] x 100

Where, $A_{treated}$: absorbance of treated cells, $A_{negative}$: absorbance of negative control cells, A_{sham}: absorbance of sham treated cells. IC_{50} values were calculated from sigmoidal dose-response curves generated by at least two independent biological replicates, with quadruple technical replicates for each set using GraphPad Prism v.5.04 software (GraphPad Software, Inc, La Jolla, CA). For combinational experiments on the KB-C2 cell line, CTR compounds and paclitaxel were used in six different ratios; namely, $0.5IC_{50}$:$0.5IC_{50}$, $0.5IC_{50}$:IC_{50}, IC_{50}:IC_{50}, IC_{50}:$0.5IC_{50}$, IC_{50}:$0.25IC_{50}$ and IC_{50}:$0.125IC_{50}$. The combination index (CI) was calculated using the following formula (Chou 2006).

$$CI = \frac{(D)_1}{(D_x)_1} + \frac{(D)_2}{(D_x)_2} = \frac{(D)_1}{(D_m)_1[f_a/(1-f_a)]^{1/m1}} + \frac{(D)_2}{(D_m)_2[f_a/(1-f_a)]^{1/m2}}$$

Where, D: Dose of the drug, D_m: Median effect dose, F_a: Fraction affected, m: slope of the curve. If the CI values were less than, equal to or more than 1, it indicated a synergistic, additive or antagonistic effect, respectively (Chou 2006). CI values were determined from four independent experiments.

2.3 Synchronization of cells

HeLa cells were synchronized at the G1/S border of the cell cycle using a double thymidine block as described previously (Romero & Lee 2008). Briefly, the cells were exposed to 2.0 mM thymidine (Sigma) for 18 h and subsequently washed with 1X PBS (2.7 mM KCl, 1.0 mM KH_2PO_4, 137 mM NaCl, 10 mM NaH_2PO_4, pH

7.5). Cells were then maintained in drug-free medium for 11 h followed by a second thymidine exposure for 14 h. The cells were then washed again with 1X PBS and released into complete medium in the absence (sham) or presence of 3.0 μM CTR-17 for different durations.

2.4 Cell cycle analysis by flow cytometry

Cell cycle analysis by flow cytometry using propidium iodide was carried out as described previously (Solomon et al. 2009). Exponentially growing cells treated with different concentrations of CTR-17 were harvested using a cell scraper at the scheduled time points. Cell pellets were collected by centrifugation at 1,100 rpm (AllegraTM X-12 centrifuge, Beckman Coulter, Mississauga, ON, Canada) for 5 min. The cells were then washed once with 1X PBS and fixed with 75% ethanol at -20°C for 18 h. Cells were then washed twice, with 1X PBS to remove ethanol by centrifugation at 1,100 rpm (AllegraTM X-12 centrifuge) for 5 min. Cells were then stained with propidium iodide (Life Technologies, Burlington, ON, Canada) solution (PI) for 1 h, protected from light. The PI solution contained 0.1% v/v PBS, 0.3% v/v Nonidet P-40, 100 μg/ml RNase A and 100 μg/ml propidium iodide. Samples were then analyzed using a Beckman Coulter Epics Elite FC 500 Flow Cytometer (Mississauga, ON, Canada). The forward scatter/side scatter (FS/SS) plot was used to exclude potential doublets and debris were excluded during the analysis of the total counts. To determine if the activity of the compounds were reversible, HeLa cells were treated for 12 h with CTR-17 or CTR-20. The floating cells were collected by centrifugation at 1,100 rpm (AllegraTM X-12 centrifuge), washed twice with 1X PBS and released into

fresh culture medium. The adherent cells were washed with 1X PBS and fresh medium was also added to these plates. At scheduled time points, both the populations of cells (adherent and floating) were harvested as previously explained, prior to performing flow cytometry. Data were generated from at least three biological replicates.

2.5 Immunofluorescence staining

Cells were plated on coverslips placed in 35 mm tissue culture plates or 6-well cluster dishes, and allowed to adhere overnight. Immunofluorescence staining was carried out as described previously (Santi & Lee 2011). Cells were then either sham-treated or treated with CTR-17 or CTR-20 for scheduled durations. Subsequently, the cells were fixed with 100% methanol for 15 min at -20°C and washed with 1X PBS thrice. The cells were then blocked with PBST (1X PBS and 0.1% v/v Triton X-100) supplemented with 1% v/v FBS for about 1 h and incubated overnight at 4°C in a PBST solution containing primary antibody. In the case of double staining, a mixture of antibodies was added in equal ratio with gentle agitation. Unbound antibodies were washed off with PBST (3X) and secondary antibody solution was added and incubated for 1 h, in protection from light. The secondary antibody solution contained Alexa488 and Alexa568 conjugated antibodies (Life Technologies). Draq 5 or Dapi was used to stain nuclei. Subsequently, the coverslips were washed thrice using PBST for 10 min each and mounted onto slides with 90% glycerol in 1X PBS. Each slide was visualized with a Carl Zeiss 510 Meta laser scanning microscope or axioscope, and analysis was done with LSM image examiner (Carl Zeiss, North York, ON,

Canada). For each staining experiment, a background control (without secondary antibody) and bleed-through controls (cells labeled with each fluorophore separately) were used to avoid any potential bleed-through artifacts. A minimum of 10 fields per coverslip or 200 cells were captured for every sample and each experiment was repeated at least twice.

2.6 EdU labeling

To examine the effect of CTR-17 on DNA synthesis, EdU labeling was performed as described previously (Salic & Mitchison 2008). The DTP analogue EdU (5-ethynyl-2′-deoxyuridine) was added, and its incorporation into DNA was detected using a Cu (I)-catalyzed cycloaddition reaction with a fluorescent azide. Cells that were allowed to adhere overnight on coverslips in 35 mm tissue culture plates were either sham-treated or treated with CTR-17 for 24 h. During the final 1 h, 10.0 µM EdU (Life Technologies) was added to cell culture in dark at 37°C with 5% CO_2. EdU-labeled cells were then fixed with 4% formaldehyde for 15 min at room temperature and were rinsed with TBS (40 mM Tris pH 8.05, 150 mM NaCl) three times, 10 min each. The cells were then stained in a freshly-made staining solution containing 100 mM Tris, pH 8.5, 1 mM $CuSO_4$, 1 µg/ml Alexa546-azide (Active Motif through Cedarlane) and 100 mM ascorbic acid (added last to the staining mixture) for 30 min in dark at 22°C with gentle shaking. The cells were subsequently washed several times (or sometimes overnight) with TBS and counterstained with Draq 5. Coverslips were then mounted and visualized as described previously. The results were generated from three biological replicates.

2.7 Live cell imaging

About 10,000 Hek293T cells were plated in each 35 mm tissue culture plate and allowed to adhere overnight. The cells were then transfected for 16 h with 3.0 µl of CellLight Tubulin-GFP (C10613, Life Technologies) to label the microtubules, according to the manufacturer's instructions. It is a fusion construct of human tubulin and emGFP in a baculovirus vector. Each CellLight® reagent has 1×10^8 particles/ml, and for efficient transfection, it was ensured that each cell received an average of 30 of these particles. The medium was then replaced with a FluoroBrite™ DMEM (Life Technologies) with or without CTR-17, and immediately visualised by live cell microscopy (IX73 inverted microscope-Olympus, Toronto, ON, Canada). Time-lapse fluorescence images were obtained for 24 h at 5 min intervals. The live cell imaging was performed at least in two biological replicates for individual samples.

2.8 Western blotting

Western blot analysis was performed as described previously (Santi & Lee 2010). Exponentially growing cells were treated with CTR-17 or CTR-20 and collected at scheduled time points using a cell scraper. Cells were centrifuged at 1,100 rpm (AllegraTM X-12 centrifuge) and then washed once with 1X PBS and lysed on ice for 10 min using lysis buffer (20 mM Tris-HCl, pH 7.5, 150 mM NaCl, 1 mM EDTA and 1% (v/v) Triton X-100, supplemented with 1 mM phenylmethylsulfonyl fluoride (PMSF), 5 mM protease inhibitor and 5 mM dithiothreitol just before use). The lysates were cleared by centrifugation at 10,000 rpm for 10 min at 4ºC (Microfuge 22R centrifuge, Beckman Coulter) and

the protein concentration in the supernatant was determined using a BCA (Bicinchoninic acid) assay (Pierce, Thermo Fisher Scientific). The protein extracts were then diluted with 5X SDS-PAGE loading buffer (312.5 mM Tris-HCl, pH 6.8, 10% v/v glycerol, 11.5% v/v sodium dodecyl sulphate (SDS), 0.05% w/v bromophenol blue, 5% β-mercaptoethanol) and equal amounts of proteins (25-40 µg/ml) were loaded onto 6-15% polyacrylamide gels. Proteins were separated by electrophoresis using Tris-glycine running buffer (25 mM Tris, 192 mM glycine, 0.1% w/v SDS) at 90-120V for 2 h. On the completion of electrophoresis, the proteins were transferred to nitrocellulose or polyvinylidene fluoride (PVDF) membranes (Amersham Biosciences through Cedarlane) using a semi-dry transfer system (Bio-Rad, Mississauga, ON, Canada) and protein transfer buffer (50 mM Tris, 40 mM glycine, 0.04% w/v SDS, 20% v/v methanol) at 25 V for 1 h. The membranes were then blocked for 45 min in a blocking solution containing TBS and 5% w/v skim milk powder (Carnation®). The membranes were then incubated overnight at 4°C with different antibodies diluted in TBS with 5% w/v skim milk powder or TBS with 5% w/v bovine serum albumin (BSA), when detecting phosphorylated proteins. The membrane was then washed three times with TBST (TBS with 0.05% Tween-20) and incubated for 1 h in a solution containing horseradish peroxidase (HRP)-conjugated secondary antibody in TBST and 5% w/v skim milk powder. The membranes were washed again three times in TBST and the immunoreactivity was visualized using X-ray film exposure and enhanced chemiluminescence (ECL) western blot reagents (Amersham Biosciences).

2.9 Immunoprecipitation

Immunoprecipitation was performed as described previously (Kim & Lee 2008). Synchronised cells following double thymidine treatment were either sham treated or treated with the indicated drugs for scheduled durations. Cell lysates were prepared in 1X IP buffer (20 mM Tris-HCl, pH 7.5, 150 mM NaCl, 1 mM EDTA and 1% (v/v) Triton X-100, supplemented with 10 mM sodium fluoride, 1 mM sodium orthovanadate and 5 mM cocktail of protease inhibitors), and then pre-cleared for 3 h using 50 µl of protein A/G agarose beads, sc-2003 (Santa Cruz Biotechnology, Dallas, TX) at 4°C with gentle agitation. Subsequently, immunoprecipitation was performed with 5.0 µg of a rabbit polyclonal anti-BuBR1 antibody (Table A1, page 147), or 5.0 µg of a rabbit polyclonal normal IgG (Table A1) as negative control. 50 µl of protein A/G beads were added for an additional 5 h at 4°C (gentle agitation) and centrifuged at 2,500 rpm for 5 min at 4ºC (Microfuge 22R centrifuge) to recover these immunocomplexes. They were then subsequently washed five times in IP lysis buffer and boiled for 5 min prior to SDS-PAGE and Western blotting. Cdc20 was detected using a rabbit polyclonal anti-cdc20 antibody (Table A1). Data were generated from at least two biological replicates.

2.10 Microtubule assays

2.10.1 Microtubule polymerization assay

The effects of CTR compounds on the ability to assemble purified tubulin were determined using a tubulin polymerization kit (BK004P, Cytoskeleton Inc. through Cedarlane) according to the manufacturer's instructions. Each reaction mixture

contained 4.0 mg/ml of porcine tubulin in G-PEM buffer (1.0 mM guanosine triphosphate (GTP), 80 mM piperazine-*N,N′*-bis[2-ethanesulfonic acid] sequisodium salt (PIPES), pH 6.9, 0.5 mM ethylene glycol-bis(2-aminoethylether)-*N,N,N′,N′*-tetraacetic acid (EGTA) and 2.0 mM $MgCl_2$), supplemented with 10 % glycerol. 10.0 µM of paclitaxel which is an MT stabilizer (provided in the same assay kit), 5.0 µM of nocodazole, an MT destabilizer (sc-3518; Santa Cruz Biotechnology) and G-PEM buffer without drugs were used as controls for the assay. The assay kit is based on the principle that the light scattered by the microtubules is directly proportional to the polymer mass of the microtubules when measured at 37°C at 340 nm. Absorbance was measured using an automated plate reader (Synergy H4 Hybrid Multi-Mode Microplate Reader) for 1 h at 1 min interval. The experiment was performed in three biological replicates.

2.10.2 Differential tubulin extraction

A two-step extraction procedure, as described was used to differentially extract tubulin heterodimers and microtubules from sham or treated cells (Tokési et al. 2010). Exponentially growing cells were treated with 50 nM of paclitaxel, 50 ng/ml nocodazole, 3.0 µM of CTR-17 or 1.0 µM of CTR-20 for 12 h. The cells were then harvested and lysed with a pre-warmed microtubule stabilizing buffer (80 mM PIPES, pH 6.8, 1mM $MgCl_2$, 1 mM EGTA, 0.5% Triton X-100, 10% glycerol, and 5.0 mM protease inhibitor cocktail). The lysate was then centrifuged at 2,500 rpm for 5 min at room temperature (Sorvall™ Legend™ Micro 17 centrifuge, Thermo Scientific). The supernatant containing the soluble tubulin

heterodimers was transferred to fresh tubes. To ensure that the soluble tubulin was completely extracted, the cell pellet was washed once again with the microtubule stabilizing buffer and the supernatants were pooled to form the soluble tubulin fraction. The polymerized tubulin fraction was then extracted from the cell pellet in microtubule destabilizing buffer (20 mM Tris, pH 7.4, 150 mM NaCl, 1% Triton X-100, 10 mM $CaCl_2$, and 5.0 mM protease inhibitor cocktail). The extract was cleared by centrifugation at 2,500 rpm for 5 min at room temperature (Sorvall™ Legend™ Micro 17 centrifuge) to obtain the insoluble microtubule fraction. An equal volume of both the soluble and polymerized fractions and 40 µg of protein for sham-treated and treated samples as determined by a BCA assay were resolved by SDS-PAGE. The resultant Western blot was analysed by densitometry using AlphaEaseFC 4.0 software (Alpha Innotech Corp. San Leandro, CA). The experiment was performed in three biological replicates.

2.10.3 Determination of the dissociation constant using tryptophan fluorescence of tubulin

Intrinsic tryptophan fluorescence was used to determine the binding constants of CTR-17 and CTR-20 as reported previously (Rai et al. 2012). Purified porcine tubulin (T240) was purchased from Cytoskeleton Inc. 0.4 µM of tubulin was dissolved in 25 mM PIPES buffer, pH 6.8, and incubated in the absence or presence of different concentrations of compounds for 30 min at 37°C. The intrinsic fluorescence of tryptophan residues in the tubulin heterodimers was monitored by excitation at 295 nm and the emission spectra were recorded from

315-370 nm. All measurements were corrected for the inner filter using the formula $F_{corrected} = F_{observed}$ X antilog $[(A_{ex}+A_{em})/2]$, where A_{ex} and A_{em} are the absorbance of the reaction mixture at the excitation and emission wavelengths, respectively. GraphPad Prism software was used to determine the dissociation constants of CTR-17 and CTR-20 binding to tubulin using the following formula:

$$\Delta F = \frac{\Delta Fmax \times C}{Kd + C}$$

Where, ΔF is the change in fluorescence intensity of tubulin when bound to CTR compounds, ΔF_{max} is the maximum change in the fluorescence intensity when tubulin is bound with the drugs, C is the concentration of CTR-17/CTR-20, and K_d is the dissociation constant of CTR-17 or CTR-20. The experiment was performed in five biological replicates.

2.10.4 Competitive binding assay

Competition binding assays were performed as shown previously (Rai et al. 2012). For BODIPY® FL Vinblastine competition assay, 25.0 µM of CTR-17, CTR-20, colchicine, C9754 (Sigma), vinblastine, ab141475 (Abcam) was incubated with 0.4 µM purified tubulin for 1 h at 37°C. Subsequently, BODIPY® FL Vinblastine, V12390 (Life Technologies) was added to the tubulin complexes to a final concentration of 5.0 µM, and incubated further for 30 min at the same temperature. For the colchicine competition assay, tubulin (0.4 µM) was incubated with different concentrations of CTR-17, CTR-20 or vinblastine for 1 h at 37°C. Subsequently, colchicine was added to the CTR-17/CTR-20-tubulin or vinblastine-tubulin complexes. To determine the inhibition constant (Ki),

colchicine was added to a final concentration of 3.0 μM, 5.0 μM or 8.0 μM to different concentrations of CTR-17-tubulin complexes, and 1.0 μM, 3.0 μM, 5.0 μM and 8.0 μM to different concentrations of CTR-20-tubulin complexes. Fluorescence was monitored using an automated plate reader (Synergy H4 Hybrid Multi-Mode Micro plate Reader). For the vinblastine competition assay, fluorescence was monitored by excitation at 490 nm and the emission spectra were recorded at 510-550 nm. For the colchicine competition assay, the fluorescence of the tubulin complexes was determined with an excitation wavelength of 360 nm and emission wavelength at 430 nm. A modified Dixon plot was used to analyze the competitive inhibition of colchicine binding to tubulin and to determine the Ki of CTR-17 and CTR-20. The experiment was performed in four biological replicates.

2.11 Molecular docking

Molecular Operating Environment (MOE) (Chemical Computing Group Inc, Montreal, Quebec, Canada) was used to predict the interaction model of CTR-17 and CTR-20 binding to the colchicine binding domain of the β-tubulin subunit. The crystal structure of the tubulin-colchicine complex (PDB Code: 1SA0) was used as the target structure and was subjected to energy minimization and protonation via the same software. The protocol for docking was adopted from that posted to the MOE website and an induced-fit protocol was used (http://www.chemcomp.com/ MOE-Structure_Based_Design.htm). CTR-17 and CTR-20 were docked close to the colchicine-binding site and the best docking pose was determined based on the minimum free energy for binding. The

contributions of hydrogen bonds, hydrophobic, ionic and Van der Waals interactions were taken into consideration when calculating the free energy of binding.

2.12 Scratch-wound healing assay

A scratch-wound healing assay (Liang et al. 2007) was used to measure the migration of cells *in vitro* in the presence or absence of CTR-17 in a time-dependent manner. Human MDA-MB231 cells were plated to 90% confluency to obtain a monolayer on a 35 mm tissue culture dish. After the cells were allowed to adhere overnight, a scratch was made in a straight line using a p200 pipette tip and the cells were then washed once with 1XPBS. To completely remove any debris, the monolayer was washed two more times with regular media. The cells were then either sham-treated or treated with CTR-17 and immediately subjected to time-lapse imaging for 72 h with an IX73 inverted microscope. The percentage of wound closure was then quantified using ImageJ software, which is an open access software, developed by the National Institute of Health (rsb.info.nih.gov/ij). The experiment was conducted in three biological replicates.

2.13 Estimation of doubling time in cancer *vs* non-cancer cells

The doubling time of the cancer *vs* non-cancer cells was used to determine if the cancer cell specificity of the CTR compounds was due to the difference in the doubling time of cancer *vs* non-cancer cells. Two different approaches were used to estimate the doubling time of HeLa, MDA-MB231, MDA-MB468, Hek293T, 184B5 and MCF10A.

Approximately, 15,000 cells/ml were plated in a 35 mm dish (trypan blue exclusion assay) or a 24-well culture plate (SRB assay). For a trypan blue exclusion assay (Strober 2001), the cells were trypsinised and the cell pellets were collected by centrifugation at 1,100 rpm (AllegraTM X-12 centrifuge) for 5 min. Cell pellets were then re-suspended in 1.0 ml of culture medium. An aliquot was mixed in an equal volume of 0.4% Trypan blue solution (Sigma). For SRB assay, the cells were fixed and stained as outlined in section 2.2. Both the assays were conducted for eight consecutive days and the growth curves were constructed using Microsoft excel. The log phase of the curve was used to determine the doubling time of each cell line. Doubling times were determined using trypan blue exclusion assay, conducted once and SRB assay which was performed in two independent replicates.

2.14 CTR cell permeability test

The intracellular concentration of the CTR compounds in cancer *vs* non-cancer cells was determined by high performance liquid chromatography (HPLC) method as previously described with minor modifications (Ren & Wei 2004; Jorfi et al. 2015). Cells were either sham-treated or treated with 3.0 µM of CTR-17 for scheduled time points. The medium was removed and the cells were washed twice with 1X PBS. The cells were then harvested using a cell scraper and cell pellets were collected by centrifugation at 1,100 rpm (AllegraTM X-12 centrifuge) for 5 min. The pellets were then re-suspended in 200 µl lysis buffer (20 mM Tris-HCl, pH 7.5, 150 mM NaCl, 1 mM EDTA and 1% (v/v) Triton X-100). The extract was sonicated for 2 min on ice using a sonic dismembrator, model 100 (Thermo

Fisher Scientific). 100 µl of acetonitrile (Thermo Fisher Scientific) was added to the extract, followed by centrifugation for 10 min at 17,000 x g (Sorvall™ Legend™ Micro 17 centrifuge) to remove proteins. The protein precipitation process was repeated again. The supernatant was collected in fresh tubes, filtered using Target2 Nylon Syringe Filters, F2504-2 prior to performing HPLC: pore sizes of the filters were 2.0 µm and the diameters were 4.0 mm (Thermo Fisher Scientific). The HPLC system consisted of a Shimadzu LC20AB pump (Laval, QC, Canada), equipped with an autosampler and a diode array detector. An injection volume of 5.0 µl of CTR-17 was introduced into a Restek LC column; Ultra C18 column (4.6 mm X 150 mm, 3.0 µm) and the absorbance of the samples were monitored at 350 nm. The system was run in an isocratic mode with a mobile phase containing methanol to water at a ratio of 70:30 (v/v). The flow rate used was 0.75 ml/min. The experiment was performed in two biological replicates.

2.15 Assessment of combination effects using CTR compounds and X-ray radiation

T98G brain cancer cells express high levels of the enzyme O6-methylguanine-DNA methyltransferase (MGMT) that confers resistance to temozolomide (TMZ) (Christmann et al. 2011). Therefore, CTR compounds were used in combination with X-rays to determine the combinatorial effects, in which T98G cells were exposed to X-ray radiation simultaneously with CTR compounds (Chou 2006; Pearce et al. 2001). When cells were scheduled for radiation, the 96-well plates were treated with increasing doses of radiation (2-10 Gy) using a RS320

Radiation System (Gulmay Medical Inc. Scarborough, Canada). The plates were placed on the fourth shelf within the X-ray machine, on top of the Perspex plate to reduce backscatter. Cells received a dose ranging from 2-10 Gy (300 kV, 9 mA) in 2-10 min respectively. The drug treatment was performed as outlined in section 2.2. The time point at which the cells were exposed to CTR-17 and CTR-20 was considered as 0 h. After 72 h, the cells were fixed and the cytotoxicity was assessed using an SRB assay (section 2.2). Combination effects of CTR compounds and X-ray radiation were determined using two biological replicates.

2.16 Statistical analyses

All values were expressed as mean ± SEM of at least three independent experiments, unless stated otherwise. Analyses were performed using GraphPad Prism software. To determine any significant difference between two populations, an unpaired t-test was performed and a p-value of <0.05 was considered to be statistically significant.

3.0 Results

3.1 CTR-17 and CTR-20 induce cell death in a cancer-specific manner and are equally potent against MDR cells

Four CTR compounds (Figure 7) were initially short-listed from a series of 75 chalcone-based derivatives by preliminary cytotoxicity screening performed at the Lee Lab. Subsequent screening of these CTR compounds using three breast cancer cell lines (MDA-MB231, MDA-MB468 and MCF-7) and two matching non-cancer breast cell lines (184B5 and MCF10A) identified CTR-17 and CTR-20 as the most cancer-selective and efficient lead compounds (Table 1). To determine the effect of CTR-17 and CTR-20 on the proliferation of different cancer cells, nine other cancer cell lines (HeLa, K562, Hek293T, RPMI-8226, U87MG, T98G, NCI-H1975, A-549 and UC-3) were exposed to increasing concentrations of CTR-17 and CTR-20 (Table 2). IC_{50} values were calculated from sigmoidal dose-response curves (Figure 8) and the resultant data showed that CTR-17 and CTR-20 kill most of the cancer cells 10-25 times more effectively than non-cancer cell lines, which is a highly desirable property of anti-cancer agents. When comparing the cytotoxic activity of colchicine in cancer and non-cancer cell lines, CTR-17 and CTR-20 exhibit much better selectivity than colchicine, which is only about two to three fold more selective for cancer cells (Table 3). More attractively, CTR compounds inhibit the proliferation of multi-drug resistant cell lines with almost equal potency to the parental cells (Figure 9 & Table 4). The IC_{50} values indicate that both CTR-17 and CTR-20 kill the multidrug resistant (KB-C2, H69AR) and sensitive (KB-31, SW1271) cells with similar potency. Colchicine, paclitaxel, and vinblastine kill KB-C2 cell line more than 10 fold less than the parental KB-31 cells.

Figure 7: Chemical Structures of the CTR compounds
These quinolone chalcone hybrids were synthesized by our collaborators at the Rajiv Gandhi Technical University of India and subsequently sent to the Lee Lab for further analysis. Chemical names are provided below each compound structure.

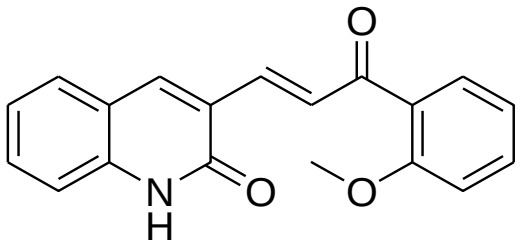

3-(3-(2-methoxyphenyl)-3-oxoprop-1-enyl) quinolin-2(1H)-one (CTR-17)

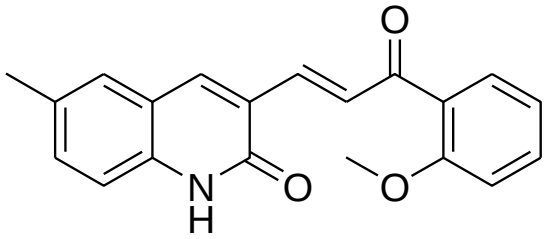

3-(3-(2-methoxyphenyl)-3-oxoprop-1-enyl)-6-methyl quinolin-2(1H)-one (CTR-18)

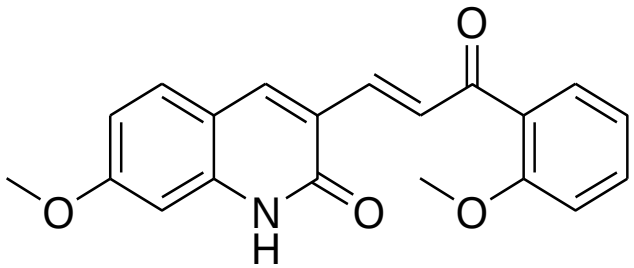

7-methoxy-3-(3-(2-methoxyphenyl)-3-oxoprop-1-enyl) quinolin-2(1H)-one (CTR-19)

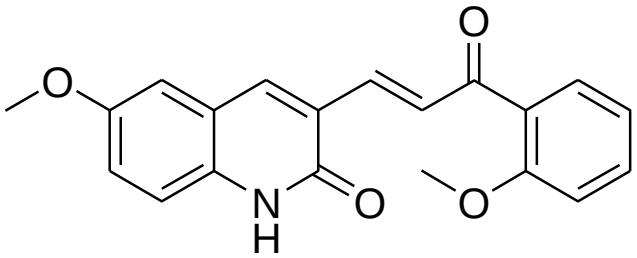

6-methoxy-3-(3-(2-methoxyphenyl)-3-oxoprop-1-enyl) quinolin-2(1H)-one (CTR-20)

Figure 8: Representative dose-response curves that were used to calculate the IC_{50} values

A: A representative sigmoidal dose-response curve of HeLa cells treated with different concentrations of CTR-17 for 72 h.

B: A representative sigmoidal dose-response curve of HeLa cells treated with different concentrations of CTR-20 for 72 h.

The curves represent the values obtained by at least three independent biological replicates, with quadruple technical replicates for each set using GraphPad Prism v.5.04 software.

A

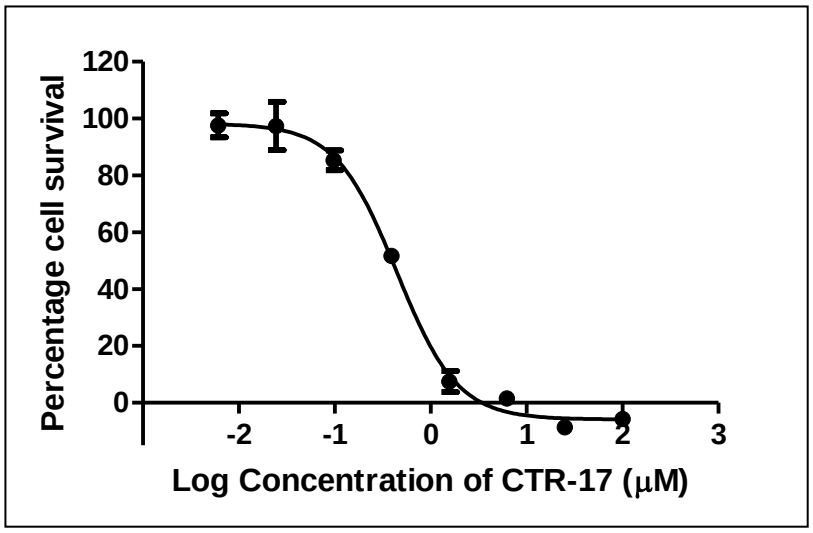
Percentage cell survival
120
100
80
60
40
20
0
-2
-1
0
1
2
3
Log Concentration of CTR-17 (μM)

B

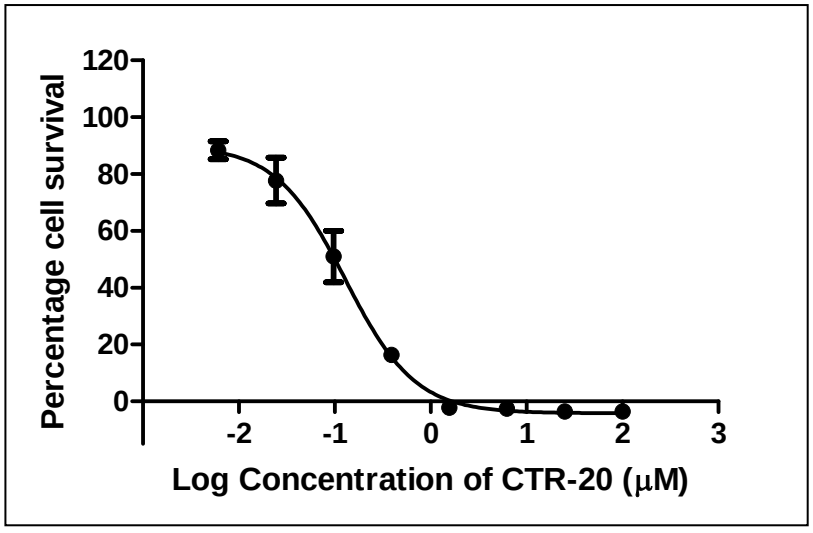
Percentage cell survival
120
100
80
60
40
20
0
-2
-1
0
1
2
3
Log Concentration of CTR-20 (μM)

Table 1: Initial screening of four CTR compounds using breast cancer cells (MDA-MB231, MDA-MB468, MCF7) and non-cancer breast cells (184B5, MCF10A) determined by SRB assays

CODE	IC_{50} (μM)[a,b]						
	MDA-MB231	MDA-MB468	MCF7	K562	HeLa	184B5[d]	MCF10A[d]
CTR-17[c]	0.41±0.02	0.15±0.33	0.52±0.17	0.15±0.10	0.33±0.06	3.49±0.03	3.95±0.14
CTR-18	0.93	0.08	0.12	0.21±0.02	ND	3.89	ND[e]
CTR-19	5.11	1.91	1.93	0.95±0.65	ND	3.94	ND
CTR-20[c]	0.12±0.09	0.12±0.02	0.14±0.06	0.13±0.02	0.10±0.02	1.24±0.06	2.37±0.21
Chloroquine	22.52	28.58	38.44	ND	ND	76.13	ND
Cisplatin	23.65	31.02	25.77	ND	ND	25.54	ND

[a] IC_{50} values were calculated from sigmoidal dose response curves (variable slope), which were generated with GraphPad Prism V. 4.02 (GraphPad Software Inc.).
[b] Values are the mean value of triplicates of at least two independent experiments.
[c] The IC_{50} values for CTR-17 and CTR-20 are represented as mean ± SEM (N=3).
[d] The 184B5 and MCF10A are non-cancer, immortalized breast epithelial cell lines, and the rest are different cancer cell lines.
[e] ND, not determined.

Table 2: Antiproliferation effects of CTR-17 and CTR-20 on other cancer cells

	IC_{50} (μM)[a]						
	U87MG (brain)	T98G (brain)	NCI-H1975 (lung)	A549 (lung)	RPMI-8226 (myeloma)	UC3 (Urinary Bladder)	Hek293T (kidney)
CTR-17	0.76 ±0.10[b]	0.82 ±0.09	0.60 ±0.14	0.41 ±0.06	0.36 ±0.04	0.39 ±0.03	0.42 ±0.07
CTR-20	0.49 ±0.13	0.22 ±0.10	0.39 ±0.14	0.13 ±0.04	0.23 ±0.00	0.12 ±0.03	0.19 ±0.00

[a] The IC_{50} values for CTR-17 and CTR-20 are represented as mean ± SEM (N=3)
[b] Numbers are IC_{50} values in μM, determined by SRB assays as described in Table 1.

Table 3: Comparison of the anti-proliferative activity of colchicine in cancer and non-cancer cells

	IC_{50} (nM)[a]					
	MDA-MB231	MDA-MB468	MCF7	HeLa	184B5	MCF10A
Colchicine	5.70±0.49[a]	2.89±0.15	8.73±0.67	4.56±0.56	16.03±1.21	11.86±0.69

[a] The IC_{50} values for colchicine are represented as mean ± SEM (N=3)
[b] Numbers are IC_{50} values in nM, determined by SRB assays as described in Table 1.

Figure 9: CTR compounds are cytotoxic towards cell lines overexpressing both MDR and MRP

Western blotting of WCEs of drug-resistant cell lines and their parental wild type cells shows the overexpression of MDR1 and MRP1 for KB-C2 and H69AR cells, respectively. H69 cells grow as large multi-cell aggregates; hence, accurate cell counts were difficult. Therefore, cytotoxicity results obtained from H69AR cells was compared to SW1271 cells which are another small cell lung carcinoma cell line

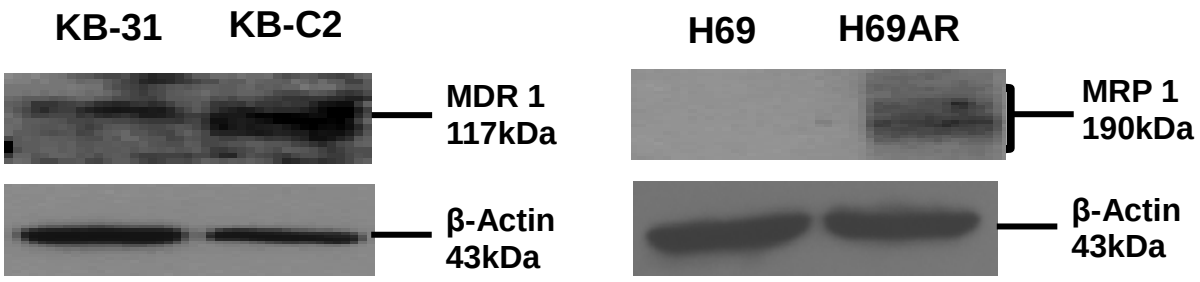
KB-31
KB-C2
MDR 1
117kDa
β-Actin
43kDa
H69
H69AR
MRP 1
190kDa
β-Actin
43kDa

Table 4: Anti-proliferation effects of CTR compounds and other MTAs in multidrug resistant cell lines

	IC_{50}[a]					
	KB-31[b]	**KB-C2**	**Resistance in fold**	**SW-1271**	**H69AR**[b]	**Resistance in fold**
Colchicine (nM)	**5.36±0.54**	**83.45±7.22**	**15.57**	**4.84±0.80**	**22.97±3.63**	**4.74**
Paclitaxel (nM)	**2.01±0.17**	**23.08±0.21**	**11.48**	**4.51±0.71**	**10.99±2.60**	**2.44**
Vinblastine (nM)	**0.61±0.09**	**9.27±3.22**	**15.20**	**1.75±0.21**	**10.20±1.97**	**5.82**
CTR-17 (µM)	**0.38±0.07**	**0.65±0.16**	**1.71**	**1.14±0.04**	**0.52±0.10**	**0.45**
CTR-20 (µM)	**0.10±0.02**	**0.25±0.03**	**2.50**	**0.95±0.01**	**0.13±0.01**	**0.13**

[a] The IC_{50} values are represented as mean ± SEM (N=3)
[b] The KB-C2 and H69AR are multidrug resistant cell lines that overexpress MDR1 and MRP1 respectively.

Figure 10: Synergistic effects of CTR compounds and paclitaxel on cell proliferation inhibition in KB-C2 cells

KB-C2 cells were plated in 96-well plates and treated with CTR-17, CTR-20, or paclitaxel alone, or with combinations of six different ratios of CTR-17 (or CTR-20) to paclitaxel. The SRB assay was used to construct a sigmoidal dose-response curve, from which the median effect dose (Dm), fraction affected (Fa) and slope of the curve (m) were determined. These values were then used to determine the combinational effect between CTR-17 or CTR-20 with paclitaxel, as outlined in methodology, section 2.2. Cell growth rates are represented as the mean ± SEM (N=4).

A: The combination of CTR-17 and paclitaxel enhanced the cytotoxic abilities against the multidrug resistant KB-C2 cell line with CI values ranging from 0.71-0.87.

B: The combination of CTR-20 and paclitaxel enhanced the cytotoxic abilities against KB-C2 cell lines with CI values ranging from 0.69-0.95.

A

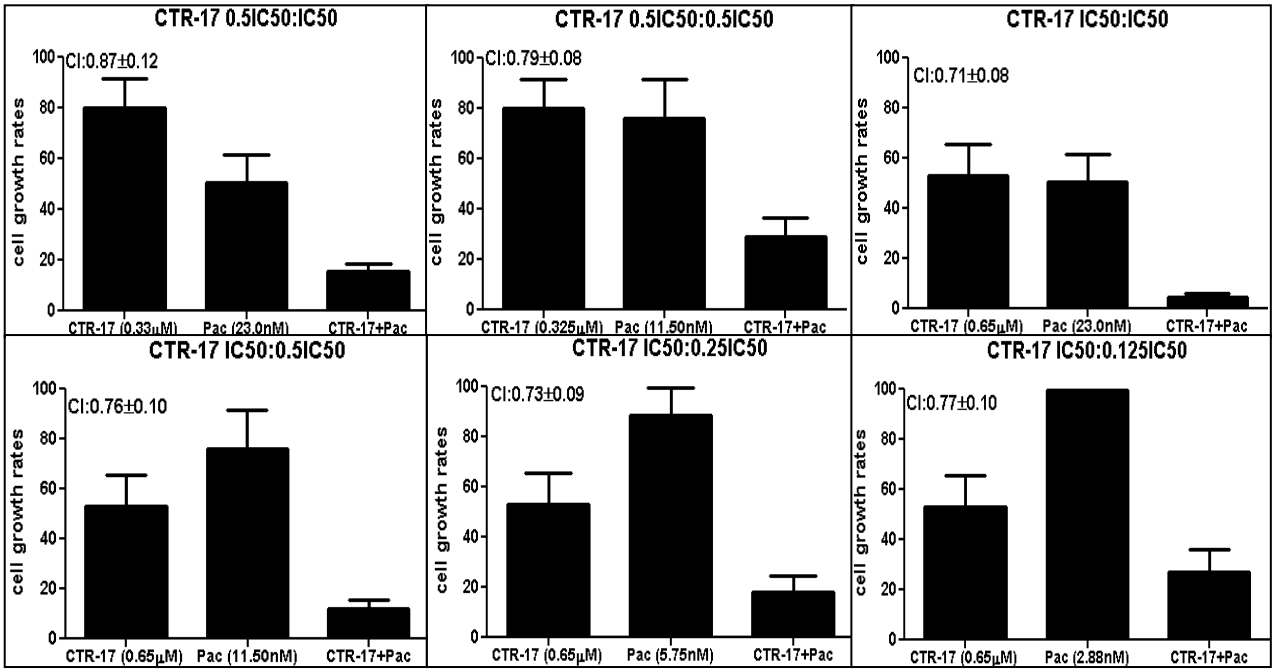
CTR-17 0.5IC50:IC50
CI:0.87±0.12
CTR-17 (0.33μM)
Pac (23.0nM)
CTR-17+Pac
CTR-17 0.5IC50:0.5IC50
CI:0.79±0.08
CTR-17 (0.325μM)
Pac (11.50nM)
CTR-17+Pac
CTR-17 IC50:IC50
CI:0.71±0.08
CTR-17 (0.65μM)
Pac (23.0nM)
CTR-17+Pac
CTR-17 IC50:0.5IC50
CI:0.76±0.10
CTR-17 (0.65μM)
Pac (11.50nM)
CTR-17+Pac
CTR-17 IC50:0.25IC50
CI:0.73±0.09
CTR-17 (0.65μM)
Pac (5.75nM)
CTR-17+Pac
CTR-17 IC50:0.125IC50
CI:0.77±0.10
CTR-17 (0.65μM)
Pac (2.88nM)
CTR-17+Pac
cell growth rates

B

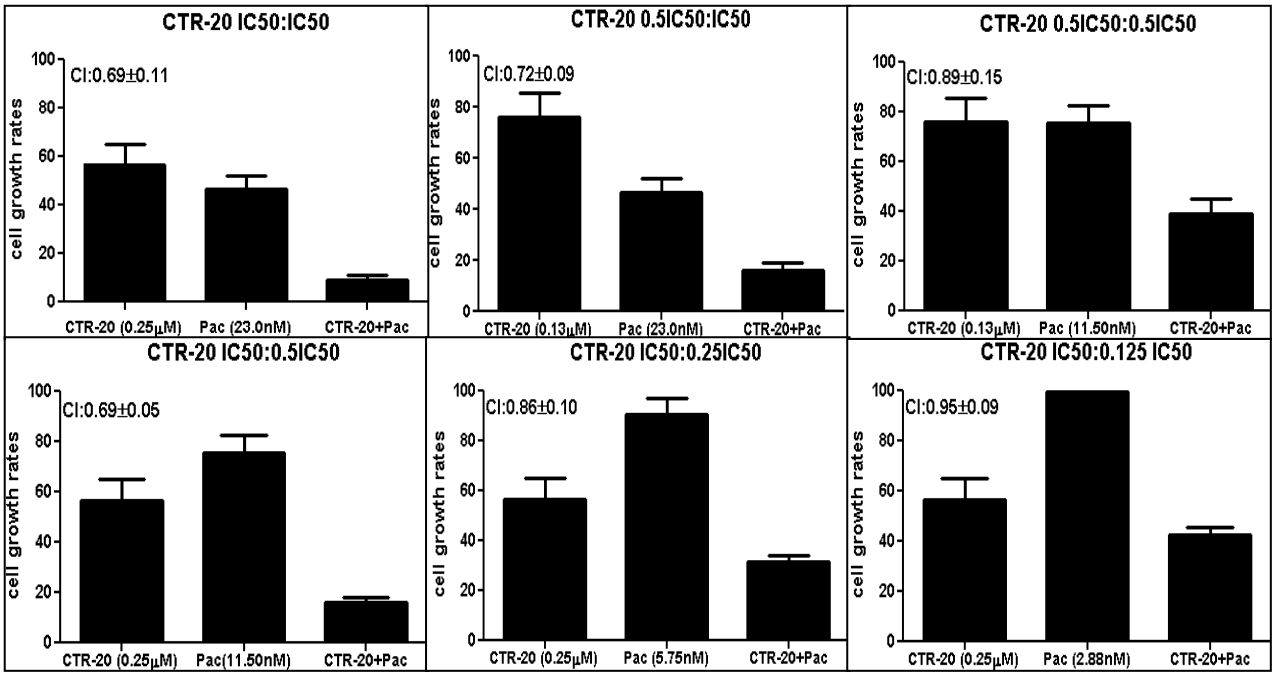
CTR-20 IC50:IC50
CI:0.69±0.11
CTR-20 (0.25μM)
Pac (23.0nM)
CTR-20+Pac
CTR-20 0.5IC50:IC50
CI:0.72±0.09
CTR-20 (0.13μM)
Pac (23.0nM)
CTR-20+Pac
CTR-20 0.5IC50:0.5IC50
CI:0.89±0.15
CTR-20 (0.13μM)
Pac (11.50nM)
CTR-20+Pac
CTR-20 IC50:0.5IC50
CI:0.69±0.05
CTR-20 (0.25μM)
Pac(11.50nM)
CTR-20+Pac
CTR-20 IC50:0.25IC50
CI:0.86±0.10
CTR-20 (0.25μM)
Pac (5.75nM)
CTR-20+Pac
CTR-20 IC50:0.125 IC50
CI:0.95±0.09
CTR-20 (0.25μM)
Pac (2.88nM)
CTR-20+Pac
cell growth rates

H69AR cells are usually more resistant to colchicine and vinblastine (about 5 fold) than paclitaxel as paclitaxel is known to be a poor substrate for MRP (Glynn et al. 2004). Moreover, in combination with paclitaxel, both CTR-17 and CTR-20 exhibited a synergistic mode of cell killing in Pgp overexpressing KB-C2 cells (Figure 10). The CI values for six different ratios of CTR compounds to paclitaxel were between 0.71-0.87 for CTR-17 with paclitaxel, and 0.69-0.95 for CTR-20 with paclitaxel. According to previously published reports, all these combinations provide synergistic effects as the CI values are below 1 (Chou, 2006).

In addition, Western blotting data of WCEs prepared from asynchronous HeLa cells showed that treatment with 3.0 μM CTR-17 caused cell death, as demonstrated by the increase in cleaved PARP in cancer cells but not in 184B5 cells (Figure 11).

3.2 CTR-17 induces a prolonged mitotic arrest that triggers cell death

Flow cytometric analysis of propidium iodide stained cells showed that CTR-17 treated cells undergo a prominent G2/M arrest within 12 h of the treatment, as demonstrated by the increase in the 4N DNA content (Figure 12). However, 184B5 and MCF10A non-cancer cells returned to near-normal flow cytometry profile by 48 h post-treatment, although a substantial portion of 184B5 contained sub-G1 DNA content.

Figure 11: CTR-17 caused cell death only in cancer cells
Western blotting of WCEs prepared from asynchronous HeLa cells showed that treatment with 3.0 μM CTR-17 for 12-48 h causes cell death in cancer cells but not in 184B5 cells.

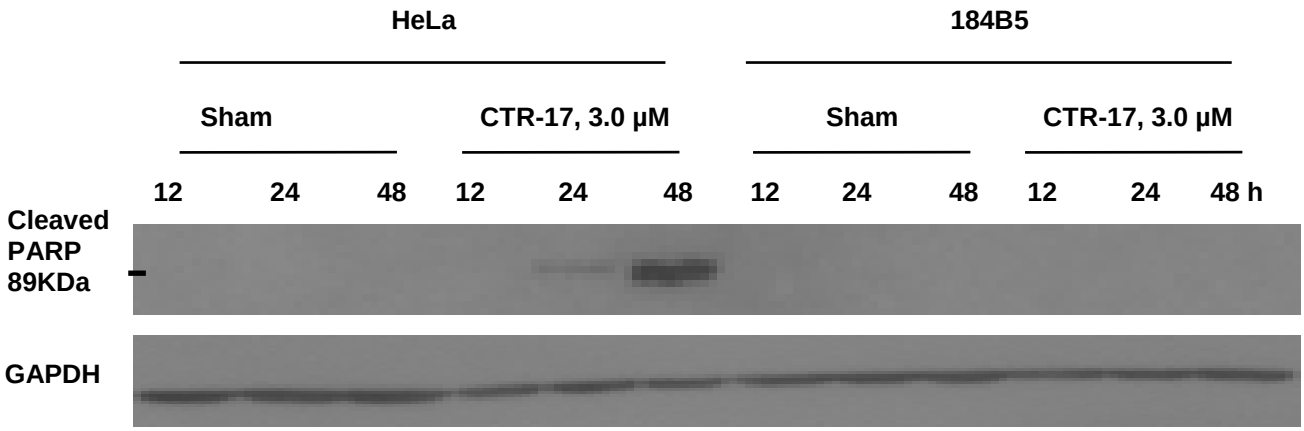
HeLa
184B5
Sham
CTR-17, 3.0 μM
Sham
CTR-17, 3.0 μM
12
24
48
12
24
48
12
24
48
12
24
48 h
Cleaved PARP 89KDa
GAPDH

Figure 12: The majority of cancer cells arrested in G2/M by 12 h in the presence of 3.0 µM CTR-17

A: 72 h post-treatment of HeLa cells with different concentrations (µM) of CTR-17.

B: Treated with 3.0 µM of CTR-17 and cell cycle progression was observed at different time points for 6-72 h. HeLa cells were collected, fixed and then stained with propidium iodide solution, and cell cycle positions were determined using flow cytometry.

C: CTR-17 selectively increased cell cycle arrest and cell death in cancer cells. Breast cancer cells (MDA-MB468 and MDA-MB231), Human embryonic kidney 293 cells that constitutively express the SV40 large T antigen (Hek293T) and non-cancer breast cells (184B5 and MCF10A) were treated with 3.0 µM CTR-17, stained with PI solution and analyzed by flow cytometry. MDA-MB468 cells undergo a prominent cell cycle arrest at G2/M phase and subsequently cell death as early as 48 h post-treatment. MDA-MB231 and Hek293T cells demonstrate prominent cell cycle arrests which accumulate with increases in exposure time to CTR-17. However, non-cancer breast cell line, MCF10A and 184B5 undergoes a less prominent cell cycle arrest, which seems to deteriorate with increase in exposure time, either with entrance to the cell cycle or minimal cell death. The data represents at least three independent experiments

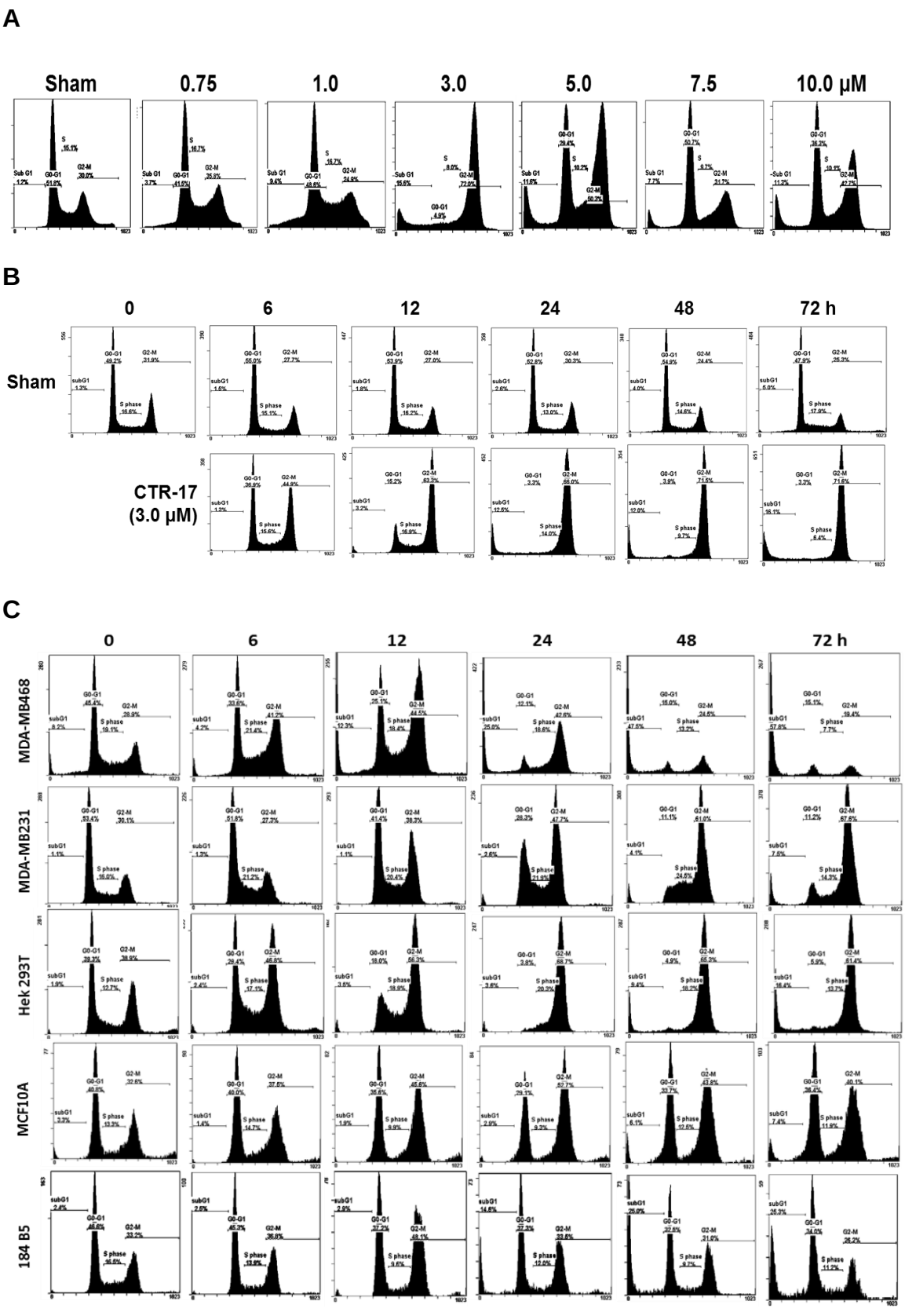
A
Sham
0.75
1.0
3.0
5.0
7.5
10.0 μM
B
0
6
12
24
48
72 h
Sham
CTR-17
(3.0 μM)
C
MDA-MB468
MDA-MB231
Hek 293T
MCF10A
184 B5

CTR-17 did not cause an impediment to DNA replication as the percentage of Edu labeled cells was not significantly different ($p > 0.05$) between sham (29.11%) and CTR-17 (27.39%) treated cells (Figure 12). CTR-17 did not cause double-stranded DNA damage as γH2AX foci was not observed in sham or CTR-17 treated cells in comparison to etoposide, even after 48 h of treatment (Figure 13).

Western blotting of WCEs prepared from asynchronous HeLa, Hek293T, MDA-MB468 and MDA-MB231 cells provides further evidence that cells are arrested in mitosis when treated with CTR-17 (Figure 14). During the mitotic entry of eukaryotic cells, cdk1 activation is governed by multiple layers of regulation. Cdk1 remains in the inactive state during G2 by the phosphorylation on the Tyr15 residue by wee1. As cells enter mitosis, cdk1 undergoes dephosphorylation on the Tyr15 residue by the cdc25C phosphatase and the level of wee1 reduces. On the other hand, cdk1 remain active by the phosphorylation on Thr161 caused by cdk activating complex (CAK). In CTR-17 treated cells, cdk1 has undergone dephosphorylation on Tyr15 and phosphorylation on Thr161 within 12 h indicating that cdk1 is still active. In addition, the increase in cyclin B suggests that cyclin B-cdk1 complex is still intact, indicating that cells are in mitosis. The increase in phosphorylation of cdc25C on Thr48 (activating phosphorylation) and decrease in phosphorylation on Ser 216 (inhibitory phosphorylation) suggests that cdc25C is active. This positive feedback loop results in an extended activation of the cyclin B-cdk1 complex that prevents mitotic exit.

Figure 13: CTR-17 has no significant effect on DNA replication and does not cause DNA damage

A: Detection of EdU incorporated into DNA of HeLa cells treated with CTR-17 showed that CTR-17 does not significantly affect DNA replication. Sham-treated or CTR-17 (3.0 µM) treated HeLa cells were incubated with culture medium containing 10.0 µM of EdU for one hour prior to 24 h. The cells were subsequently fixed and stained with a staining solution containing 1.0 µg/ml Alexa546-azide. After several washing steps, cells were then counterstained with Draq 5 and imaged by fluorescence microscopy. At least 10 different fields were analysed in three independent experiments to determine the percentage mean ± SEM of EdU labeled cells.

B: Data from γH2AX staining shows that 3.0 µM CTR-17, even after incubation as long as 48 h, did not cause DNA double-stranded breaks. 50.0 µM of DNA-damaging agent, etoposide, was used as a positive control to detect the γH2AX foci. At least 10 different fields were analysed in three independent experiments.

A

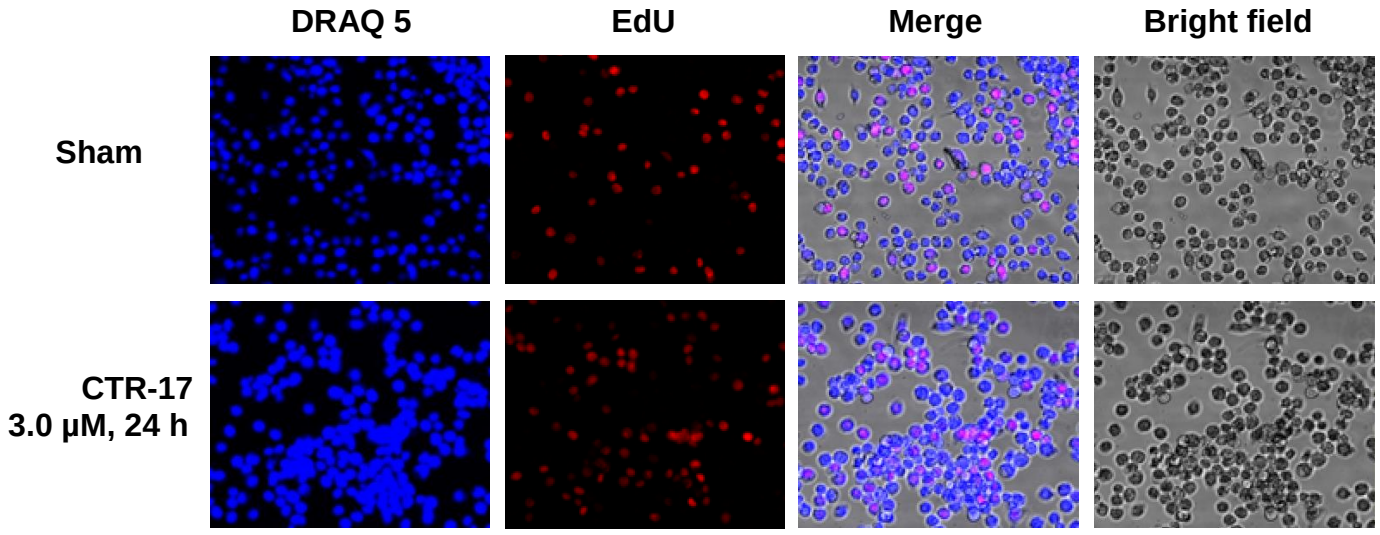

	Sham-treated	3.0 μM CTR-17
% of EdU labeled cells[a]	29±1*	27±4*

[a] Percentage of EdU labeled cells are expressed as mean ± SEM (N=3)
*p > 0.05 for sham-treated *vs* CTR-17 treated

B

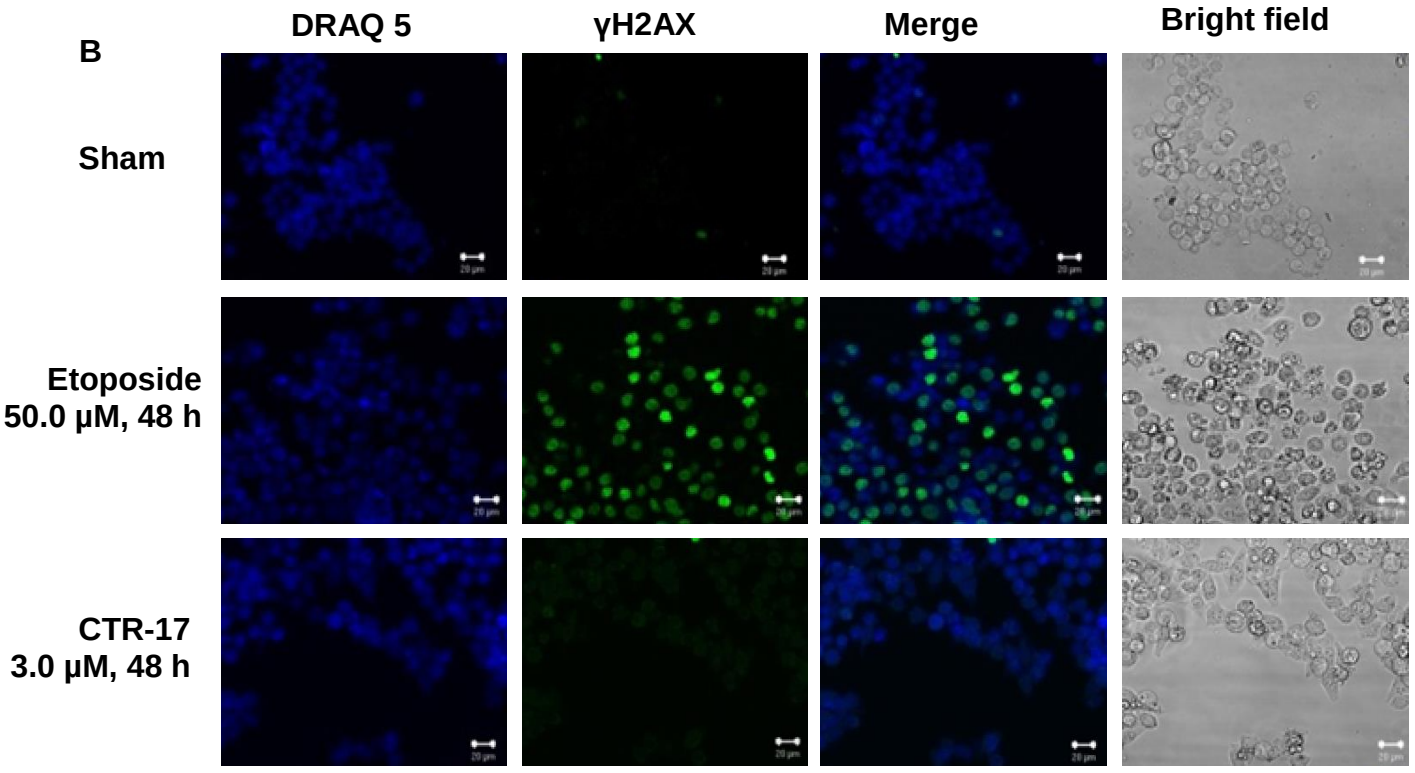

Figure 14: CTR-17 arrested cells in mitosis not in G2
Western blotting data of WCEs prepared from asynchronous **(A)** HeLa, **(B)** Hek293T, **(C)** MDA-MB468, and **(D)** MDA-MB231 showed that cells are arrested in mitosis when treated with 3.0 µM CTR-17 at different time points. Equal protein samples were resolved by SDS-PAGE and immunoblotted using the antibodies against the proteins listed. GAPDH was used as a loading control. "p-" denotes phosphorylation. Numbers above gels are post-treatment in hour (h)

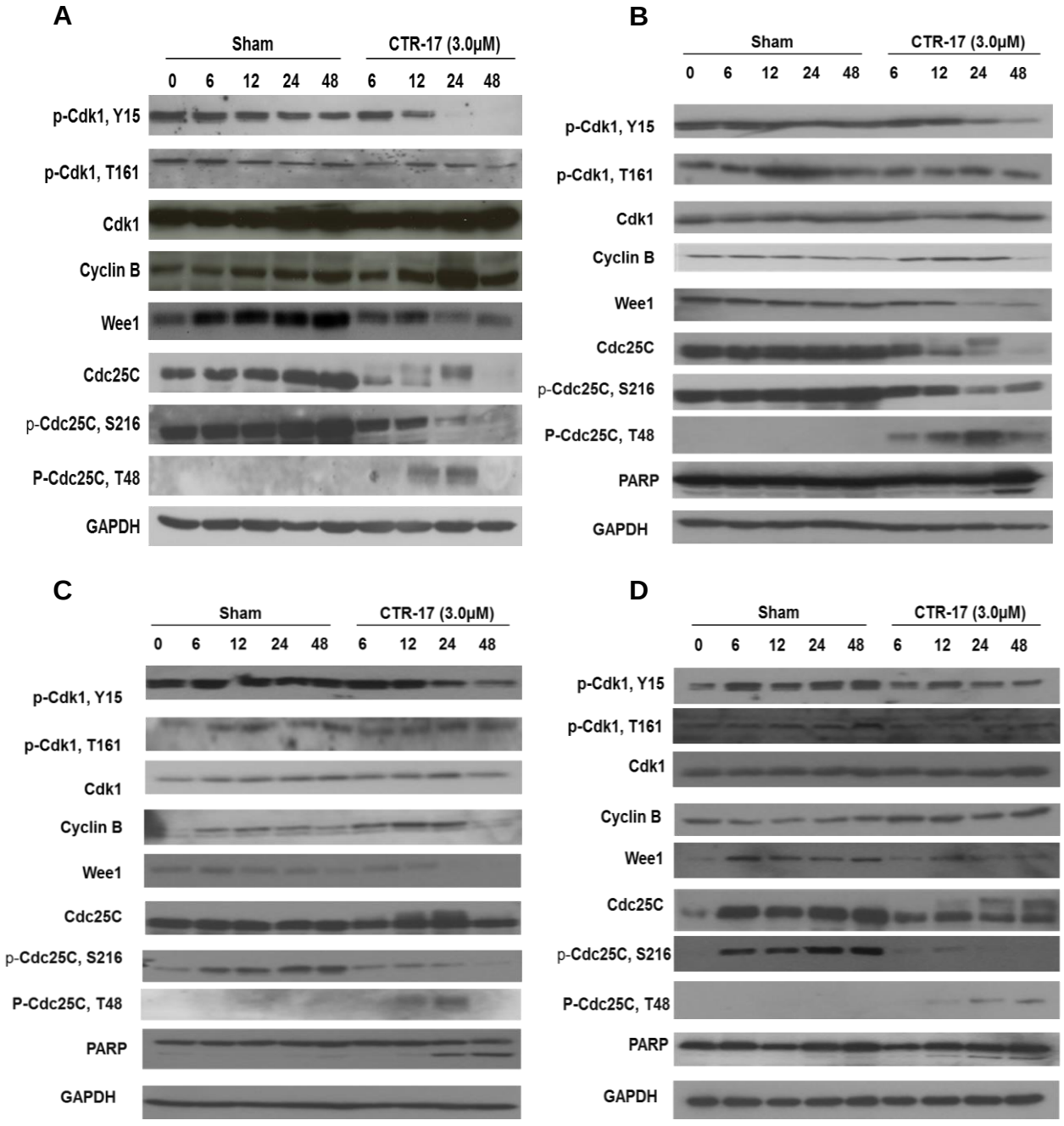
A
Sham
CTR-17 (3.0μM)
0 6 12 24 48 6 12 24 48
p-Cdk1, Y15
p-Cdk1, T161
Cdk1
Cyclin B
Wee1
Cdc25C
p-Cdc25C, S216
P-Cdc25C, T48
GAPDH
B
Sham
CTR-17 (3.0μM)
0 6 12 24 48 6 12 24 48
p-Cdk1, Y15
p-Cdk1, T161
Cdk1
Cyclin B
Wee1
Cdc25C
p-Cdc25C, S216
P-Cdc25C, T48
PARP
GAPDH
C
Sham
CTR-17 (3.0μM)
0 6 12 24 48 6 12 24 48
p-Cdk1, Y15
p-Cdk1, T161
Cdk1
Cyclin B
Wee1
Cdc25C
p-Cdc25C, S216
P-Cdc25C, T48
PARP
GAPDH
D
Sham
CTR-17 (3.0μM)
0 6 12 24 48 6 12 24 48
p-Cdk1, Y15
p-Cdk1, T161
Cdk1
Cyclin B
Wee1
Cdc25C
p-Cdc25C, S216
P-Cdc25C, T48
PARP
GAPDH

To determine if CTR-17 affected the mitotic entry of the cells and to determine the exact stage of cell cycle arrest by CTR-17, HeLa cells were synchronised at the G1/S border and then released in the presence or absence of CTR-17 (Figure 15). The similar patterns of cdk1 dephosphorylation on Tyr15 and phosphorylation on Thr161 in sham and CTR-17 treated cells suggest that cells enter mitosis without any impediment. Cyclin E has undergone complete degradation after 3 h in both sham and CTR-17 treated cells. However, unlike in sham-treated cells, cyclin E never reappears in CTR-17 treated cells at 12 h. This suggests that sham-treated cells have moved forward in the cell cycle, whereas CTR-17 treatment cause the cells to never move beyond mitosis. This conclusion is also strengthened by the continuous phosphorylation on serine 10 residue of histone H3 in CTR-17 treated cells. The lack of cyclin B and securin degradation at least up to 20 h post-DT indicates that cells never enter anaphase in the presence of CTR-17, raising the possibility that cells are arrested at SAC activation step.

Using immunofluorescence staining, changes in phenotype caused by CTR-17 was analysed more closely using HeLa, Hek293T, MDA-MB468 and MDA-MB231 cells. CTR-17 treatment caused an increase in the cell population with an abnormal mitotic morphology and prolonged mitotic arrest (Figures 16 and 17). The cells appeared to be rounded up with evidence of chromatin condensation.

Figure 15: CTR-17 prevents mitotic exit of HeLa cells released from synchronisation at the G1/S border

A: Data shows flow cytometric profiles of HeLa cells synchronised at the G1/S border by double thymidine (DT) block and subsequent release into drug-free medium or medium containing CTR-17 (3.0 µM) for the indicated times.

B: HeLa cells arrest at prometaphase-metaphase in the presence of CTR-17. Data shows Western blotting carried out with WCEs isolated from cells that had been arrested at G1/S by DT treatment and subsequently released into complete medium in the absence (sham) or presence of 3.0 µM CTR-17. Equal protein samples were resolved by SDS-PAGE and immunoblotted with antibodies against the proteins listed. GAPDH was used as the loading control. “p-“ denotes phosphorylation. Both flow cytometry profiles and Western blots show that mitotic progression is disturbed and mitotic exit is prevented. Data indicates: (1) By 6 h post-DT, most cells in the presence or absence of CTR-17 reach to G2/M; (2) by 12 h post-DT, all of the cells in the sham control enter G1 of new cell cycle, while those treated with CTR-17 are trapped M phase; (3) by 48 h post-DT, most of the cells treated with CTR-17 are either still in M phase or undergo cell death.

A

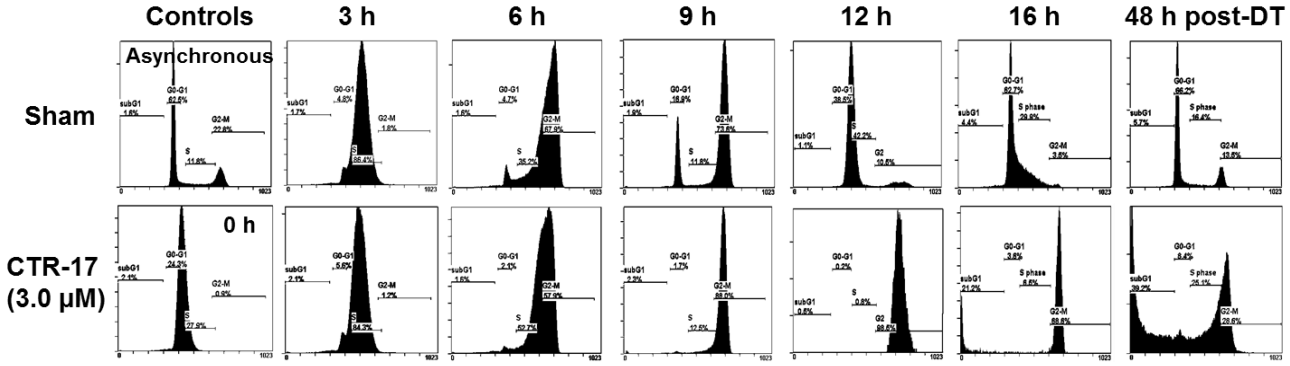
Controls
3 h
6 h
9 h
12 h
16 h
48 h post-DT
Sham
Asynchronous
CTR-17
(3.0 μM)
0 h

B

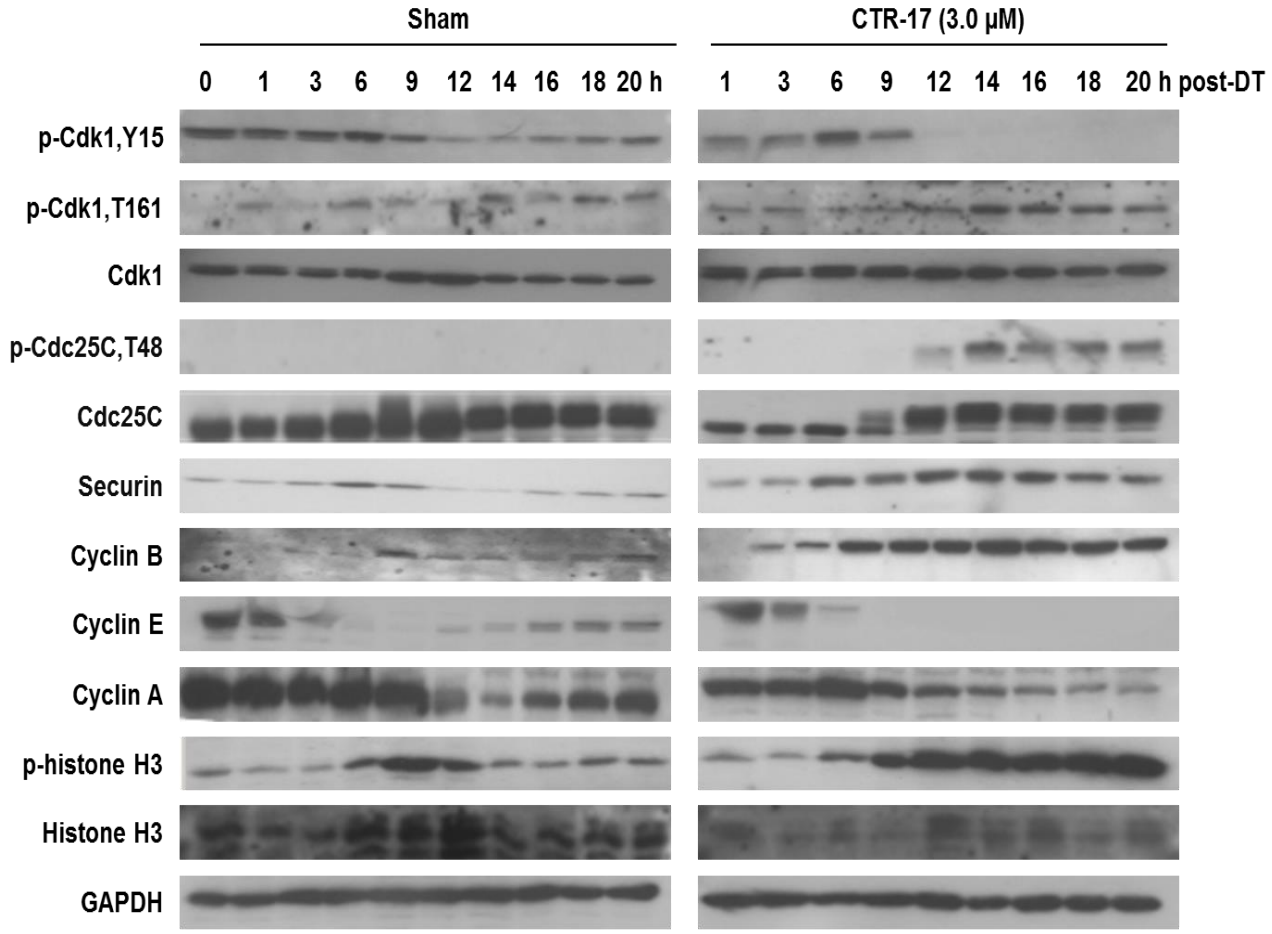
Sham
CTR-17 (3.0 μM)
0 1 3 6 9 12 14 16 18 20 h
1 3 6 9 12 14 16 18 20 h post-DT
p-Cdk1,Y15
p-Cdk1,T161
Cdk1
p-Cdc25C,T48
Cdc25C
Securin
Cyclin B
Cyclin E
Cyclin A
p-histone H3
Histone H3
GAPDH

Figure 16: CTR-17 treatment caused monopolar or uneven chromosome distribution

Cells were treated (or not treated) with 3.0 µM CTR-17 for 12 h, fixed in methanol and stained with antibodies specific for gamma-tubulin (green) and alpha-tubulin (red), and then counterstained with DAPI (blue) to visualise the chromosomes.

A: Sham-treated cells (top panels) are mostly in interphase and a higher magnification of a metaphase cell shows chromosomes positioned between the spindle poles equidistantly. However, CTR-17 treated cells (bottom panels) show groups of chromosomes (denoted by arrows) at the spindle poles which are incapable of resolving at the metaphase plate.

B: Treatment of other cancer cells (Hek293T, MDA-MB468 and MDA-MB231) with 3.0 µM CTR-17 demonstrates a similar abnormal mitotic spindle that eventually leads to a monopolar or an abnormal chromosome division

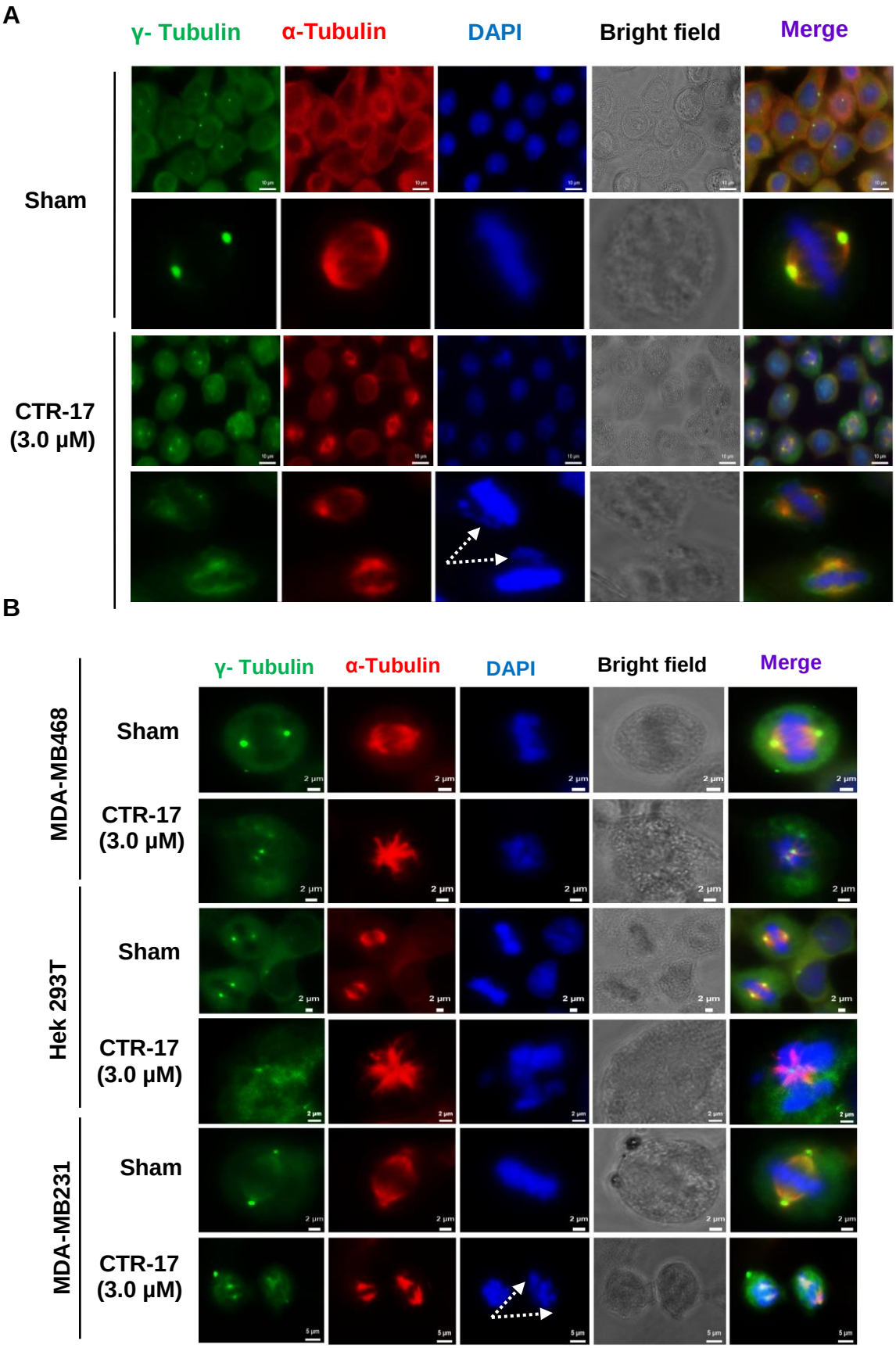
A
γ- Tubulin
α-Tubulin
DAPI
Bright field
Merge
Sham
CTR-17
(3.0 μM)
B
γ- Tubulin
α-Tubulin
DAPI
Bright field
Merge
MDA-MB468
Sham
CTR-17
(3.0 μM)
Hek 293T
Sham
CTR-17
(3.0 μM)
MDA-MB231
Sham
CTR-17
(3.0 μM)

Figure 17: CTR-17 selectively increased the mitotic index of cancer cells with an accumulation of abnormal and monopolar centrosomes

A: CTR-17 selectively increased the percentage of cells in mitosis in a time-dependent manner. Different cell types were either sham-treated or treated with 3.0 µM CTR-17 for 12 h or 24 h. The mitotic index was determined by fluorescence microscopic analysis of about 200 cells for each cell type, either sham-treated or treated with CTR-17, and the data were expressed as percentage mean ± SEM of at least two independent experiments.

B: Percentage of monopolar and abnormal chromosome division, under the same conditions as in (A) are tabulated. ACD denotes abnormal chromosome division among the mitotic cells.

C: The average distance between the centrosomes of sham-treated *vs* cells treated with CTR-17 shows that the interpolar distance was about 35% less than in sham-treated cells. The average distance between the centrosomes were determined by fluorescence microscopic analysis of 100 cells in three independent replicates and the data were expressed as percentage mean ± SEM of at least three independent experiments.

A

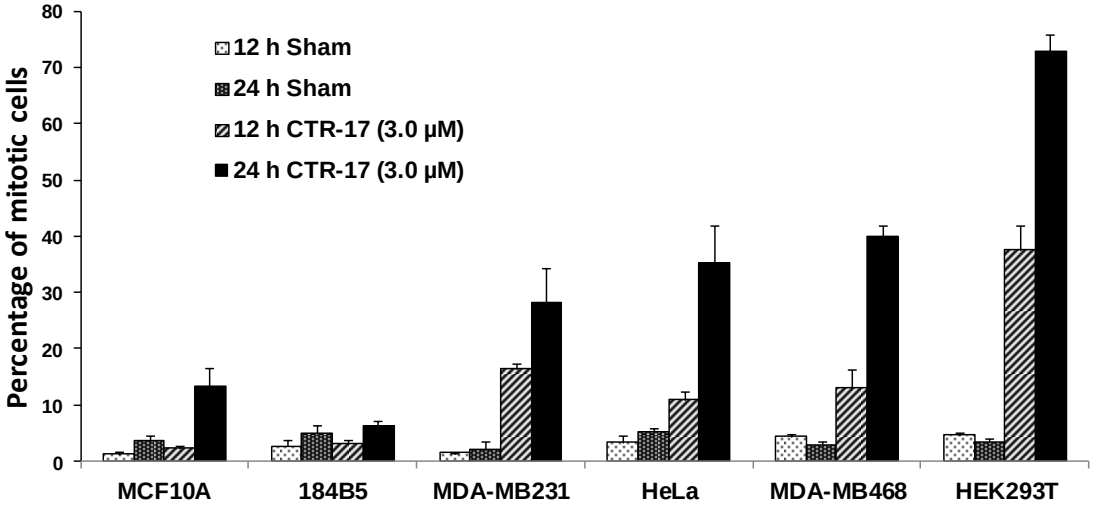

B

	12 h post-treatment		24 h post-treatment	
	Monopolar	ACD	Monopolar	ACD
HeLa	80.0±4.5	20.0±4.5	100.0±0.0	0.0±0.0
MDA-MB231	40.0±10.2	60.0±10.2	44.9±5.7	55.1±5.7
MDA-MB468	55.3±8.9	44.7±8.9	76.0±5.9	24.0±5.9
HEK293T	50.5±10.1	48.2±10.1	93.2±3.4	0.1±0.0

C

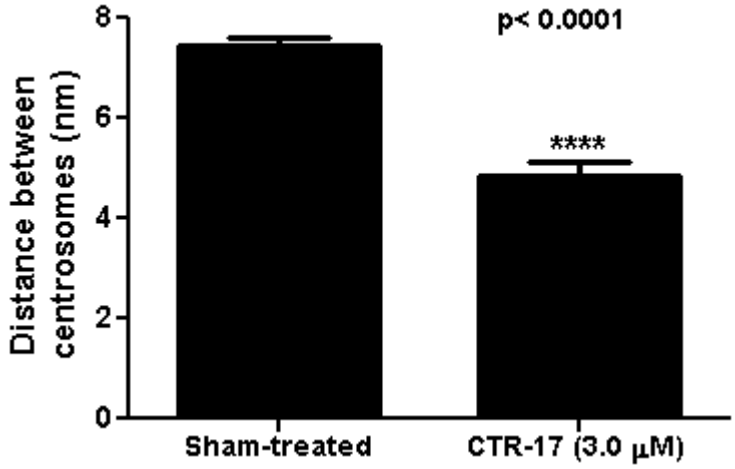

The distance of two centrosomes in a single cell was shorter by 35% compared to sham-treated cells. CTR-17 treatment leads to: (1) abnormal chromosome division (ACD); and (2) monopolar centrosomes. The incidence of each phenotype varies among cells and depends on the stage of the cell cycle when CTR-17 is administered. If cells are in interphase during CTR-17 treatment, centrosomes may not be able to separate.

This agrees with previously published reports which indicate the use of MTs in centrosome separation (Uzbekov et al. 2002). However, if the cells are already in mitosis, when CTR-17 is administered, the chromosomes may not be able to accurately resolve at the metaphase plate due to the absence of tension and attachment between the chromosomes and the mitotic spindle leading to ACD.

The presence of unattached kinetochores results in the activation of SAC. To examine if CTR-17 causes mitotic arrest by SAC activation, BuBR1, one of the core proteins in the SAC complex was studied in detail. BubR1 associates with cdc20 (represented by red asterisks in Figure 18A) to inhibit the cdc20-mediated activation of the APC/C complex. To determine if BubR1 interacts with cdc20, BubR1 was immunoprecipitated and immunoblotted with an antibody specifically directed towards cdc20 at scheduled time points (6-9 h, post-DT). Nocodazole causes the activation of SAC, and hence was used as a positive control (Collin et al. 2013). Both nocodazole and CTR-17 arrest the cells at the SAC step where BubR1 is associated with cdc20, in comparison to the sham-treated cells.

Figure 18: CTR-17 prevented mitotic exit by prolonged spindle checkpoint activation

A: Immunoprecipitation of BuBR1 revealed its association with cdc20, rendering APC/C-cdc20 complex inactive and causing the spindle assembly checkpoint activation. HeLa cells synchronised at the G1/S boundary by double thymidine block and release were either sham-treated or treated with 20 ng/ml nocodazole or 3.0 µM CTR-17, and then harvested at the indicated time points. BuBR1 was immunoprecipitated from the whole cell lysates, and the immunoprecipitates were then resolved by SDS-PAGE and immunoblotted using an antibody specifically directed towards cdc20 (represented by red asterisks). WCEs were immunoblotted with cdc20 and used as the loading control.

B: The presence of a slow migrating band of BubR1 in DT-synchronised CTR-17 treated HeLa cells is another evidence of SAC activation.

C: Representative images showing BuBR1 accumulation at the kinetochores of CTR-17 treated HeLa cells. HeLa cells were either sham or CTR-17 (3.0 µM) treated for 12 h. Cells were subsequently fixed and stained with anti-BubR1 and CENP-B, to stain the centromeres. Accumulation of BubR1 at the kinetochores indicates the lack of proper tension between the kinetochores and the mitotic spindle and thus the continuous activation of spindle assembly checkpoint.

A

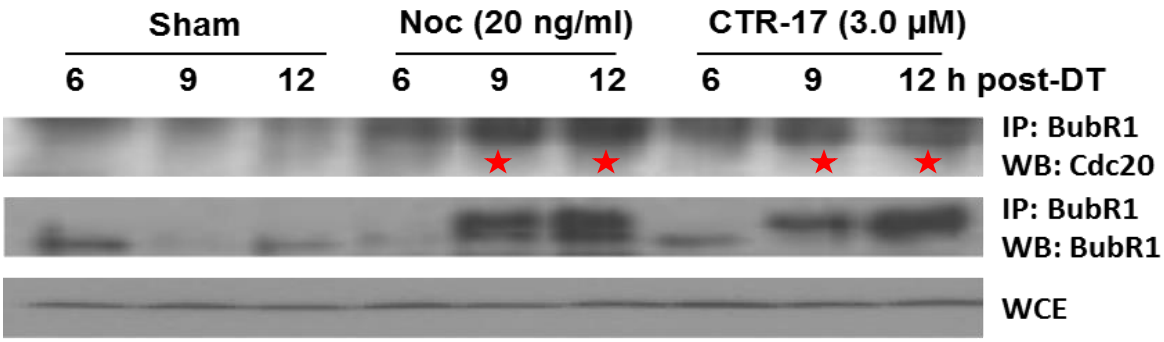
Sham
Noc (20 ng/ml)
CTR-17 (3.0 μM)
6
9
12
6
9
12
6
9
12 h post-DT
IP: BubR1
WB: Cdc20
IP: BubR1
WB: BubR1
WCE

B

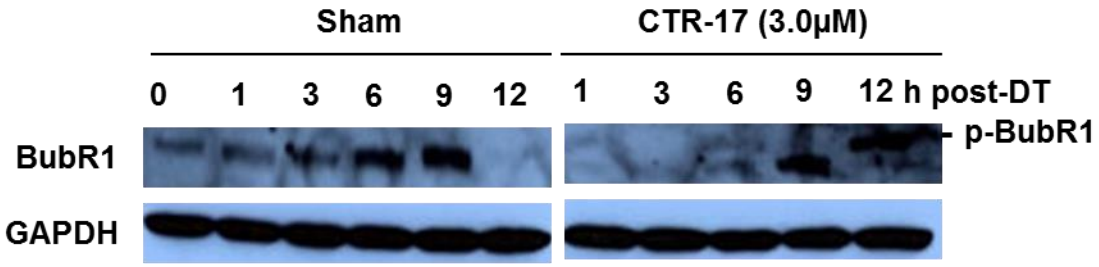
Sham
CTR-17 (3.0μM)
0
1
3
6
9
12
1
3
6
9
12 h post-DT
BubR1
p-BubR1
GAPDH

C

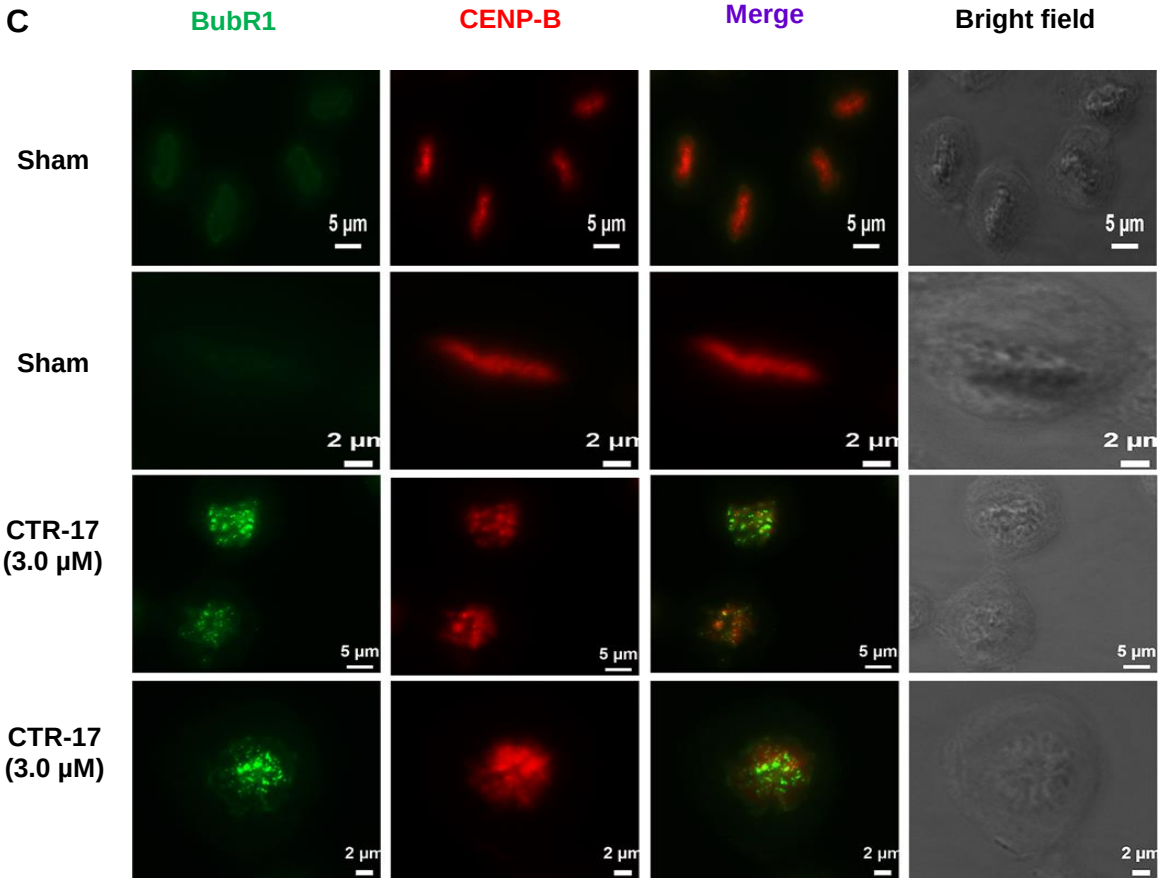
BubR1
CENP-B
Merge
Bright field
Sham
Sham
CTR-17
(3.0 μM)
CTR-17
(3.0 μM)
5 μm
2 μm

When whole cell extracts (WCEs) isolated after DT-based synchronization were released in the absence (sham) or presence of 3.0 μM CTR-17 and then resolved by SDS-PAGE, a bandshift in BubR1 was observed in the CTR-17 treated cells by 12 h post-DT (Figure 18B). This observation strongly agrees with previous reports that a phosphorylation-dependent band-shift occurs when cells are treated with MTAs (Taylor et al. 2001).

BubR1 is reported to accumulate at the unattached kinetochores and to aid in the recruitment of other SAC proteins including CENP-E, Mad1, Mad2, Bub1 and, Bub3. Therefore, the localisation of BubR1 at unattached kinetochores was examined by using an antibody specifically directed towards CENP-B. CTR-17 leads to the accumulation of BuBR1 at the kinetochores, suggesting that the APC/C-Cdc20 complex is inactive in CTR-17-treated cells, thus confirming SAC activation and inhibition of mitotic exit (Figure 18C).

To determine if mitotic arrest caused by CTR-17 and CTR-20 was reversible, HeLa cells were treated for 12 h with CTR compounds and then the drug-containing medium was removed, washed with 1X PBS, and replaced with fresh culture medium. The cells were harvested at scheduled time points and subjected to flow cytometry. The flow cytometry profiles showed that both CTR-17 and CTR-20 are reversible and the cells progressed to the next cycle within 3-6 h after washing (Figure 19).

Figure 19: CTR-17 and CTR-20 causes a reversible mitotic arrest in HeLa cells

A: HeLa cell cycle histograms show a G2/M cell cycle arrest in CTR-17 (3.0 µM) and CTR-20 (1.0 µM) treated cells after 12h (t=0 h). At t=0 h, the adherent and floating cells were washed separately twice with 1X PBS, followed by re-suspension of the cells in 10 ml of pre-warmed, drug-free medium for the indicated duration.

B: HeLa flow cytometry profiles show that CTR-17 and CTR-20 cause a reversible mitotic arrest, during which cells progress in the cell cycle and overcome the robust mitotic arrest as early as 3 h from the release.

C: Treated HeLa cells released into drug-free medium progress normally in mitosis. Representative images of cells released into drug-free medium collected at the indicated time points.

A

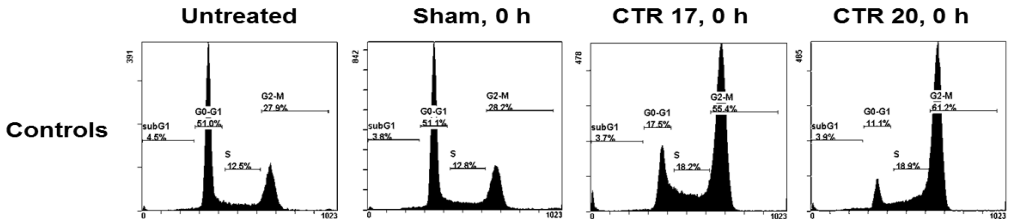
Untreated
Sham, 0 h
CTR 17, 0 h
CTR 20, 0 h
Controls

B

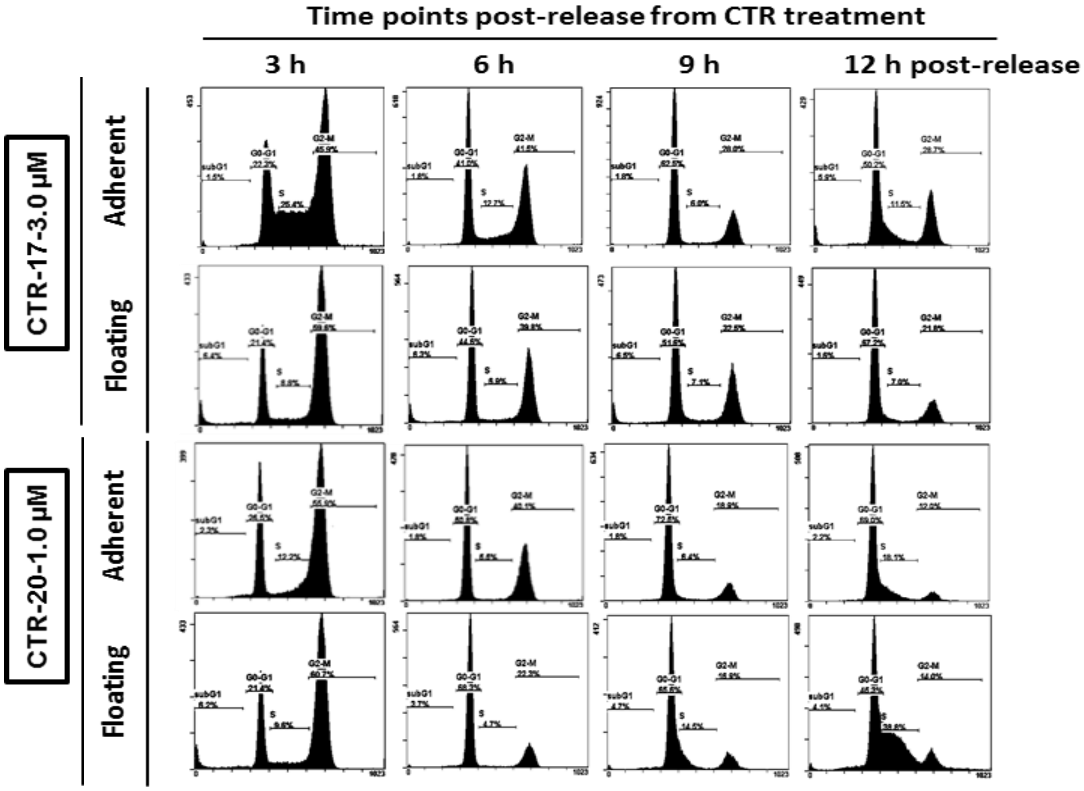
Time points post-release from CTR treatment
3 h
6 h
9 h
12 h post-release
CTR-17-3.0 µM
CTR-20-1.0 µM
Adherent
Floating

C

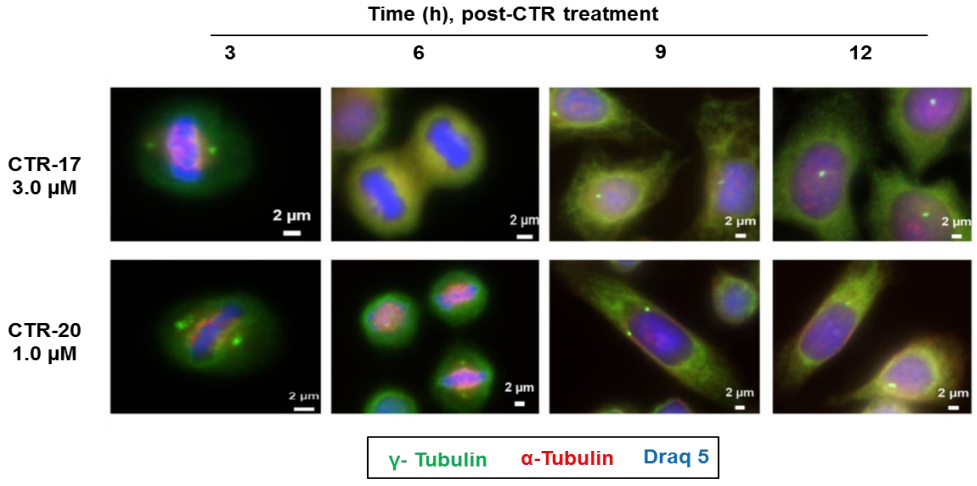
Time (h), post-CTR treatment
3
6
9
12
CTR-17
3.0 µM
CTR-20
1.0 µM
2 µm
γ- Tubulin
α-Tubulin
Draq 5

3.3 CTR compounds inhibit MT polymerization

The morphological features observed by the treatment of cells with CTR compounds were very similar to other MTAs such as vinblastine, nocodazole and podophyllotoxin (Jordan et al. 1992). CTR compounds caused aberrant mitotic spindles with a shorter distance between the spindle poles and some chromosomes remain at the spindle poles, leading to prolonged mitotic arrest with disregulated chromosome alignment. Hence, the effect of CTR compounds on the MT polymerization was examined using an *in vitro* MT assembly assay (Figure 20). A polymerization curve was then constructed to represent 3 stages of the MT polymerization process, including MT nucleation, growth, and finally the steady state equilibrium. If a compound interacts with MT, one of the above phases should be altered. For example, paclitaxel, an MT stabilizer, completely eliminates the nucleation phase and achieve steady state equilibrium in a shorter duration (Schiff et al. 1979). In contrast, nocodazole, an MT destabilizer shows a longer growth phase and achieves a steady state after an extended period of time in the process of MT assembly (Chao et al. 2002). Data in Figure 20 shows that CTR-17 and CTR-20 cause an inhibition of MT polymerization; whereas, paclitaxel promoted MT assembly. Similarly to CTR compounds, nocodazole inhibited MT polymerization. It is noted that CTR-17 and CTR-20 showed a prolonged MT growth phase and took a longer time to reach a steady equilibrium state (≥60 min). In contrast, paclitaxel reached equilibrium as early as 18 min. According to the experimental set up, (i.e., a working volume of 100 µl and a path length of 0.5 cm), OD 0.1 at 340 nm is approximately equivalent to 1.0 mg/ml of MT polymer mass.

Figure 20: CTR-17 and CTR-20 inhibit the polymerization of purified tubulin
10.0 µM paclitaxel, 3.0 µM CTR-17, 1.0 µM CTR-20 or 5.0 µM nocodazole were added to reaction mixtures containing purified porcine tubulin in G-PEM buffer. Polymerization of tubulin was then monitored at 340 nm and 37°C using a spectrophotometer every 1 min for one hour. CTR-17 and CTR-20 cause an extended growth phase and takes a longer duration to achieve steady state equilibrium, similar to nocodazole but contrarily to paclitaxel, indicating that they are inhibitors of tubulin polymerization. The Figure is a representative of at least three independent experiments.

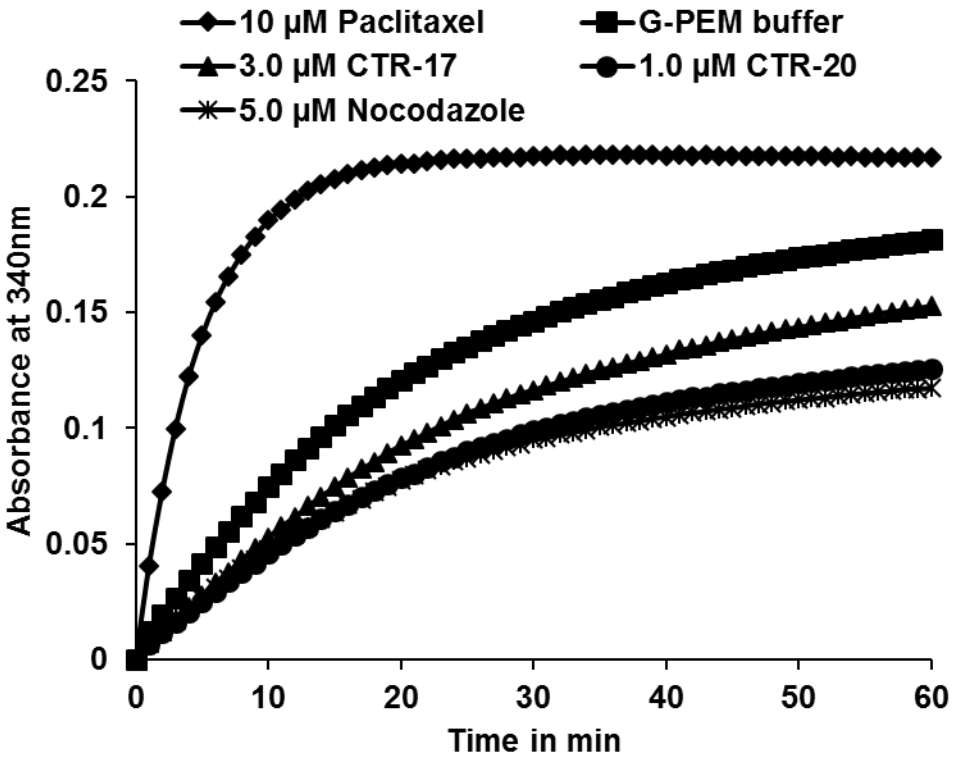
10 μM Paclitaxel
G-PEM buffer
3.0 μM CTR-17
1.0 μM CTR-20
5.0 μM Nocodazole
Absorbance at 340nm
0.25
0.2
0.15
0.1
0.05
0
0
10
20
30
40
50
60
Time in min

Hence, paclitaxel, G-PEM buffer control, CTR-17, CTR-20 and nocodazole polymerised about 55%, 40%, 30%, 25% and 24%, respectively, at 30 min. Therefore, CTR-17 and CTR-20 were identified as MT polymerization inhibitors.

Live cell imaging using sham or CTR-17 (3.0 µM) treated Hek293T cells transfected with GFP-tubulin showed that CTR-17 led to the formation of aberrant spindles (Figure 21). The centrosomes were unable to establish the bipolarity of the cells for as long as 24 h. As a result, normal cell cycle progression was disrupted and mitotic exit is prevented, strongly agreeing with the data obtained from immunofluorescence, immunoblotting and flow cytometry experiments.

The effect of CTR compounds on MT polymerization in the cell was then determined. Intracellular tubulin occurs in two forms, namely the polymerized (cytoskeletal) tubulin and monomeric (soluble) tubulin. MT stabilizers and destabilizers lead to the accumulation of polymerized and soluble tubulin, respectively (Stanton et al. 2011). To confirm the inhibition of MT polymerization of CTR compounds, the polymerised and soluble tubulin fractions were separately extracted and examined by immunoblotting. Similarly to nocodazole (50 ng/ml), both CTR-17 (3.0 µM) and CTR-20 (1.0 µM) reduced the polymerized pool of tubulin by 12 h of treatment in HeLa cells (Figure 22). This phenomenon was also observed in a dose-dependent manner in HeLa cells.

Figure 21: CTR-17 leads to disrupted spindle bipolarity
A: Sham-treated Hek293T cells transfected for 16 h using CellLight® Tubulin-GFP shows the bipolar spindle formation (indicated by a white arrow) followed by the completion of cell division and the separation of the cell into two daughter cells.
B: CellLight® Tubulin-GFP transfected Hek293T cells treated with CTR-17 tries to develop the spindle. However, they are apparently unable to maintain an adequate distance between the centrosomes (indicated by a yellow arrow) and, eventually, collapse to a monopolar spindle configuration towards the end of the capture (indicated by a red arrow).
.

A

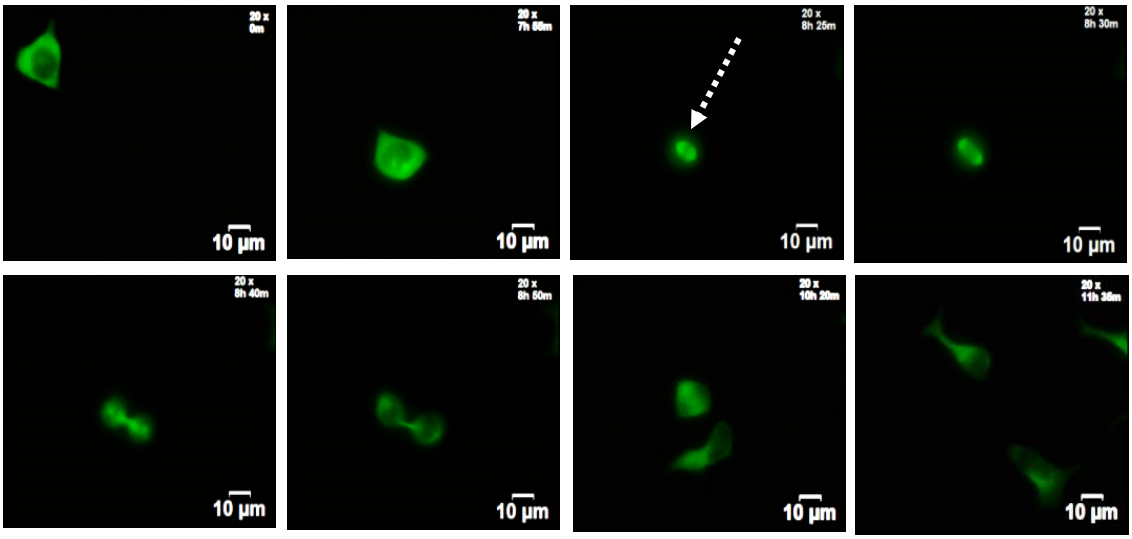
20 x
0m
10 µm
20 x
7h 55m
10 µm
20 x
8h 25m
10 µm
20 x
8h 30m
10 µm
20 x
8h 40m
10 µm
20 x
8h 50m
10 µm
20 x
10h 20m
10 µm
20 x
11h 35m
10 µm

B

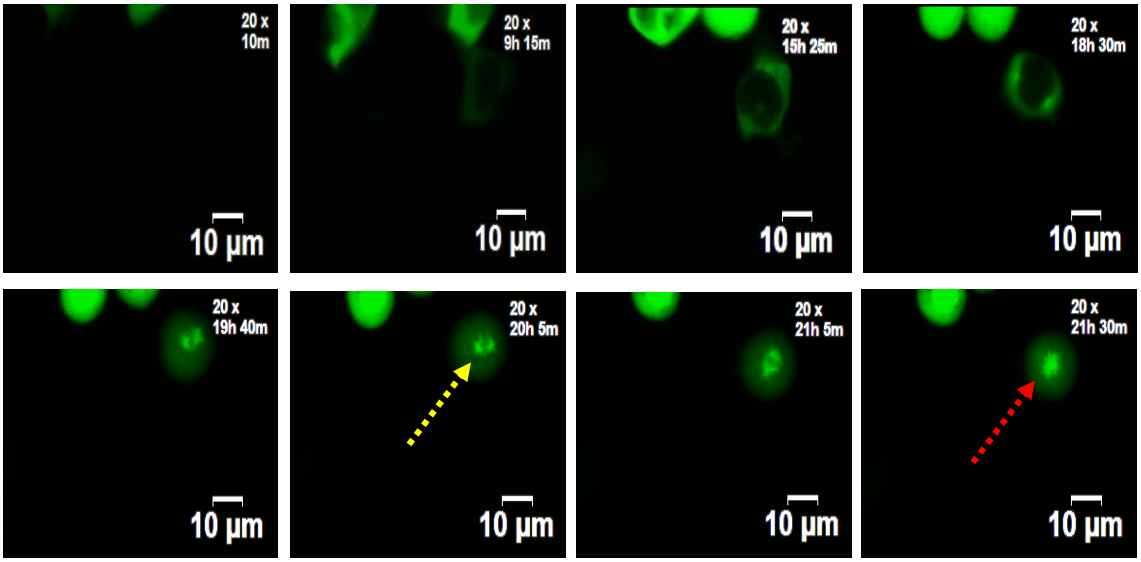
20 x
10m
10 µm
20 x
9h 15m
10 µm
20 x
15h 25m
10 µm
20 x
18h 30m
10 µm
20 x
19h 40m
10 µm
20 x
20h 5m
10 µm
20 x
21h 5m
10 µm
20 x
21h 30m
10 µm

Figure 22: CTR-17 and CTR-20 decreased the polymerized pool of tubulin
A: HeLa cells were either sham-treated or treated with 50.0 nM paclitaxel, 50.0 ng/ml nocodazole, 3.0 µM CTR-17 and 1.0 µM CTR-20 for 12 h. Lysates were subsequently separated into polymerized (Pol) and soluble (Sol) fractions, and then equal amounts of proteins were resolved by SDS-PAGE and immunoblotted with an antibody specific to alpha-tubulin. The graphs below each blot represent densitometry of the tubulin band intensities in each fraction. The results represent the mean ± SEM of at least three independent experiments. CTR compounds reduced the polymerized fraction of tubulin similar to nocodazole, but contrarily to paclitaxel. Pac and Noc denote paclitaxel and nocodazole, respectively.
B: CTR-17 and CTR-20 reduced the polymerized tubulin fraction dose-dependently in HeLa cells.
C: The MT destabilizing effect of CTR compounds were common in other cell lines, MDA-MB231 and MDA-MB468.

A

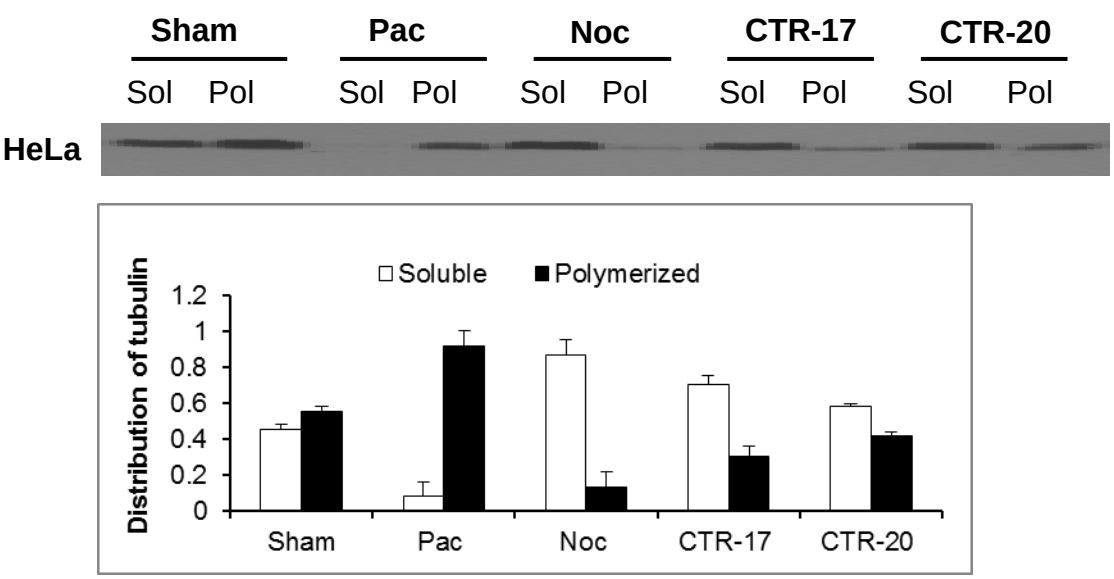
Sham
Pac
Noc
CTR-17
CTR-20
Sol Pol Sol Pol Sol Pol Sol Pol Sol Pol
HeLa
Soluble
Polymerized
Distribution of tubulin
1.2
1
0.8
0.6
0.4
0.2
0
Sham
Pac
Noc
CTR-17
CTR-20

B

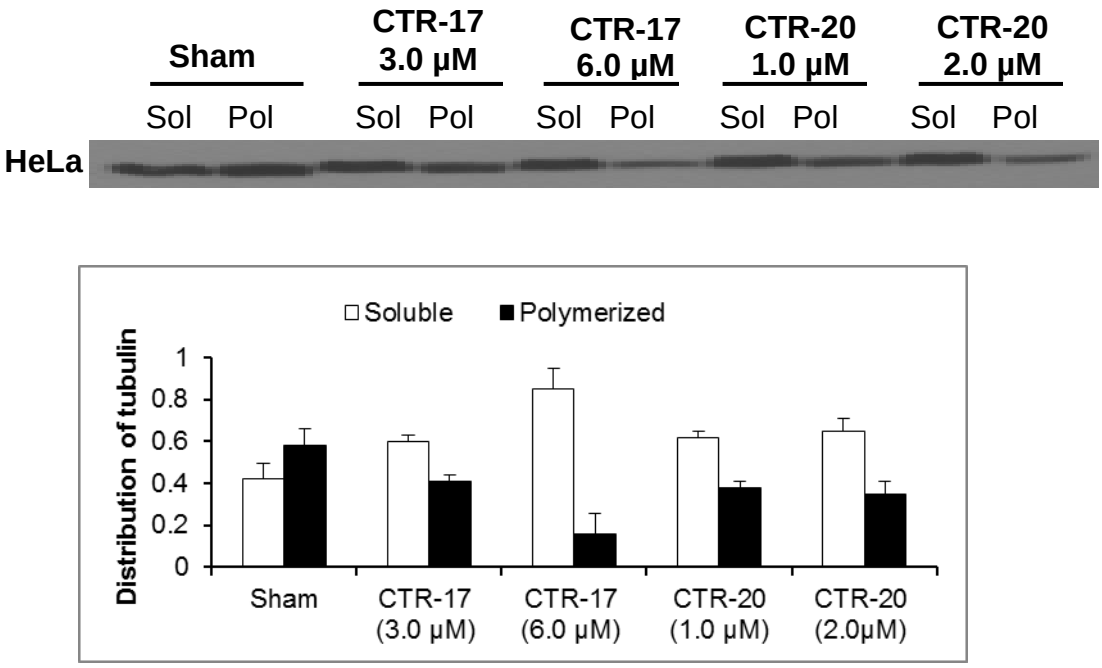
Sham
CTR-17 3.0 μM
CTR-17 6.0 μM
CTR-20 1.0 μM
CTR-20 2.0 μM
Sol Pol Sol Pol Sol Pol Sol Pol Sol Pol
HeLa
Soluble
Polymerized
Distribution of tubulin
1
0.8
0.6
0.4
0.2
0
Sham
CTR-17 (3.0 μM)
CTR-17 (6.0 μM)
CTR-20 (1.0 μM)
CTR-20 (2.0μM)

C

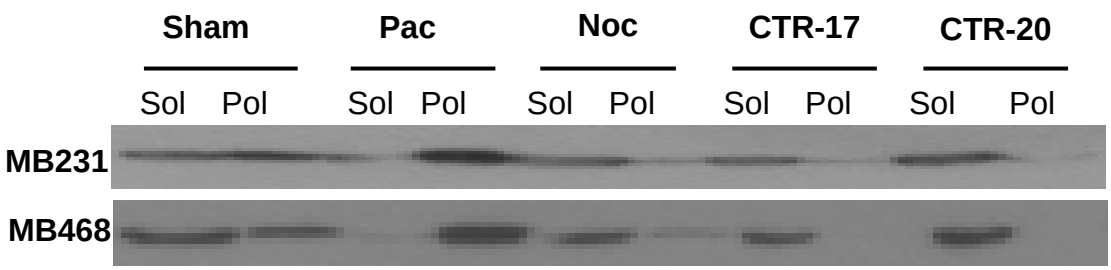
Sham
Pac
Noc
CTR-17
CTR-20
Sol Pol Sol Pol Sol Pol Sol Pol Sol Pol
MB231
MB468

When examined in other cell lines, including MDA-MB231 and MDA-MB468, the same effect was observed. However, paclitaxel (50 nM) caused the polymerised fraction of tubulin to increase in all cell lines as expected for a well-known MT stabilizing agent. Hence, CTR compounds are MT polymerization inhibitors in multiple cell lines.

3.4 CTR compounds reduced the migration abilities of MDA-MB231 cells

In addition to the disruption of cell cycle progression, MTAs also interfere with the migration capability of cells (Goldman 1971; Small et al. 2002). Many studies have shown that MTAs inhibit mitosis by abrogating the dynamic behaviour of the plus-ends of the MT (Jordan & Wilson 2004). This alteration in MT dynamicity was used to explain the inhibition of cell migration by agents that interfere with MTs (Pourroy et al. 2006).

Hence, the effect of CTR-17 on the migration ability of MDA-MB231 cells in comparison to a sham-treated cell population for a period of 72 h was examined (Figure 23A). For the scratch wound healing assay, a scratch was introduced using a p200 pipette tip on a monolayer of MDA-MB231 cells and then the cells were either sham-treated or treated with 3.0 µM CTR-17 before being subjected to live cell microscopy. The cell images were captured every 10 min for 72 h and the percentage of wound closure was measured using Image J software, an open access software developed by the National Institute of Health (rsb.info.nih.gov/ij).

Figure 23: CTR-17 disrupted the wound healing ability of MDA-MB231 cells
A: Live cell images of confluent MDA-MB231 cells containing a scratch wound that were either sham-treated or treated with CTR-17 for up to 72 h. Images were taken using a 4X objective and every 10 min intervals.
B: The values show the mean ± SEM of the percentage of wound closure (N=3).
C: Figures are presented as a bar graph. The percentage of wound closure was calculated using Image J software in triplicates for each field, and each experiment was performed in triplicates.

A

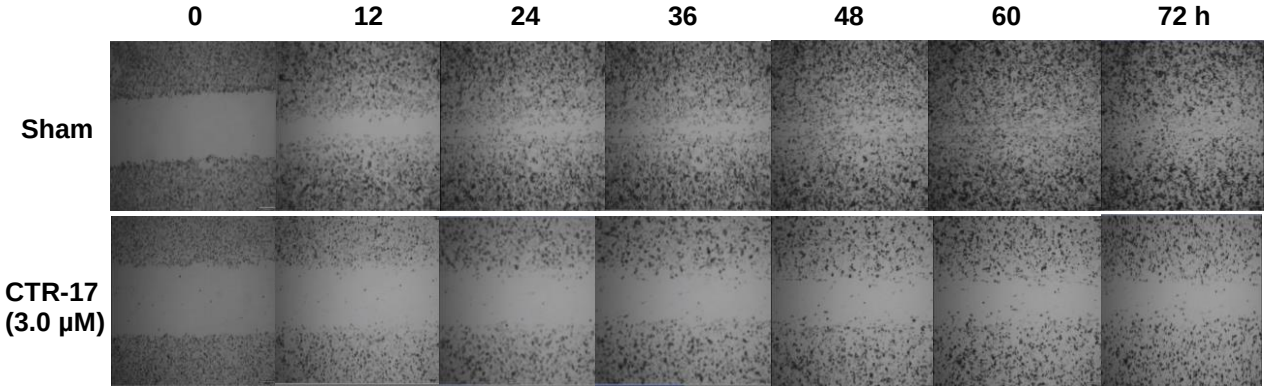

B

	Percentage of wound closure	
Time in h	Sham-treated	CTR-17 (3.0 µM)
0	0	0
12	30.80±1.85	6.22±2.48
24	48.70±6.28	10.31±1.35
36	66.22±5.95	18.49±2.38
48	78.10±2.54	32.91±2.12
60	84.27±4.77	45.47±11.11
72	92.60±7.43	50.64±9.94

C

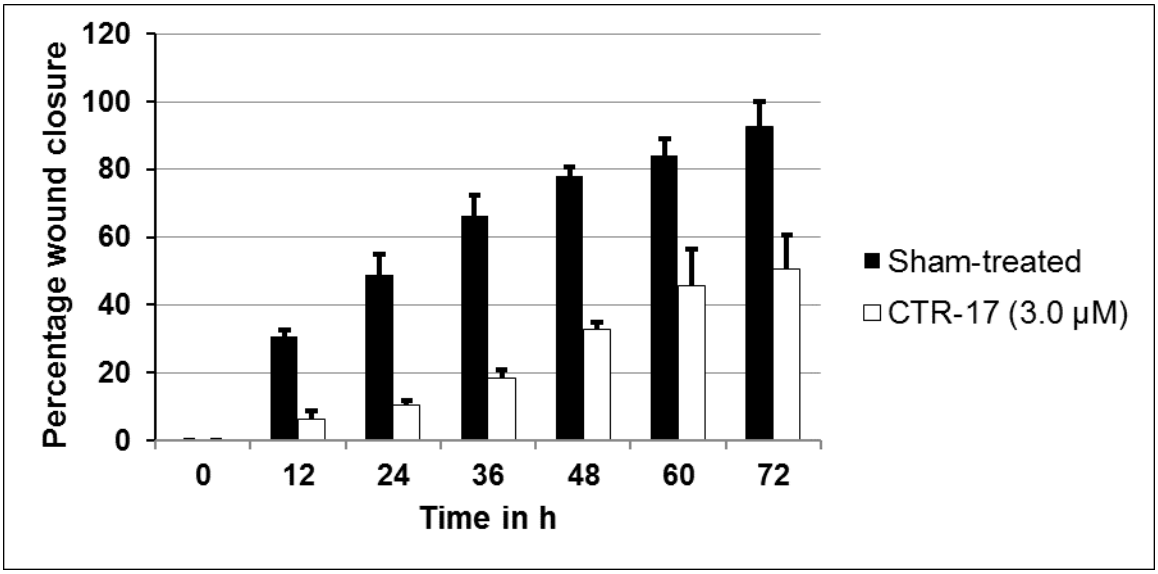

Sham-treated cells led to approximately 93% wound closure within 72 h; however, CTR-17 treated cells were only able to close the wound by 51% (Figure 23B). Looking closely at the velocity of wound closure, sham-treated cells closed the wound at a rate of ~10.0 µm/h, while CTR-17 treated cells closed the wound at approximately half of the velocity. Previous studies showed that MTAs cause the microtubules to be more static and are hence unable to remodel the cytoskeleton for the purpose of changing the shape of the cell during the cell migration (Yang et al. 2010). These observations further support the ability of CTR compounds to manifest themselves as MT interfering agents.

3.5 CTR compounds bind directly to purified tubulin

To determine if CTR compounds directly bind to tubulin and cause any changes in its tertiary structure, the fluorescence of tryptophan residues was monitored. Intrinsic tryptophan fluorescence of tubulin is now widely used as a probe to determine the binding affinity of drugs to tubulin heterodimers (Zhang et al. 2009; Venghateri et al. 2013; Rai et al. 2012; Gireesh et al. 2012). The fluorescence of the reaction mixture in the absence of any drug (but in the presence of DMSO or PIPES buffer) with tubulin was relatively higher than all the drug concentrations used. Data in Figure 24 shows a concentration-dependent quenching of the tryptophan fluorescence when purified tubulin was incubated with CTR-17 or CTR-20. For example, the incubation of 10.0 µM and 40.0 µM of CTR-17 with tubulin quenched the intrinsic fluorescence of tubulin by 34.3±1.6% and 46.4±3.6%, respectively (Figure 24A).

Figure 24: CTR-17 and CTR-20 bound to purified tubulin

A, B: CTR-17 and CTR-20 quenched the intrinsic tryptophan fluorescence of tubulin in a dose-dependent manner. Tubulin (0.4 μM) dissolved in 25 mM PIPES buffer (pH 6.8) was incubated in the absence or presence of different concentrations of CTR compounds for 30 min at 37°C. Fluorescence was then monitored by excitation of the reaction mixture at 295 nm and the emission spectra were recorded at 315-370 nm.

C, D: The changes in fluorescence were plotted against the concentration of the drugs to determine the dissociation constant. The dissociation constants suggest that CTR-17 and CTR-20 bind with comparable ability to tubulin. ΔF is the change of fluorescence intensity of tubulin when bound to CTR-17 or CTR-20. Data are the average of at least five independent experiments.

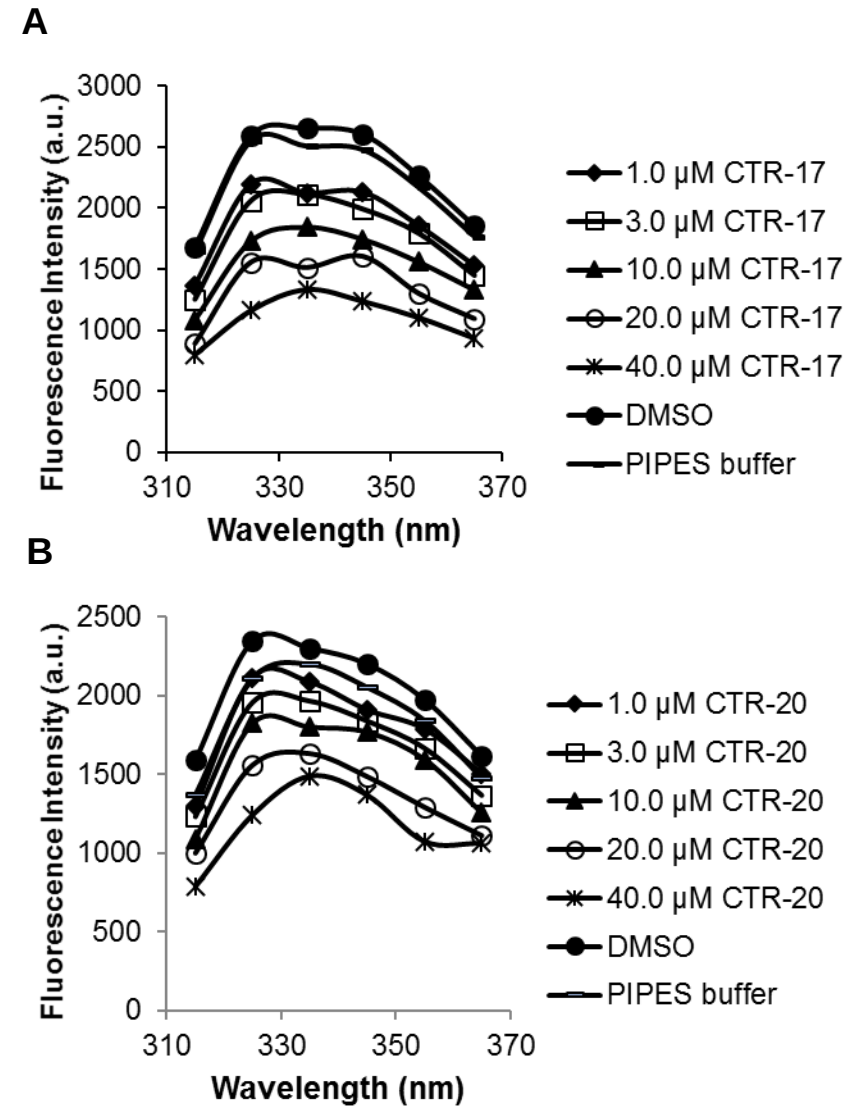
A
Fluorescence Intensity (a.u.)
3000
2500
2000
1500
1000
500
0
310
330
350
370
Wavelength (nm)
1.0 μM CTR-17
3.0 μM CTR-17
10.0 μM CTR-17
20.0 μM CTR-17
40.0 μM CTR-17
DMSO
PIPES buffer
B
Fluorescence Intensity (a.u.)
2500
2000
1500
1000
500
0
310
330
350
370
Wavelength (nm)
1.0 μM CTR-20
3.0 μM CTR-20
10.0 μM CTR-20
20.0 μM CTR-20
40.0 μM CTR-20
DMSO
PIPES buffer

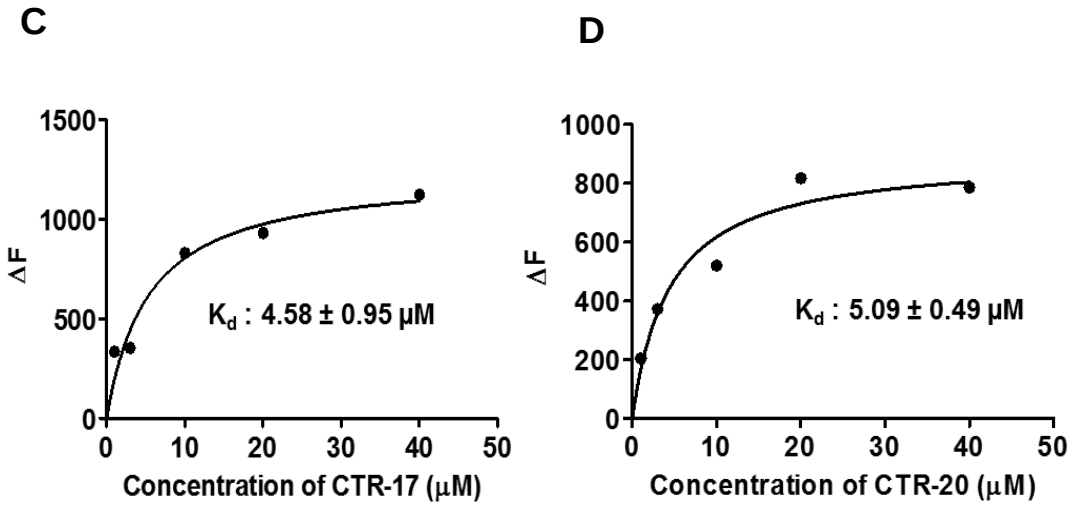
C
ΔF
1500
1000
500
0
0
10
20
30
40
50
Kd : 4.58 ± 0.95 μM
Concentration of CTR-17 (μM)
D
ΔF
1000
800
600
400
200
0
0
10
20
30
40
50
Kd : 5.09 ± 0.49 μM
Concentration of CTR-20 (μM)

The incubation of 10.0 µM and 40.0 µM of CTR-20 similarly reduced the intrinsic fluorescence of tubulin by 21.5±1.0% and 32.5±1.7%, respectively (Figure 24B). The changes in fluorescence intensity were determined relative to PIPES buffer, and the binding constants (K_d) were then determined by fitting the fluorescence changes in a binding isotherm for CTR-17 (Figure 24C) and CTR-20 (Figure 24D). During each experiment, no-tubulin controls (each concentration of drug only in PIPES buffer) were used to deduct any inherent fluorescence of the CTR compounds alone. The K_d values were found to be 4.58±0.95 µM and 5.09±0.49 µM from five independent experiments for CTR-17 and 20, respectively.

3.6 CTR compounds bind to tubulin partially overlapped to the colchicine-binding site

To pinpoint the exact binding site of the CTR compounds, competition assays in the presence of BODIPY® FL Vinblastine and colchicine were performed, as most of the MT polymerization inhibitors bind to tubulin via the colchicine or vinblastine-binding sites (Zhang et al. 2009). Upon binding to tubulin, the fluorescence intensity of colchicine and BODIPY® FL Vinblastine increases, which was used as an index to determine if CTR-17 and CTR-20 compete with either colchicine or vinblastine in binding to the respective target sites. The CTR compounds and colchicine were unable to inhibit the fluorescence enhancement caused by BODIPY® FL Vinblastine binding to tubulin, even at a high concentration of 25 µM; however, vinblastine did reduce the fluorescence of the BODIPY® FL Vinblastine-tubulin complex. This suggests that CTR compounds do not bind to the vinblastine site (Figure 25A).

Figure 25; CTR-17 and CTR-20 do not bind to the vinblastine-binding site
A: CTR-17 and CTR-20 do not quench the fluorescent enhancement of BODIPY FL vinblastine-tubulin complex, similarly to colchicine but contrary to vinblastine. Tubulin (0.4 µM) was incubated with 25.0 µM of CTR-17, CTR-20, colchicine, vinblastine for one hour at 37°C and 5.0 µM of BODIPY® FL Vinblastine was then added to the tubulin complexes and incubated under the same conditions for additional 30 min. Fluorescence was then monitored by excitation of the reaction mixture at 490 nm and the emission spectra were recorded at 510-550 nm.
B: Unlike vinblastine, CTR-17 inhibits the fluorescence enhancement of the colchicine-tubulin complex in a dose-dependent manner. Tubulin (0.4 µM) was incubated with different concentrations of CTR-17 or vinblastine for one hour at 37°C, and then 5.0 µM of colchicine was added to the tubulin complexes, followed by incubation for 30 min under the same conditions. Fluorescence was then monitored by excitation of the reaction mixture at 360 nm and emission was recorded at 430 nm. F is the fluorescence of the CTR-17-colchicine-tubulin or vinblastine-colchicine-tubulin complexes, and F0 is the fluorescence of the colchicine-tubulin complex. Each experiment was repeated at least twice more.

A

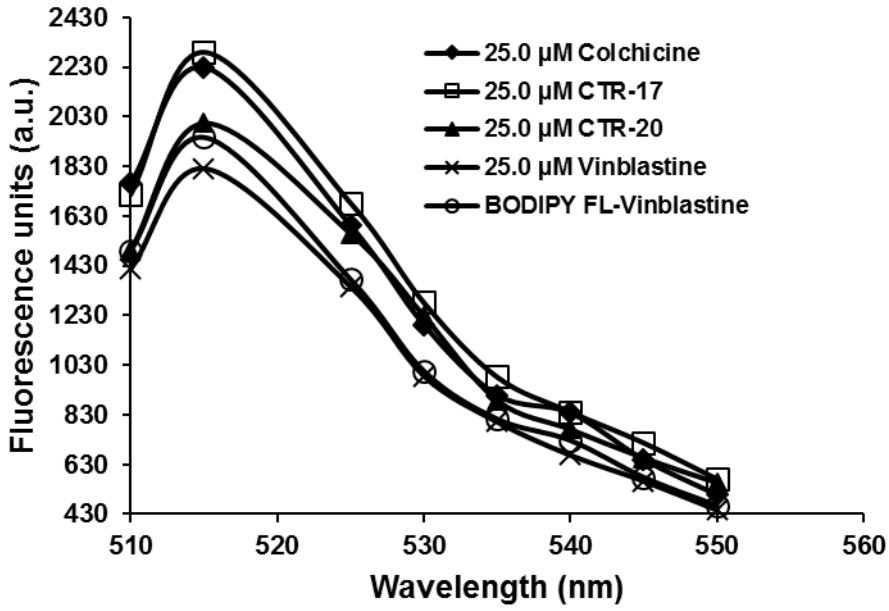
2430
2230
2030
1830
1630
1430
1230
1030
830
630
430
Fluorescence units (a.u.)
510
520
530
540
550
560
Wavelength (nm)
25.0 μM Colchicine
25.0 μM CTR-17
25.0 μM CTR-20
25.0 μM Vinblastine
BODIPY FL-Vinblastine

B

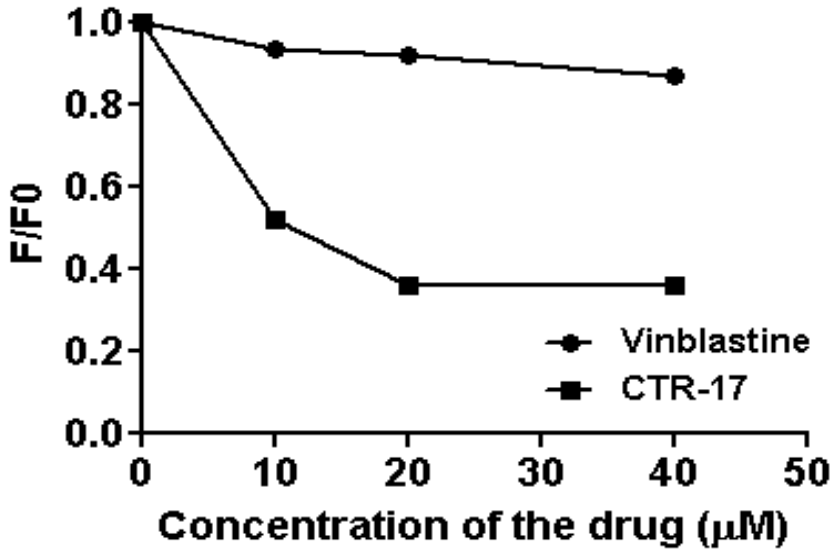
1.0
0.8
0.6
0.4
0.2
0.0
F/F0
0
10
20
30
40
50
Concentration of the drug (μM)
Vinblastine
CTR-17

However, the fluorescence of the colchicine-tubulin complex was reduced in a concentration-dependent manner by the CTR compounds, suggesting that both CTR-17 and CTR-20 bind to tubulin at or near the colchicine-binding site. Figure 25B shows the change in fluorescence of the colchicine (5 μM)-tubulin complex, when incubated with vinblastine or CTR-17 at the same concentration. Unlike vinblastine, CTR-17 reduced the fluorescence of the complex in a dose-dependent manner. To determine the mode of inhibition of the CTR compounds, different concentrations of colchicine were used. For example, 1, 3, 10 and 20 μM CTR-17 decreased the fluorescence of the colchicine (3 μM)-tubulin complex by 44±6%, 59±6%, 65±4% and 74±7%, respectively, and colchicine (5 μM)-tubulin complex by 30±4%, 44±6%, 53±3% and 67±6% (Figure 26A). CTR-20, when bound to tubulin, caused an enhancement of fluorescence at the same wavelength; therefore, the concentration range of CTR-20 was reduced. This may be because CTR-20 binds to the colchicine site more strongly than CTR-17. For example, 0.5, 1.5 and 3.0 μM CTR-20 decreased the fluorescence of the colchicine (3 μM)-tubulin complex by 27±11%, 34±8% and 59±11%, respectively, and colchicine (5 μM)-tubulin complex by 18±7%, 29±10% and 37±8% (Figure 26B). Thereafter, modified Dixon plots (Figures 25C and D) were constructed to determine the inhibition constants (Ki) and the mode of inhibition of the CTR compounds. An intersecting family of lines were obtained in a Dixon plot by plotting 1/F versus the inhibitor concentration (CTR) for each substrate concentration (colchicine).

Figure 26: CTR-17 and CTR-20 bind partially overlapping to the colchicine-binding site

A: CTR-17 and CTR-20 reduces the fluorescence enhancement of different concentrations of colchicine-tubulin complexes. CTR-17/CTR-20-tubulin complexes containing increasing concentrations of CTR-17 or CTR-20 were incubated for 30 min with different concentrations of colchicine, and the fluorescence of the final tubulin complex was determined by exciting the complexes at 360 nm and recording their emissions at 430 nm.

B: Modified Dixon plots for both the CTR compounds show a competitive mode of inhibition and the Ki values were 5.68±0.35 µM and 1.05±0.39 µM for CTR-17 and CTR-20, respectively. F is the fluorescence of the CTR-17- or CTR-20-colchicine-tubulin complexes, and F0 is the fluorescence of the colchicine-tubulin complex. Data are the average of at least four independent experiments.

A

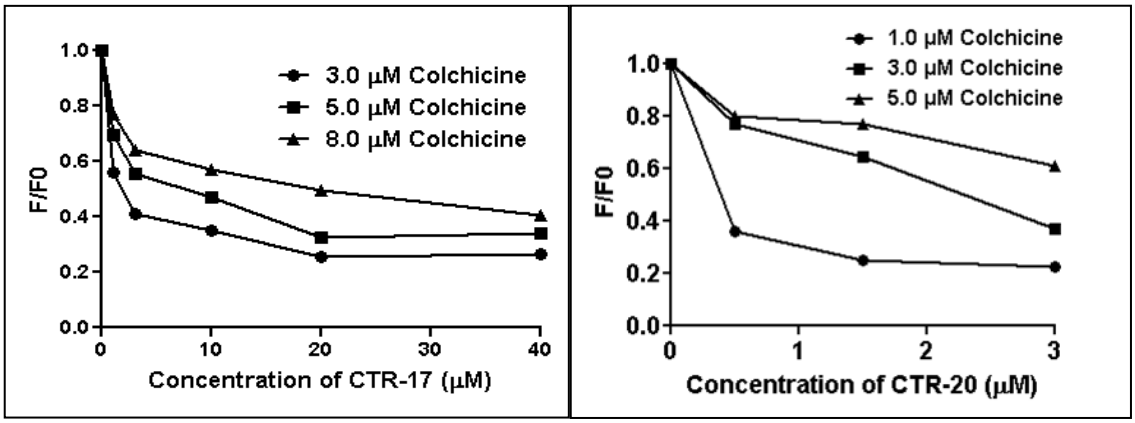
3.0 μM Colchicine
5.0 μM Colchicine
8.0 μM Colchicine
F/F0
Concentration of CTR-17 (μM)
1.0 μM Colchicine
3.0 μM Colchicine
5.0 μM Colchicine
F/F0
Concentration of CTR-20 (μM)

B

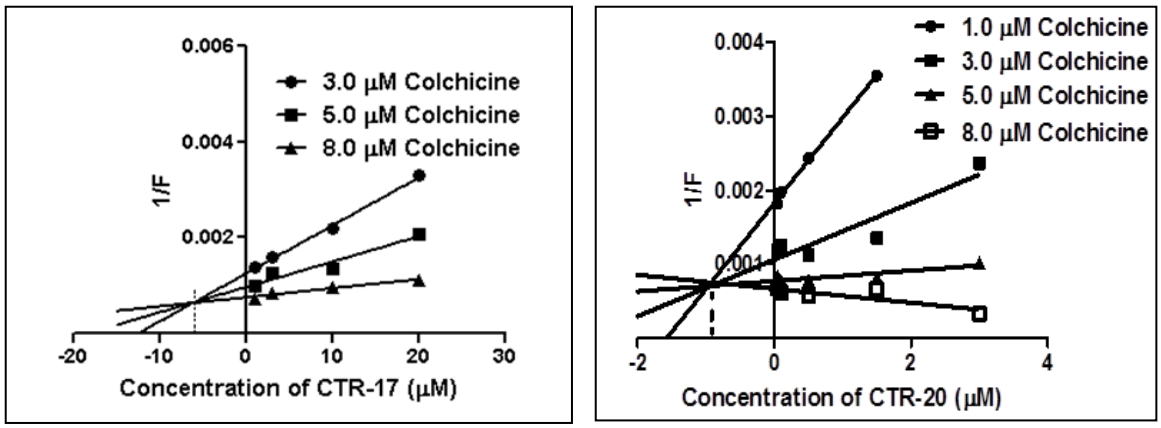
3.0 μM Colchicine
5.0 μM Colchicine
8.0 μM Colchicine
1/F
Concentration of CTR-17 (μM)
1.0 μM Colchicine
3.0 μM Colchicine
5.0 μM Colchicine
8.0 μM Colchicine
1/F
Concentration of CTR-20 (μM)

These lines converge and intersect above the x-axis, which in this case of a competitive inhibitor, and on the x-axis in the case of a non-competitive inhibitor. The value of the inhibitor concentration, where the lines intersect, shows the Ki value. Ki values signify the concentrations of the inhibitor (in this case, CTR compounds) required to cause half of the maximum inhibition (Cornish-Bowden 1974). The mode of inhibition was found to be competitive for both the CTR compounds, and the Ki values were determined to be 5.68±0.35 μM and 1.05±0.39 μM from four independent experiments for CTR-17 and CTR-20, respectively. These values suggest that the concentration of CTR-20 required to inhibit 50% of binding ability of colchicine to tubulin is about five times less than CTR-17, indicating that CTR-20 binds at or near the colchicine site about five times more efficiently than CTR-17.

Computation-based docking study was carried out to provide further evidence in determining the binding site of the CTR compounds. Data from the molecular modeling is consistent with the conclusion that CTR-17 and CTR-20 interact with tubulin at close proximity to the colchicine-binding site. These two chalcone derivatives embed well within the colchicine binding pocket and are stabilized by both covalent and non-covalent interactions (Figure 27). There are 10 amino acids commonly found surrounding both colchicine and CTR-20 (Figure 27, red squares), 19 amino acids surrounding both colchicine and CTR-17 (Figure 27, yellow squares) and 10 amino acids surrounding both CTR-17 and CTR-20 (Figure 27, blue squares).

Figure 27: Docking poses of CTR-17 and CTR-20 at the colchicine-binding site

Interactions between tubulin heterodimer (PDB code: 1SA0) and colchicine (A), CTR-20 (B), and CTR-17 (C) are shown in 3D pattern in the left panels. 2D ligand interaction diagrams show the bonds and amino acids within a distance of 4 Å to colchicine (A'), CTR-20 (B') and CTR-17 (C'). There are three hydrogen (H) bonds between the tubulin and colchicine, and two and one H bonds between tubulin and CTR-20 and CTR-17, respectively. Green arrow denotes that the H bond is formed via the side chain, and the blue arrow via the backbone of the amino acid. A number of hydrophobic and polar residues show overlap in colchicine and two CTR compounds' docking images. Amino acids which are common to colchicine and CTR-20 are within red boxes, amino acids common to colchicine and CTR-17 are in yellow boxes, and amino acids that are common to CTR-17 and CTR-20 are in blue boxes. Polar residues are shown in pink and hydrophobic resides in green. Basic residues contain a blue ring and acidic residues a red ring. Atoms in the ligand surrounded by a blue cloud indicates the surface area of the ligand atoms exposed to the solvent, and light blue clouds around the amino acid residues denote the strength of the interaction. The dotted lining indicates the steric possibility of a methyl group substitution and the dotted lining is broken if the ligand is close to a fully exposed atom.

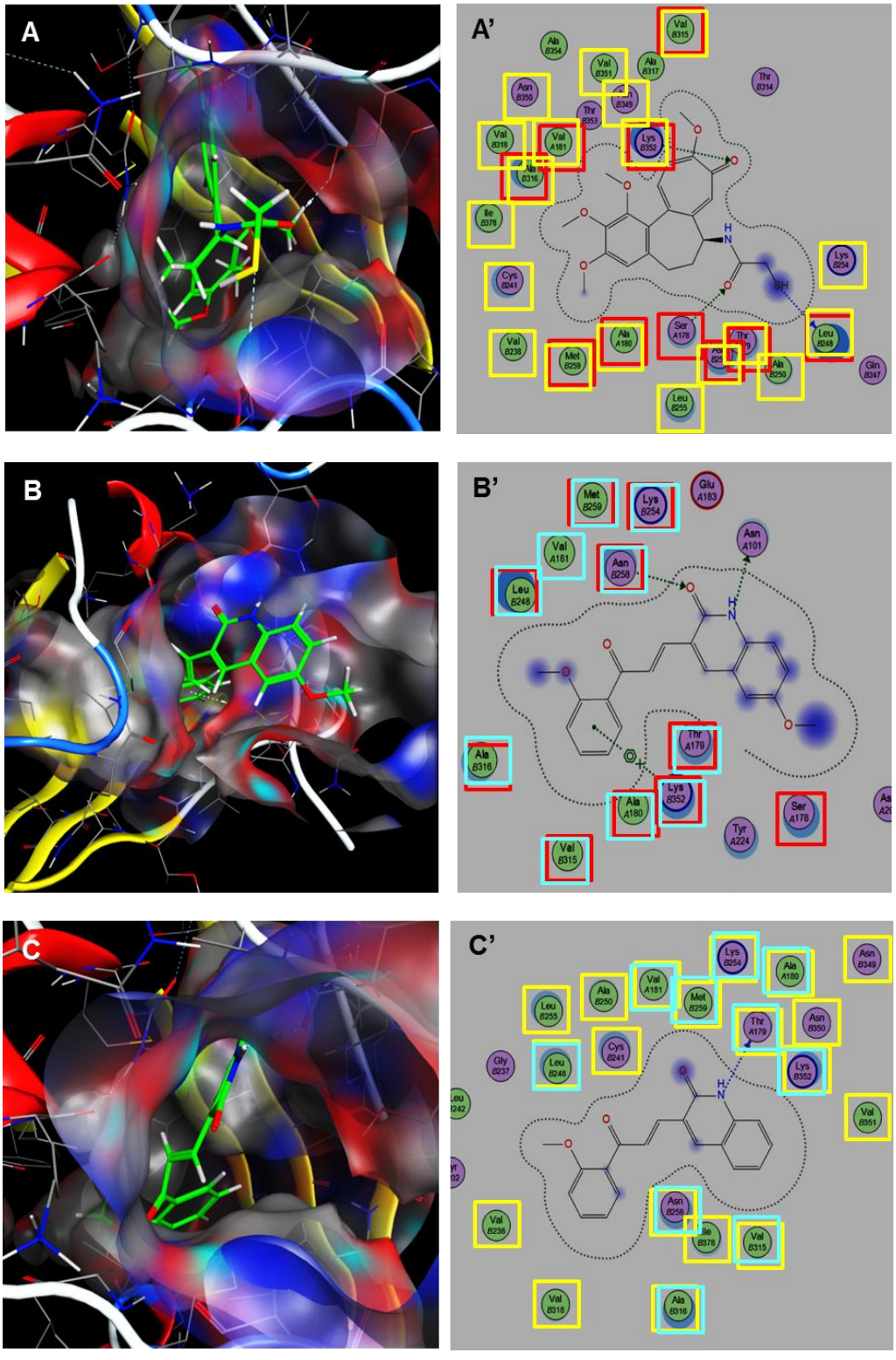
A
A'
B
B'
C
C'

There are three hydrogen bonds between the tubulin and colchicine. The direction of the arrows suggests that colchicine is the donor of one hydrogen (H) bond and the tubulin moiety is the donor of the other two hydrogen bonds. The green arrows indicate that the H bonds are formed with the side chains of the amino acid residues and the blue arrow shows that it is formed with its backbone (Deschênes & Sourial 2007). CTR-20 forms two H bonds and an arene-cation interaction with the tubulin moiety. CTR-20 is the donor of one H bond and tubulin donates the other H bond and both are formed with the side chains of the amino acid residues. CTR-17 is the donor of the single H bond that is formed with the back bone of the amino acid. Surrounding amino acids in the ligand interactions are within 4 Å distance and stabilizes the interaction between each compound and the tubulin moiety by Van der Waals forces.

In spite of striking differences in the structures of colchicine, podophyllotoxin and the two CTR compounds, all of these compounds can occupy the same binding pocket within the tubulin moiety as demonstrated by the overlapping docking images (Figure 28).

3.7 Specificity of CTR compounds in preferential cancer cell killing is neither due to a shorter doubling time of cancer cells nor differences in cell permeability

To determine if the cancer-cell specificity of the CTR compounds is due to the shorter doubling times of cancer than non-cancer cells, the doubling times of four cancer cell lines and two non-cancer cell lines were determined.

Figure 28: CTR-17 and CTR-20 overlap colchicine and podophyllotoxin-binding sites

A: The overlap of tubulin-bound colchicine (blue), CTR-17 (green), CTR-20 (magenta), podophyllotoxin (yellow) and vinblastine (red) in the 3D X-ray structure of tubulin (PDB code: 1SA0).

B: The structures of colchicine (blue), CTR-17 (green), CTR-20 (magenta) and podophyllotoxin (light red) are shown to aid the visualization of the overlap when bound to tubulin.

A

Colchicin CTR-17 CTR-20
Podophyllotoxin Vinblastine

B

Colchicine
CTR-20
CTR-17
Podophyllotoxin

The differences in doubling times, determined from the growth curves of each cell line (Figure 29) are not found to be justifying the preferential cancer cell killing of the CTR compounds (Table 5). The two non-cancer cell lines that were used for the study were (1) 184B5, a chemically transformed, immortalized, non-malignant breast cell line, and (2) MCF10A, which is a non-tumorigenic breast epithelial cell line. As summarized in Table 6, the doubling times of HeLa, MDA-MB231, MDA-MB468, Hek293T, MCF10A, and 184B5 were 24 h, 25 h, 39 h, 16 h, 20 h and 26 h respectively. These doubling times are similar to those previously determined by others. For example, the doubling times for HeLa, MDA-MB231, MDA-MB468, Hek293T, MCF10A and 184B5, according to previous publications were about 24 h (Rahbari et al. 2009), 28 h (Limame et al. 2012), 48.5 h (Iyer et al. 2013), 16-20 h (Kamei et al. 2011), 26 h (Molitor & Traktman 2013) and 18 h (Zajchowski et al. 1993), respectively.

To determine if the doubling times reflect the cytotoxicity caused by the CTR compounds in different cell lines, linear regression analysis was performed (Dariolli et al. 2013). The results showed that there was no relationship between the doubling times of the cell lines and the cytotoxicity caused by CTR-17 and CTR-20. When the degree of cytotoxicity of CTR-17 or CTR-20, expressed as the Mean IC_{50} values were plotted against the doubling times of different cell lines, the slopes of the regression line, R^2 values, and the p values were -0.044, 0.041, and 0.701 for CTR-17 and -0.009, 0.007, and 0.878 for CTR-20 respectively (Figure 30).

Figure 29: The difference in doubling times in cancer and non-cancer cells do not justify the cancer cell specificity of the CTR compounds
Proliferation curves of HeLa, MDA-MB231, MDA MB-468, Hek293T, 184B5 and MCF10A show the essential features of a typical growth curve that includes a lag phase, an exponential log phase and a stationary phase.

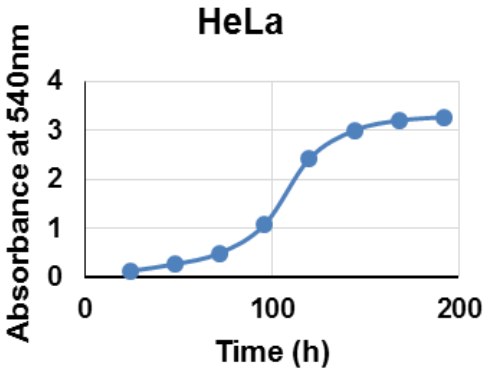
HeLa
Absorbance at 540nm
0
1
2
3
4
0
100
200
Time (h)

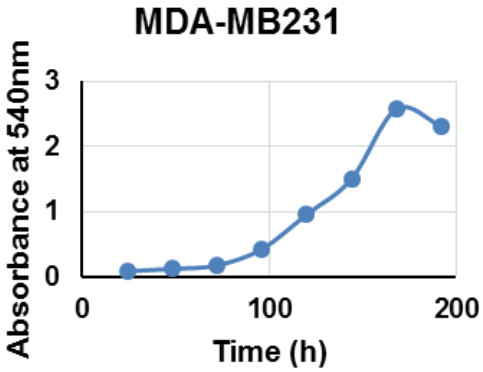
MDA-MB231
Absorbance at 540nm
0
1
2
3
0
100
200
Time (h)

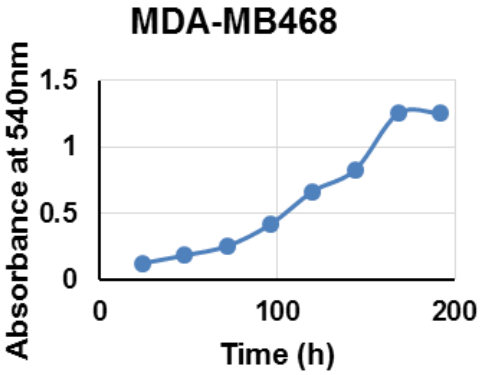
MDA-MB468
Absorbance at 540nm
0
0.5
1
1.5
0
100
200
Time (h)

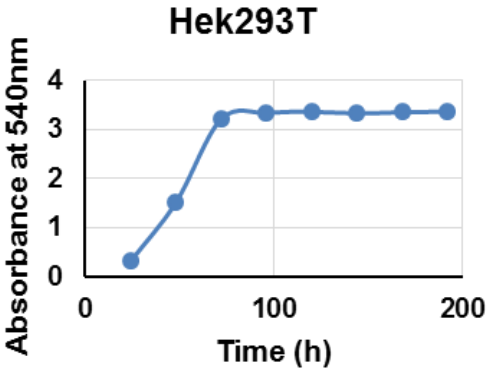
Hek293T
Absorbance at 540nm
0
1
2
3
4
0
100
200
Time (h)

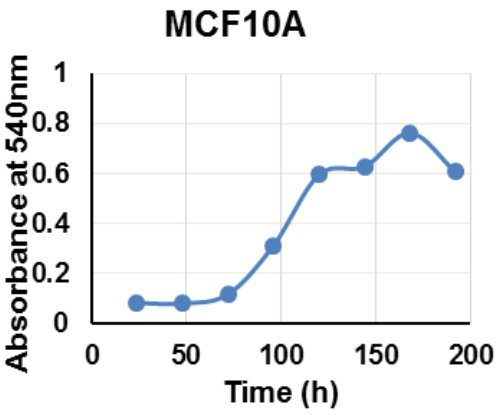
MCF10A
Absorbance at 540nm
0
0.2
0.4
0.6
0.8
1
0
50
100
150
200
Time (h)

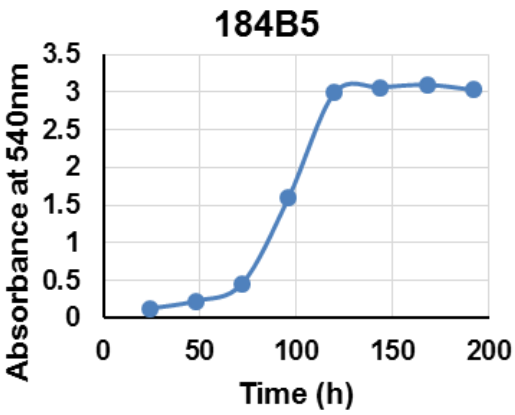
184B5
Absorbance at 540nm
0
0.5
1
1.5
2
2.5
3
3.5
0
50
100
150
200
Time (h)

Table 5: IC_{50} values of CTR-17 and CTR-20

	HeLa	MDA-MB231	MDA-MB468	Hek293T	184B5	MCF10A
CTR-17	0.33±0.06[a]	0.41±0.02	0.15±0.33	0.42±0.07	3.49±0.03	3.95±0.14
CTR-20[c]	0.10±0.02	0.12±0.09	0.12±0.02	0.19±0.00	1.24±0.06	2.37±0.21

[a] Numbers are IC_{50} values in µM, determined by SRB assays as described in Table 1.

Table 6: Doubling times of cancer and non-cancer cells

	Doubling time (h)					
	HeLa	MDA-MB231	MDA-MB468	Hek293T	184B5	MCF10A
Trial 1 (Trypan blue)	19.52	25.18	ND[a]	ND	17.62	21.3
Trial 2 (SRB)	21.12	21.67	37.32	18.51	21.24	22.59
Trial 3 (SRB)	31.81	26.61	40.8	12.69	21.09	35.15
Mean ± SEM	24.2±3.9	24.5±1.5	39.1±1.7	15.6±2.9	19.9±1.2	26.4±4.4

[a] ND, not determined.

Figure 30: Cytotoxicity caused by CTR compounds is not related to the doubling times of different cells

A: Linear regression analysis of the mean IC_{50} values of CTR-17 and the doubling times of different cell lines.

B: Linear regression analysis of the mean IC_{50} values of CTR-20 and the doubling times of different cell lines.

A

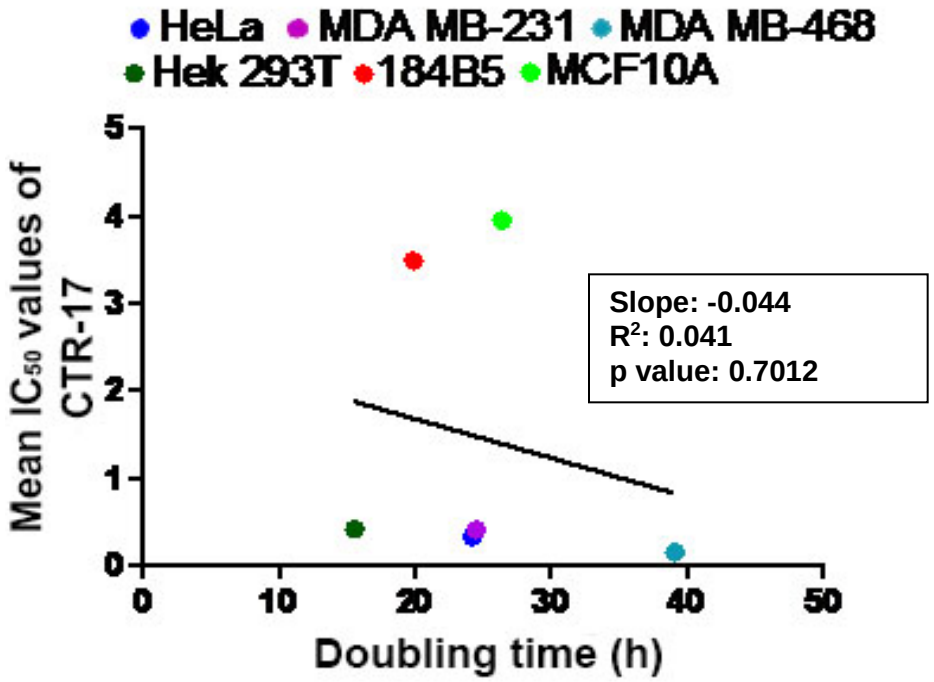
HeLa
MDA MB-231
MDA MB-468
Hek 293T
184B5
MCF10A
Mean IC50 values of CTR-17
Doubling time (h)
Slope: -0.044
R2: 0.041
p value: 0.7012

B

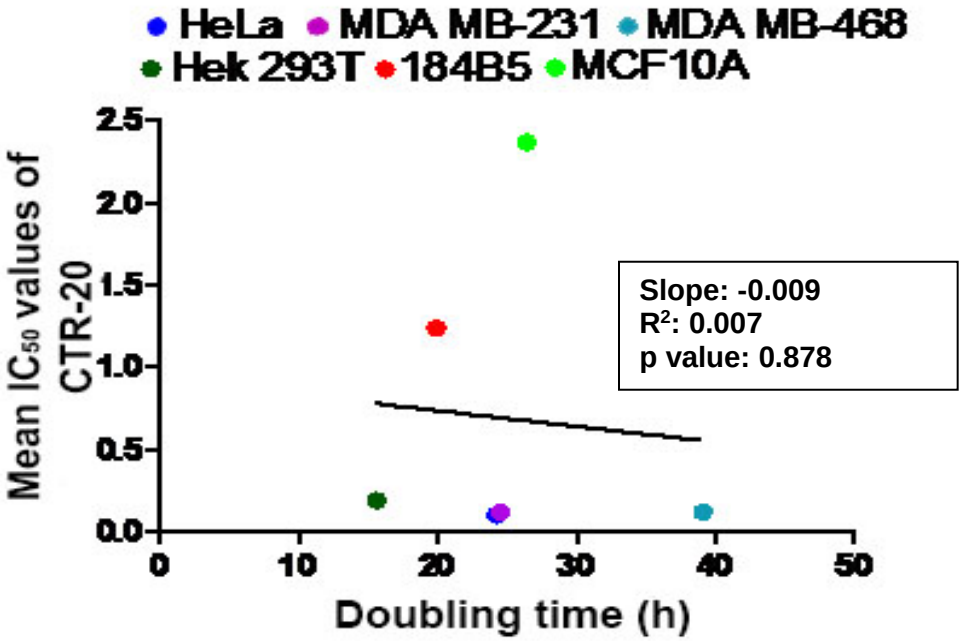
HeLa
MDA MB-231
MDA MB-468
Hek 293T
184B5
MCF10A
Mean IC50 values of CTR-20
Doubling time (h)
Slope: -0.009
R2: 0.007
p value: 0.878

The negative slopes suggest that the mean IC_{50} values increase, while the doubling time decreases and vice versa. However, if at all the doubling times and cytotoxicity were related, we would expect the faster growing cells (lower doubling times), such as 184B5 and Hek293T to be more responsive to the drugs (lower IC_{50} values) than the slower replicating cells, like MDA-MB468. This is because CTR compounds are MT inhibitors and highly proliferating cells would be more susceptible to these agents as MT organization is crucial for mitosis (Stanton et al. 2011). However, the IC_{50} values show that this was not the case, as 184B5 cell line was one of the more resistant cell lines to both CTR-17 (3.49 µM) and CTR-20 (1.24 µM) as compared to slower growing MDA-MB468 (CTR-17:0.15 µM and CTR-20:0.12 µM).

The R^2 value determines if the values in X and Y axes follow a linear relationship. When the R^2 value is closer to 1, this suggests that the values fall on straight line with no random scatter, however when R^2 value is closer to 0, this suggests that that values in X and Y axes are not related. The R^2 values for both CTR-17 (0.044) and CTR-20 (0.007) suggest that the mean IC_{50} values and the doubling times are not related. The p value determines the probability of values to lie on a regression line away from the horizontal, the null hypothesis being that the overall slope equals zero (no linear relation between X and Y axes). The p values, in both CTR-17 (0.701) and CTR-20 (0.878) indicates that the slopes are not significantly deviating from a zero slope, indicating a poor goodness-of-fit and

no relation between the doubling times and the levels of cytotoxicity by both the CTR compounds (Dariolli et al. 2013).

Since the doubling times were not distinctly different between cancer and non-cancer cells, the differences in permeability of cancer (MDA-MB231) and non-cancer (184B5) cell line to CTR-17 were evaluated. Both the cell lines were exposed to 3.0 µM CTR-17 and harvested at the scheduled time points. The intracellular concentration of CTR-17 was then determined in the cell lines using HPLC and expressed as the area of CTR-17 peak per µg of protein in each cell line (Figure 31). In sham-treated cells and at 0 h, there was no CTR-17 found in both types of cells. When cells were incubated for longer periods of time, the amount of CTR-17 (area of the peak per µg of protein) was 14.57, 18.02, and 20.41 at 6 h, 12 h, and 24 h respectively, in 184B5 cells and 13.13, 13.98, and 17.93 at 6 h, 12 h, and 24 h in MDA MB-231 cells. Hence, there was no significant difference in the concentration of CTR-17 within both the cell types. This may be because CTR-17 is a small molecule with molecular weight of 305.33 kDa, hence, apparently there is no differential permeability between cancer and non-cancer cells. Interestingly, 184B5 cells were actually slightly more permeable to CTR-17 than MDA-MB231 cells. However, the degree of cytotoxicity and mitotic arrest, caused by CTR compounds is clearly distinct among the cancer and non-cancer cells. Therefore, the mechanism of preferential cancer cell killing by CTR-17 and CTR-20 is still to be elucidated.

Figure 31: The intracellular concentration of CTR-17 does not correlate with the specificity of CTR compounds

A: HPLC profile of CTR-17 (0.5 mg/ml) standard at retention time of 5.88 min. HPLC conditions included an injection volume of 5.0 µl of the CTR-17 into an ultra C18 column (4.6 mm X 150 mm, 3.0 µm). Detection at 350 nm for 10 min. Mobile phase consisted of an isocratic system of methanol to water at a ratio of 70:30 (v/v) with a flow rate of 0.75 ml/min.

B: The intracellular concentration of CTR-17, represented here as the area of the peak/µg of protein, is not significantly different between MDA-MB231 and 184B5 cells. Both cell lines were treated with 3.0 µM CTR-17 for the scheduled time points. Cells were washed twice, harvested and lysed with lysis buffer and sonication. The proteins were then precipitated out from the extracts and filtered before performing HPLC.

C: The bar graphs show that the intracellular concentration of CTR-17 is not significantly different between MDA-MB231 and 184B5 cells ($p>0.05$, using an unpaired t-test). Data presented in the bar graphs are mean ± SEM of two independent experiments.

A

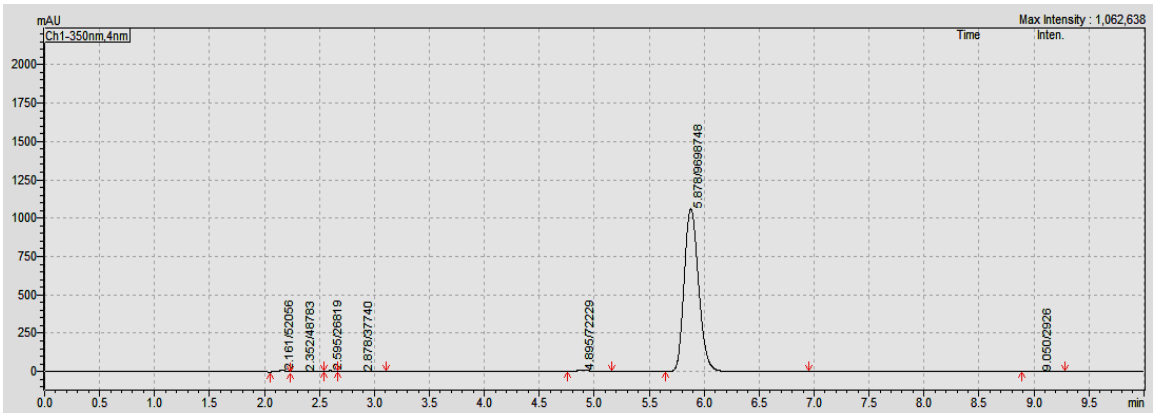
mAU
Ch1-350nm,4nm
Max Intensity : 1,062,638
Time
Inten.
2000
1750
1500
1250
1000
750
500
250
0
2.161/52056
2.352/48783
2.595/26819
2.878/37740
4.895/72229
5.878/99698748
9.050/2926
0.0 0.5 1.0 1.5 2.0 2.5 3.0 3.5 4.0 4.5 5.0 5.5 6.0 6.5 7.0 7.5 8.0 8.5 9.0 9.5 min

B

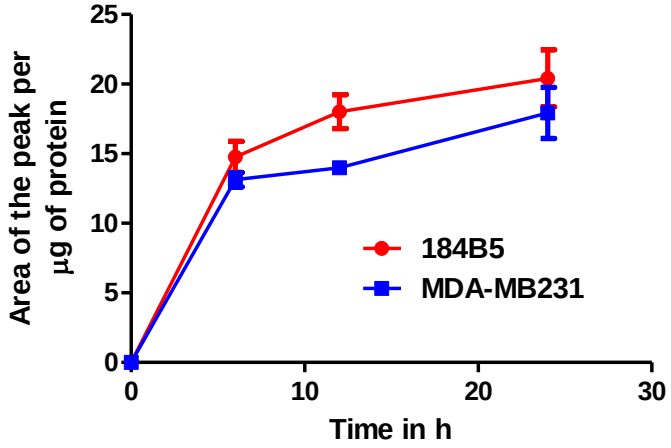
Area of the peak per µg of protein
25
20
15
10
5
0
0
10
20
30
Time in h
184B5
MDA-MB231

C

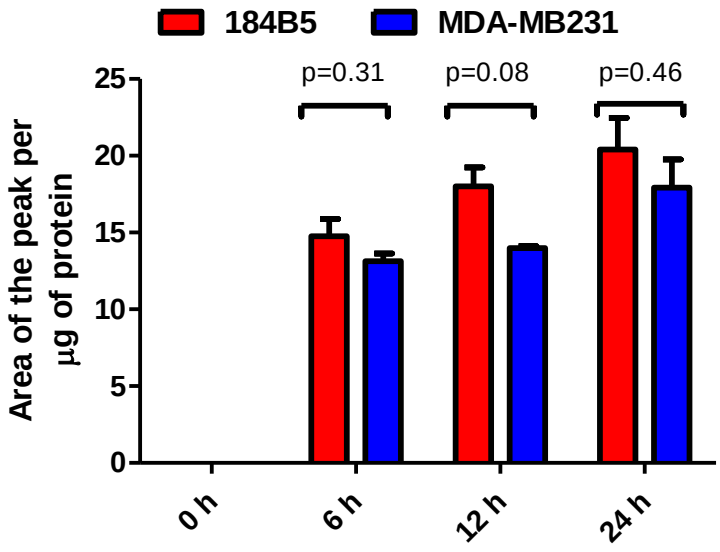
184B5
MDA-MB231
p=0.31
p=0.08
p=0.46
Area of the peak per µg of protein
25
20
15
10
5
0
0 h
6 h
12 h
24 h

3.8 CTR compounds do not radiosensitize T98G cells

Temozolomide (TMZ)-based chemotherapy along with neurosurgery has proven to be successful in the treatment of glioblastoma multiforme (GBM) (Huang et al. 2012). However, resistance to this treatment occurs in some patients. TMZ is an alkylating agent that methylates several residues including N7 of guanine, N3 and O6 of adenine. The O6 methylation is repaired by the enzyme, MGMT. Increased expression of MGMT levels is associated with resistance to TMZ (Montaldi & Sakamoto-Hojo 2013; Bobola et al. 1995). The combinatorial effects of CTR compounds and X-ray radiation were assessed using three different concentrations of CTR-17 and CTR-20. To establish a lesser toxic combinatorial regimen, the IC_{50} concentrations and two more concentrations below it were used, for each compound against the T98G cells.

The surviving fractions show that T98G cells are not radiosensitized by both CTR-17 and CTR-20 (Figure 32). When radiation was used in the absence of any drug, the surviving fractions were 100%, 80%, 85%, 77%, 51% and 39% for 0, 2, 4, 6, 8 and 10 Gy, respectively. When cells were treated with both radiation and CTR-17, the cell viability showed no considerable change, in comparison to radiation alone. For example, in the presence of 0.05 µM CTR-17 with 0, 2, 4, 6, 8 and 10 Gy, the survival fractions were 103%, 82%, 84%, 79%, 61% and 39%, respectively. In the presence of 0.2 µM CTR-17 with 0, 2, 4, 6, 8 and 10 Gy, the cell viability was 101%, 86%, 87%, 83%, 57% and 39%, respectively.

Figure 32: CTR compounds do not radiosensitize T98G cells
The combination of three different CTR-17 (A) and CTR-20 (B) concentrations with increasing doses of radiation introduces no enhanced therapeutic benefit in comparison to each treatment modality alone. T98G cells were cultured in 96-well plates and co-treated with three different concentrations of CTR compounds and five different doses of radiation (2-10 Gy). SRB assays were performed after 72 h. Data presented in the bar graphs are mean ± SEM of two independent experiments.

A

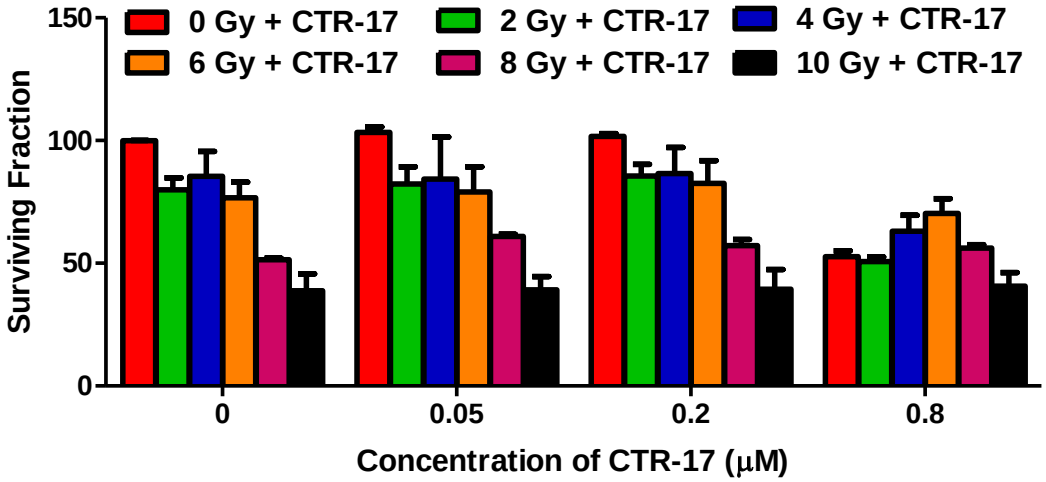
0 Gy + CTR-17
2 Gy + CTR-17
4 Gy + CTR-17
6 Gy + CTR-17
8 Gy + CTR-17
10 Gy + CTR-17
Surviving Fraction
150
100
50
0
0
0.05
0.2
0.8
Concentration of CTR-17 (μM)

B

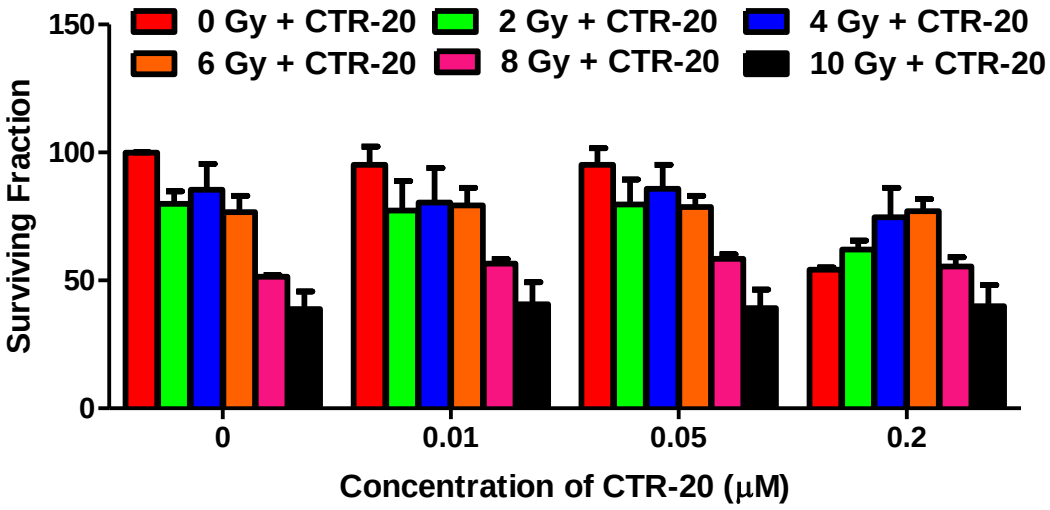
0 Gy + CTR-20
2 Gy + CTR-20
4 Gy + CTR-20
6 Gy + CTR-20
8 Gy + CTR-20
10 Gy + CTR-20
Surviving Fraction
150
100
50
0
0
0.01
0.05
0.2
Concentration of CTR-20 (μM)

In the presence of 0.8 µM CTR-17, which is the IC_{50} for T98G cells, the cell viability in combination with 0, 2, 4, 6, 8 and 10 Gy was 53%, 51%, 63%, 70%, 56% and 41%, respectively.

In addition, the use of CTR-20 together with radiation also did not induce any considerable changes to percentage cell survival. For example, in the presence of 0.01 µM CTR-20 with 0, 2, 4, 6, 8 and 10 Gy, the survival fractions were 95%, 77%, 80%, 79%, 57% and 41%, respectively. In the presence of 0.05 µM CTR-20 with 0, 2, 4, 6, 8 and 10 Gy, the cell viability was 95%, 80%, 86%, 79%, 58% and 39%, respectively. In the presence of 0.2 µM CTR-20, which is the IC_{50} for T98G cells, the cell viability in combination with 0, 2, 4, 6, 8 and 10 Gy was 54%, 62%, 75%, 77%, 55% and 40%, respectively.

Together, the data from the combination studies show that both CTR-17 and CTR-20 do not radiosensitize the T98G cells. In fact, when the surviving fractions are closely analysed for the combinations, in comparison to radiation and drug alone, there is a slight inhibitory effect when both the modalities are used in combination. This may be because radiation causes a G2 phase arrest (Sui et al. 2012; Sui et al. 2004) which subsequently abrogates the cytotoxicity of CTR compounds that is functional at mitosis as both CTR-17 and CTR-20 are MTAs.

4.0 Discussion

4.1 Cancer-cell specific cytotoxicity of CTR compounds

Four CTR compounds were initially short-listed from a series of 75 chalcone-based derivatives by preliminary cytotoxicity screening performed at the Lee Lab. Further studies showed that CTR-17 and CTR-20 inhibited the growth of cancer cells 10-25 times more effectively than non-malignant cells (Table 1). In addition, Western blot analysis using an anti-PARP antibody showed that CTR-17 induced cell death by 48 h post-treatment in HeLa cells but not in 184B5 non-cancer cells (Figure 11). As cancer-cell specific cytotoxicity is a highly desirable property for the success of anticancer drugs, extensive evaluations on the functional mechanisms were carried out as a part of my PhD research project.

Previous studies have recognised the value of chalcones and their derivatives as potential anticancer agents. Several different modes of action by chalcone derivatives have been identified including their ability to inhibit MT polymerization and angiogenesis, initiation of apoptosis, and overcoming MDR phenotype (Ducki 2007). JAI-51 (*N*-methyl indolyl chalcone), a novel chalcone derivative, was shown to possess anti-proliferative effects on one murine and four glioblastoma cell lines (Boumendjel et al. 2009). JAI-51 inhibits MT polymerization with an added benefit of inhibiting Pgp and MRP drug efflux pumps (Boumendjel et al. 2009). However, at least 10 µM JAI-51 needs to be used to induce an effective decrease in the proliferation of these cells (Boumendjel et al. 2009), which is approximately 33-100 fold higher in concentration than the effective concentration of the CTR compounds. Modzelewska et al. (2006) evaluated the selective cytotoxic ability of a series of

chalcones and bis-chalcones with boronic acid moieties, and found 4-6 fold selectivity against breast cancer cells (MDA-MB 231 and MCF-7) over non-cancer breast cell lines (MCF10A and MCF12A) (Modzelewska et al. 2006). Since the discovery of chalcones as potential anti-cancer agents in 1970s (Edwards et al. 1990), the specificity towards certain cancer cells and their selectivity towards malignant cell lines have been broadly studied.

When considering cell cycle-specific anticancer therapy, anti-mitotic agents including paclitaxel and vinblastine are recognised as the most successful drugs, partly due to their specific interference of the mitosis with minimal effects on non-dividing and quiescent cells (Chan et al. 2012) . However, MTs play an important role in different stages of cell cycle, including interphase functions such as axonal transport, vesicular trafficking and maintenance of cell shape. Therefore, MTAs often render side effects such as myeloid and neurotoxicity due to their damage to non-proliferating cells (Schmidt & Bastians 2007). Other anti-mitotic agents such as kinase inhibitors (Chk1/2, Cdk1, Aurora A, B, C and Plk1 inhibitors) and anti-motor proteins (Eg5 and CENP-E inhibitors) have been extensively studied. However, data from clinical trials show that these agents do not meet their initial promises (Chan et al. 2012). This may be because: (1) they are active against cells only in mitosis and tumor cells residing in interphase are not responsive to the cell-killing effects of the drugs; and (2) in patients, the doubling time of tumor cells is much longer (about 300 days and 700 days for solid and hematopoietic carcinomas, respectively) than cell lines or animal models (about 1-6 and 1-7

days, respectively) (Chan et al., 2012; Komlodi-Pasztor, Sackett, & Fojo, 2012). Therefore, the success of drugs like paclitaxel is partly attributable to their adverse effects on cells in interphase. Hence, an ideal drug would be: (1) cancer-cell specific by differential permeability or specific target of action (eg: monoclonal antibodies) ; and (2) active against vulnerable cell cycle stages (eg: mitosis) of proliferating cells, in order to avoid dose-limiting toxicities to the normal tissues.

The chalcone derivatives, CTR-17 and CTR-20 are less effective against immortalized non-cancer cells (184B5 and MCF10A) as compared to the cancer cells hence satisfies one of the requirements for a desirable drug. Secondly, they are agents that interfere with the process of mitosis as outlined subsequently, hence identifying CTR-17 and CTR-20 as potentially safe and more effective anticancer therapeutics.

4.2 CTR-17 and CTR-20 display potent cytotoxicity towards cell lines overexpressing MDR or MRP

Drug resistance is one of the major causes of chemotherapy failures and prolonged exposure to a single chemotherapeutic agent often results in the emergence of simultaneous resistance towards several different chemotherapeutic agents, leading to a phenomenon known as multidrug resistance (MDR) (Gottesman et al. 2002). MDR is usually induced by proteins that belong to the ABC (ATP-binding cassette) transporter family, including:

- ABCB1, p-glycoprotein (Pgp) or MDR1

- ABCC1 or MDR associated protein-1 (MRP1)
- ABCG2 or breast cancer resistance protein (BCRP)
- ABCC2, MRP2 or cMOAT

To determine if CTR-17 and CTR-20 overcome MDR, their cytotoxic properties were evaluated using KB-C2, an ABCB1 overexpressing cervical carcinoma cell line and H69AR, an ABCC1 overexpressing small cell lung cancer cell line. KB-C2 cell line was at least 15-fold more resistant to both colchicine and vinblastine and more than 10-fold resistant to paclitaxel in comparison to the parental cell line (KB-31). In contrast, both CTR-17 and CTR-20 induced cytotoxicity with equal potency to both KB-31 and KB-C2. Both CTR-17 and CTR-20 were also effective against H69AR cells (Figure 9). A technical problem faced was that the parental H69 cells were always aggregated during cell culturing, making it difficult to accurately count cell numbers. To overcome this problem, another small cell lung cancer cell line (SW 1271) was used to compare cytotoxic results of H69AR. It is evident that CTR compounds overcome MDR, suggesting that these compounds may not be substrates for aforementioned drug efflux proteins.

Although the discovery of compounds with a specific target has been the ultimate goal of anticancer therapy, there are drawbacks associated with this approach (Zhang et al. 2014). The emergence of acquired resistance and dose-limiting side effects, limits the continuous application of single drugs (Sams-Dodd 2005). Hence, combinations of drugs may provide better results (Lehár et al. 2009).

Therefore, the combination of CTR compounds with paclitaxel was explored to improve efficacy and overcome MDR (Figure 10). The concentration of the drugs used was less than for each drug alone and showed an effective anti-proliferative effect. The CI values for six different ratios of CTR compounds to paclitaxel were between 0.71-0.87, for CTR-17 with paclitaxel and 0.69-0.95, for CTR-20 with paclitaxel. According to previously published reports, all these combinations provide synergistic effects as the CI values are below 1 (Chou 2006). Hence, each drug could be used at a lower dose to overcome the toxic side effects caused by single drugs at high doses, even in the drug-resistant KB-C2 cells.

4.3 CTR-17 is a specific anti-mitotic compound

Data from flow cytometry profiles showed that CTR-17 treatment for 72 h caused a G2/M arrest of 71.6, 61.4 and, 67.4% in HeLa, Hek293T and MDA-MB231 respectively (It was later found by microscopy and Western blot analysis that the arrest point is actually prometaphase-see below). All of these cells eventually underwent cell death. For MDA-MB468, the cells accumulated in G2/M phase starting from as early as 6 h, and then underwent a massive cell death after 48 h of treatment. However, in 184B5 non-cancer cells, only about 25% of cells underwent cell death, and the remaining cells progressed a normal cell cycle (Figure 12).

The G2/M arrest observed during CTR-17 treatment may actually be; (1) a G2 arrest that allows time to repair DNA damage before entering into mitosis, or (2) a mitotic arrest caused by an aberrant spindle formation (DiPaola 2002). To

determine if CTR-17 treatment causes DNA damage or affects DNA replication, γH2AX staining and EdU labelling experiments were used. In comparison to etoposide, which is a topoisomerase II inhibitor (Baldwin & Osheroff 2005), CTR-17 did not cause any DNA damage as any γH2AX foci were not observed. CTR-17 was also not an impediment to DNA replication as no noticeable difference was found in EdU labelling patterns in sham *vs* CTR-17-treated cells (Figure 13). Hence, the possibility of a G2 arrest in response to CTR-17 was partially ruled out. Western blot analysis further confirmed a mitotic arrest and an inhibition of mitotic exit. However, mitotic entry was not impeded (Figures 14 & 17). Further studies showed that CTR-17 treatment arrests the cells in mitosis via the prolonged activation of the spindle checkpoint (Figure 18), thereby delaying mitotic exit by the inhibition of anaphase promoting complex/cyclosome (APC/C) ubiquitin ligase activity (Zeng et al. 2010). Previous reports showed that anti-mitotic agents, especially the MTAs, cause cell death by inducing a prominent mitotic arrest via the activation of the spindle checkpoint. It is also suggested that if the mitotic arrest is less than 15 h, the cells manage to escape mitosis, leading to several other fates (Bekier et al. 2009). In this case, while some cells die in interphase others arrest or even survive by undergoing several cycles of cell division (Gascoigne & Taylor 2008). This phenomenon is observed with aurora kinase inhibitors. The use of an aurora kinase inhibitor, ZM447439, attenuates the SAC, which leads to the degradation of cyclin B, mitotic slippage, and re-replication of genomes (endocycle) (Bekier et al. 2009; Gascoigne & Taylor 2008). Hence, when cells are treated with anti-mitotic agents, the cell fate is

regulated by two competing networks: (1) activation of cell death pathway, and (2) prevention of cyclin B degradation. Each of these networks is governed by a threshold. If cyclin B degrades below the mitotic exit threshold, the cells undergo slippage, however if the cell death threshold is breached first, the cells undergo mitotic catastrophe (Gascoigne & Taylor 2008). CTR compounds, similar to other MTAs cause a prolonged mitotic arrest which in all cases last longer than 20 h as shown previously by the flow profiles and eventually undergoes cell death as indicated by the PARP cleavage.

4.4 CTR-17 and CTR-20 are MT polymerization inhibitors

Additional studies revealed that CTR-17 and CTR-20 disrupt the mitotic spindle by inhibiting microtubule polymerisation. Jordan et al. (1992) studied the effects of MT depolymerizing drugs namely, vinblastine, podophyllotoxin and nocodazole in a concentration-dependent manner. They observed interesting phenotypes associated with their mechanism of action: (a) astral MTs were longer and denser than in control; (b) few chromosomes remained at the spindle poles instead of the metaphase plate; (c) mitotic spindles were shorter than untreated cells; and, (d) centrosomal materials were more fragmented and diffused (Jordan et al. 1992). Immunofluorescent staining revealed that CTR-17 and CTR-20 cause all of these phenotypes. Therefore, the effects on the MTs were studied with CTR-17 and CTR-20. A microtubule polymerisation assay showed that both CTR-17 and CTR-20 reduced the polymerisation ability of the MTs (Figure 20). The linear segment of the polymerisation curves could be used to calculate the V_{max} values. The V_{max} value for 10.0 µM paclitaxel was 22.8 mOD/min, for G-PEM

buffer 6.1 mOD/min, for 3.0 µM CTR-17 4.4 mOD/min and for both 1.0 µM CTR-20 and 5.0 µM nocodazole, the V_{max} values were 3.7 mOD/min. Hence, paclitaxel has enhanced the V_{max} of the reaction by ~4 fold and CTR compounds and nocodazole reduced the V_{max} value by ~1.5-2.0 folds relative to the buffer control. Therefore, it was concluded that CTR compounds are MT polymerisation inhibitors.

Cell treated with CTR-17 were unable to form a normal bipolar mitotic spindle and the inter-polar distance between the centrosomes were approximately 35% shorter than in the sham-treated HeLa cells. Data from live cell microscopy further supported the cell morphology observed by the fixed cells (Figure 21). CTR-17 treatment led to the formation of an aberrant mitotic spindle, partly because it affects the MT dynamics during mitosis and partly because it reduces the MT polymer mass, which then eventually collapse into a monopolar-like spindle. Differential extraction of polymerised and soluble pools of tubulin further confirmed the ability of the CTR compounds to inhibit MT polymerization. Paclitaxel (50 nM) enhanced the polymerised pool of tubulin by 90%. In contrast, nocodazole (50 ng/ml) reduced the polymerized pool by 80% and the two CTR compounds by ~50%. Both CTR-17 and CTR-20 also enhanced their depolymerising ability in a dose-dependent manner. Further, the phenomenon was observed in two other cell lines, namely MDA-MB231 and MDA-MB468, suggesting that the MT depolymerizing ability of these compounds is a general mechanism in cancer cells (Figure 22).

Numerous reports have shown the involvement of MTs in cell migration, and since cell migration plays a vital role in tumor metastasis, the use of MT inhibitors to prevent cell movement is widely studied (Schwartz 2009; Palmer et al. 2011; Goldman 1971; Vasiliev et al. 1970). CTR-17 not only reduced the degree of wound closure but also reduced the average velocity of the migration of MDA MB-231 cells. These findings strongly agree with previous reports of cell migration inhibition by MTAs such as colchicine and colcemid (Goldman 1971; Vasiliev et al. 1970). Additional studies showed that inhibition of cell locomotion is not necessarily due to the reduction of the MT polymer mass but due to the poor dynamics of MTs (Yang et al. 2010). Another study by the same group showed the involvement of MTs in cell migration using a simplified model (Ganguly et al. 2012). The authors' observations are summarized below. (1) In a normally migrating cell, lamellipodia occurs in random directions. In the presence of chemotactic signals, MT dynamics are suppressed in a particular region of the cells, causing MT stabilization and disruption of the lamellipodia retraction, which then allows the establishment of lamellipodia in the leading edge of the cells. MTs directed towards the forward direction of the cells aid in the feeding of the cells' leading edge via the distribution of vesicles. These MTs are higher in density but lower in their dynamicity. However, MTs at the trailing end of the cell are more dynamic and undergo rapid remodeling, which will allow the cell to retract the tail of the cell, allowing the cell to move in the forward direction. This cellular polarity permits the cells to either move along a chemical gradient or even during wound closing process. (2) In the presence of drug in low

concentrations, MT dynamics are abrogated globally; hence, the MTs towards the trailing edge of the cell are less capable of remodelling. This causes the cells to polarize but are not able to retract their trailing edge, disrupting the forward migration of the cell. (3) In the presence of drug at high concentrations, MTs are completely eliminated. Nevertheless, there are short-lived lamellipodia and cells can move in the directionless fashion.

Therefore, in the presence of MTAs such as CTR-17, cell motility can either be completely abrogated or directionless, suggesting a possible role of CTR compounds in suppressing tumor metastasis (Figure 23).

4.5 The binding sites of CTR-17 and CTR-20 to tubulin largely overlap with that of colchicine-binding site

The goal was then to determine if CTR compounds directly bind to tubulin protein by fluorescence microscopy. Fluorescence microscopy is one of the most sensitive approaches to evaluate the properties of different biological systems based on the changes incurred by various structural and molecular properties (Guha et al. 1996). Each tubulin dimer consists of eight tryptophan residues which emits an intrinsic fluorescence when excited at 295 nm. The presence of a ligand that binds to tubulin may directly cause the quenching of the intrinsic fluorescence, which could be used as a probe to determine the binding constant (Bhattacharyya et al. 1993). CTR-17 and CTR-20 reduced the intrinsic tryptophan fluorescence of tubulin, and the K_d values were found to be 4.58±0.95 μM and 5.09±0.49 μM for CTR-17 and CTR-20, respectively, indicating that CTR

compounds directly bind to tubulin (Figure 24). CTR-17 and CTR-20 bind to tubulin with stronger affinity than other MTAs such as vinblastine (K_d of 43 µM) (Lee et al. 1975), estramustine (K_d of 30 µM) (Panda et al. 1997) and dolastatin 15 (K_d of 30 µM) (Cruz-Monserrate et al. 2003; Ludueña et al. 1992). However, binding of CTR-17 and CTR-20 is weaker than colchicine which binds with a dissociation constant of 0.5 µM (Panda et al. 1992). This strong affinity of colchicine to tubulin leads to a poorly reversible colchicine-tubulin complex. Hence, the cytotoxic effects caused by colchicine are irreversible, hampering the use of colchicine as a chemotherapeutic agent (Thomas et al. 2014; Dumontet & Jordan 2010). CTR-17 and CTR-20, on the other hand, are reversible mitotic agents as shown in Figure 19. This might be due to: (1) reversible binding of CTR compounds to tubulin; or (2) absence of long-term retention within cells. Hence CTR-17 and CTR-20 may be safer drugs to be used in anticancer therapy.

There are a number of other chalcone derivatives that directly bind to tubulin and their degree of binding varies significantly. For example, JAI-51 (K_d of 5.0 µM) exhibits a similar binding ability to tubulin as the CTR compounds (Boumendjel et al. 2009). However, (*E*)-3-(6-Chloro-2*H*-chromen-3-yl)-1-(3,4,5-trimethoxy phenyl)prop-2-en-1-one, also known as compound 14 (K_d: 9.4 µM) (Aryapour et al. 2012) binds to tubulin with a lower affinity while MDL-27048 (K_d: 0.36 µM) (Peyrot et al. 1992; Peyrot et al. 1989) binds to tubulin with a much higher affinity than the two CTR compounds.

MT polymerisation inhibitors generally interact with tubulin through either the colchicine or vinblastine-binding site (Dumontet & Jordan 2010; Singh et al. 2008). Vinblastine-binding site was initially examined to determine if the two CTR compounds bind to tubulin via the same site, using a fluorescent analogue of vinblastine, BODIPY® FL Vinblastine. When BODIPY® FL Vinblastine binds to tubulin, the fluorescence intensity was enhanced, which was quenched by a compound that binds close to or at the vinblastine-binding site (eg: vinblastine). However, neither the CTR compounds nor colchicine were able to inhibit the fluorescence development of BODIPY® FL Vinblastine-tubulin complex, suggesting that CTR compounds and colchicine do not bind to the vinblastine site. (Figure 25A)

Therefore, the possibility of binding of the two CTR compounds to the colchicine-binding site was then examined. Intrinsic fluorescence of colchicine increases upon forming the tubulin-colchicine complex which could be used as an index to evaluate the competition between colchicine and CTR compounds to bind to the colchicine-binding site (Bhattacharyya & Wolff 1974). Both the CTR compounds dose-dependently quenched the intrinsic fluorescence of the colchicine-tubulin equilibria, suggesting that both CTR-17 and CTR-20 bind at or near the colchicine-binding site. CTR-17 and CTR-20 competitively inhibited the binding of colchicine with a Ki of 5.68±0.35 μM and 1.05±0.39 μM, respectively, as determined by modified Dixon plots. Ki value indicates the degree of potency of

an inhibitor (Burlingham & Widlanski 2003). In this case, the concentration of CTR-20 required to inhibit half of the maximum colchicine binding was approximately five times less than CTR-17 (Figure 26). This suggests that CTR-20 binds to the colchicine site more strongly than CTR-17, which also further assured by docking analysis as is discussed below.

Molecular modeling data revealed that the binding sites of both CTR-17 and CTR-20 on the tubulin largely overlap with that of colchicine or podophyllotoxin, but distinct to the vinblastine-binding site (Figures 27 & 28). In binding, many amino acids are shared among colchicine and the two CTR compounds, according to the prediction of ligand interactions. Hence, it is reasonable to assume that CTR-17 and CTR-20 occupy a site very close to the colchicine-binding site to tubulin. However, the mode of binding may be different among the three compounds. Colchicine forms three H-bonds, and CTR-17 and CTR-20 form only one and two H-bonds, respectively. It is possible that these differences may lead to changes in the efficacy, toxicity and reversibility of colchicine versus the CTR compounds.

4.6 Why are CTR compounds selective towards cancer cells?

To determine the selectivity of CTR compounds, their efficacy on twelve cancer cell lines and two non-cancer cell lines (184B5 and MCF10A) was compared. CTR-17 and CTR-20 were approximately 10-25 fold more selective in killing cancer cells than the non-cancer cells. To probe the mechanism of selectivity of the CTR compounds, the doubling time of different cell lines were evaluated to

examine whether the selectivity is rendered by fast growth. However, the doubling times of cancer and non-cancer cells were largely similar (Figure 29 and Table 6). In addition, linear regression analyses indicated that no relation exists between the cytotoxicity caused by both CTR compounds and the doubling times of different cells (Figure 30). Therefore, cancer cell selectivity of the CTR compounds is not due to differences in cell proliferation rates.

To gain better insight into their cancer cell selectivity, the intracellular concentration of CTR-17 in MDA-MB231 (cancer) and 184B5 (non-cancer) cells (Figure 31) was examined. There was no significant difference in the quantity of CTR-17 in the two different cell lines, suggesting that the permeability of CTR-17 is similar for both cancer and non-cancer cells. Hence the selectivity of the two CTR compounds needs to be further elucidated at this point and requires additional investigation.

4.7 Combination of CTR compounds and radiation shows no improved cytotoxicity

When increasing doses of radiation was administered in combination with both CTR-17 and CTR-20 to T98G cells, there was no enhancement in the cytotoxicity of each treatment modality (Figure 32). In fact, when both the CTR compounds were used at their IC_{50} concentration, in combination with radiation, the cytotoxicity was reduced in radiation doses, 4, 6, and 8 Gy. For example, in the absence of any radiation, 0.8 µM of CTR-17 led to 50% cell viability. When CTR-17 was used at the same concentration in combination with 4, 6, and 8 Gy,

however, the survival fractions increased to 63%, 70% and 56%, respectively. In addition, when 0.2 µM of CTR-20 was used alone, the cell viability was 54%. In contrast, when CTR-20 was at the same concentration in combination with 2, 4, and 6 Gy, the survival fractions increased to 62%, 75%, and 77%, respectively. Therefore, the combination of radiation and CTR compounds show no enhanced cytotoxicity but a slight reduction in efficacy.

The above combinational effect has been previously demonstrated using other microtubule drugs, including paclitaxel and vinblastine. The use of paclitaxel in combination with radiation has shown cell cycle-dependent antagonistic effects (Sui et al. 2004). Further, the combination of vinca alkaloids, including vincristine and vinblastine along with radiation was shown to antagonise the cytotoxic effects in both breast and human epidermoid cancer cells (Sui & Fan 2005). This may be because radiation causes G2 arrest, which is prior to the CTR functional point. Additionally, the presence of UCN-01 which leads to the abrogation of G2 checkpoint was shown to inhibit the radiation-induced arrest in the G2 phase. This led to the reduction in the radiation-induced inhibition on mitotic arrest and apoptosis, causing an enhanced cytotoxicity in breast (BCap37) and human epidermoid (KB) cancer cells (Sui et al. 2012). Hence, if CTR compounds were eventually to be used in combination with radiation, the use of a G2 checkpoint inhibitor may be necessary.

4.8 Conclusion

In conclusion, data presented in this thesis suggest that CTR-17 and CTR-20, novel chalcone derivatives, have a broad range of anti-tumor activity. The two

CTR compounds induce a prominent mitotic arrest through inhibition of MT polymerisation, which is caused by their binding to tubulin at the colchicine-binding site. It is important to recognise that CTR-17 and CTR-20 exert lesser toxicity to normal cells than colchicine, a highly desirable property for better therapeutic index. This is because CTR-17 and CTR-20 preferentially kill cancer cells over non-cancerous cells, despite the cell doubling times of cancer and non-cancerous cells examined were largely indistinguishable. Thus, CTR-17 and CTR-20 can be extremely desirable anticancer drugs.

A large number of the clinically efficient anticancer drugs are MTAs (Gascoigne & Taylor 2009). These anti-mitotic agents target the shortest but the most elaborate phase of the cell cycle. Although MTAs effectively target mitosis, interphase cells are also susceptible to microtubule inhibitors. Hence, MTAs usually lead to myelosuppression and cause neurotoxicity that could sometimes lead to permanent damage in central and peripheral nervous systems (Rowinsky et al. 1993). Apart from the deleterious side effects, currently available clinically successful drugs including taxanes and vinca alkaloids lead to innate and acquired resistance. Hence, the goal of modern anticancer therapy is the development of novel agents that are more specific to tumor cells and could also overcome multidrug resistance. The combination of CTR compounds and paclitaxel in treating MDR cells induces a synergistic anti-proliferative effect, even at low drug concentrations (nM range). Therefore, each of these drugs

could be used at low doses which, in turn, may overcome undesirable side effects.

Further studies, using a xenograft model of the human breast cancer cells, showed CTR-17 and CTR-20 can indeed be effective and safe drugs, when used alone or in combination with paclitaxel. In particular, the combination of 5.0 mg/kg body weight of paclitaxel and 15.0 mg/kg body weight of CTR-20 could completely inhibit tumor growth in nude mice engrafted with the MDA MB-231 metastatic breast cancer cell line (This animal-based study was carried out by another lab member).

The findings of this thesis put forth an elaborative elucidation of the mechanistic effects of CTR-17 and CTR-20. These novel MTAs are not only selective but also overcome MDR. Therefore, both CTR-17 and CTR-20 could be used as attractive lead compounds to perform further structural modifications.

4.9 Future Directions

CTR compounds are potential anticancer therapeutics, which hold much promise for the future. Both CTR-17 and CTR-20 are cancer-cell specific, which is a highly desirable property as anticancer agents. In addition, the two CTR compounds effectively kill MDR cells when used alone or in combination with paclitaxel, hence they could be used as potential drug candidates to minimise acquired resistance to currently available drugs including paclitaxel and vinblastine. CTR-17 and CTR-20 are reversible MTAs that reduce the

polymerization of tubulin. It should be noted that MTs are a well-validated target for anticancer therapy. Highly proliferating cells, such as cancer cells are more vulnerable to MTAs than normal tissues which only replicate to replace dead cells. Nevertheless many MTAs impose a certain degree of toxicity to normal cells (Stanton et al. 2011). Hence, CTR compounds are MTAs with unique benefits of selectivity, overcoming MDR, and reversibility.

However, it would still be desirable to evaluate the potential of CTR compounds in combinatorial therapies, as no single agent is used as a cure for cancer. Multimodal therapies offer enhanced long-term prognosis and may reduce side effects. Combinatorial therapies involve either the combination of two treatment modalities (chemotherapy and radiotherapy) or the simultaneous administration of two or more pharmacologically efficient drugs. The use of a combinatorial regimen can modulate multiple signalling pathways, and enhance the therapeutic benefits, while possibly reversing the resistance mechanisms (Greco & Vicent 2009).

Two different screening approaches can be implemented to determine the most effective combinatorial regimen for CTR compounds. Firstly, a biased screening approach can be used, during which currently available chemotherapeutics and other treatment modalities; such, as radiation can be explored in combination with CTR compounds, which will in part be based on previously published reports. Data from Figure 32 showed that the co-administration of radiation and

CTR compounds did not radiosensitize T98G cells. However, there are number of additional factors that influence the combinatorial effects of radiation and anticancer compounds, including duration and concentration of drugs, different cancers, different radiation schedule, and sequence of drug and radiation administration (Pawlik & Keyomarsi 2004). Therefore, these factors may be taken into consideration when performing further combination experiments of CTR compounds with radiation and other regimens.

Paclitaxel when used in combination with CTR compounds synergistically killed KB-C2 MDR cells, illustrating the role of CTR compounds in overcoming resistance (Figure 10). A previous study identified a synthetic lethal interaction between MT destabilizing drug, vinblastine and BCL-2 inhibitor, ABT-263 that enhanced the cytotoxicity against glioblastoma and non–small-cell lung cancer cells (Kitchens et al. 2011). Another study showed a synergistic induction of apoptosis by vinblastine and BI2536, a Plk1 inhibitor in rhabdomyosarcoma (RMS) cells and *in vivo* RMS models (Hugle et al. 2015). Since the mode of action of CTR compounds is similar to vinblastine, irrespective of different binding sites, the combination of CTR and ABT-263 (or BI2536) might substantially enhance efficacy.

Secondly, an unbiased siRNA screening approach can also be used to identify a novel target that may render synergistic effect when blocked the target in the presence of CTR. siRNA technology is widely used for determining the essential

genes required for the survival of cancer cells. By using siRNA synthetic lethality screening methods, we can elucidate certain proteins or signals that can effectively kill cancer cells when inhibited in the presence of CTR (Whitehurst et al. 2007). For initial assays, MDA-MB231 human breast cancer cells may be used in a CTR-20-dependent synthetic lethality screen. We can identify gene products that render cell survival in the presence of CTR-20 by siRNA high throughput sequencing in combination with stringent statistical analysis. If pharmacological inhibitors for the gene products are available, validation and further combination assays may be performed with CTR-20 to determine the most effective combinatorial regimen.

5.0 References

Ahmed, B. et al., 2003. Vascular targeting effect of combretastatin A-4 phosphate dominates the inherent angiogenesis inhibitory activity. *International Journal of Cancer*, 105, pp.20–25.

Akhmanova, A. & Steinmetz, M.O., 2008. Tracking the ends: a dynamic protein network controls the fate of microtubule tips. *Nature Reviews. Molecular Cell Biology*, 9, pp.309–322.

Aryapour, H. et al., 2012. Induction of apoptosis through tubulin inhibition in human cancer cells by new chromene-based chalcones. *Pharmaceutical Biology*, pp.1–10.

Awasthi, S.K. et al., 2009. Potent antimalarial activity of newly synthesized substituted chalcone analogs in vitro. *Medicinal Chemistry Research*, 18, pp.407–420.

Bai, R. et al., 1993. Differential effects of active isomers, segments, and analogs of dolastatin 10 on ligand interactions with tubulin. Correlation with cytotoxicity. *Biochemical Pharmacology*, 45, pp.1503–1515.

Bai, R., Pettit, G.R. & Hamel, E., 1990a. Binding of dolastatin 10 to tubulin at a distinct site for peptide antimitotic agents near the exchangeable nucleotide and vinca alkaloid sites. *Journal of Biological Chemistry*, 265, pp.17141–17149.

Bai, R., Pettit, G.R. & Hamel, E., 1990b. Dolastatin 10, a powerful cytostatic peptide derived from a marine animal. Inhibition of tubulin polymerization mediated through the vinca alkaloid binding domain. *Biochemical Pharmacology*, 39, pp.1941–1949.

Baldwin, E.L. & Osheroff, N., 2005. Etoposide, topoisomerase II and cancer. *Current Medicinal Chemistry. Anti-cancer Agents*, 5(4), pp.363–372.

Bekier, M.E. et al., 2009. Length of mitotic arrest induced by microtubule-stabilizing drugs determines cell death after mitotic exit. *Molecular Cancer Therapeutics*, 8(6), pp.1646–1654.

Bhattacharyya, A., Bhattacharyya, B. & Roy, S., 1993. A study of colchicine tubulin complex by donor quenching of fluorescence energy transfer. *European Journal of Biochemistry / FEBS*, 216(3), pp.757–761.

Bhattacharyya, B. & Wolff, J., 1974. Promotion of fluorescence upon binding of colchicine to tubulin. *Proceedings of the National Academy of Sciences of the United States of America*, 71(7), pp.2627–2631.

Bobola, M.S. et al., 1995. Contribution of O6-methylguanine-DNA methyltransferase to monofunctional alkylating-agent resistance in human brain tumor-derived cell lines. *Molecular Carcinogenesis*, 13(2), pp.70–80.

Bohlin, L. & Rosén, B., 1996. Podophyllotoxin derivatives: Drug discovery and development. *Drug Discovery Today*, 1, pp.343–351.

Bollag, D.M. et al., 1995. Epothilones, a new class of microtubule-stabilizing agents with a taxol-like mechanism of action. *Cancer Research*, 55, pp.2325–2333.

Boumendjel, A. et al., 2009. A novel chalcone derivative which acts as a microtubule depolymerising agent and an inhibitor of P-gp and BCRP in in-vitro and in-vivo glioblastoma models. *BMC cancer*, 9, p.242.

De Brabander, M. et al., 1981. Taxol induces the assembly of free microtubules in living cells and blocks the organizing capacity of the centrosomes and kinetochores. *Proceedings of the National Academy of Sciences of the United States of America*, 78, pp.5608–5612.

Brito, D.A. & Rieder, C.L., 2006. Mitotic checkpoint slippage in humans occurs via Cyclin B destruction in the presence of an active checkpoint. *Current Biology*, 16, pp.1194–1200.

Burlingham, B.T. & Widlanski, T.S., 2003. An Intuitive Look at the Relationship of Ki and IC50: A More General Use for the Dixon Plot. *Journal of Chemical Education*, 80(2), p.214.

Cassady, J.M. et al., 2004. Recent developments in the maytansinoid antitumor agents. *Chemical & Pharmaceutical Bulletin*, 52, pp.1–26.

Chan, K.-S., Koh, C.-G. & Li, H.-Y., 2012. Mitosis-targeted anti-cancer therapies: where they stand. *Cell Death and Disease*, 3(10), p.e411.

Chao, Y.Y. et al., 2002. Interaction of nocodazole with tubulin isotypes. *Drug Development Research*, 55(2), pp.91–96.

Chen, S.-M., Meng, L.-H. & Ding, J., 2010. New microtubule-inhibiting anticancer agents. *Expert Opinion on Investigational Drugs*, 19, pp.329–343.

Cheng, M.S., Li, R.S. & Kenyon, G., 2000. A solid phase synthesis of chalcones by Claisen-Schmidt condensations. *Chinese Chemical Letters*, 11, pp.851–854.

Chou, T.-C., 2006. Theoretical basis, experimental design, and computerized simulation of synergism and antagonism in drug combination studies. *Pharmacological Reviews*, 58(3), pp.621–681.

Christmann, M. et al., 2011. O(6)-Methylguanine-DNA methyltransferase (MGMT) in normal tissues and tumors: enzyme activity, promoter methylation and immunohistochemistry. *Biochimica et Biophysica Acta*, 1816(2), pp.179–190.

Clute, P. & Pines, J., 1999. Temporal and spatial control of cyclin B1 destruction in metaphase. *Nature Cell Biology*, 1, pp.82–87.

Collin, P. et al., 2013. The spindle assembly checkpoint works like a rheostat rather than a toggle switch. *Nature Cell Biology*, 15(11), pp.1378–1385.

Conde, C. & Cáceres, A., 2009. Microtubule assembly, organization and dynamics in axons and dendrites. *Nature Reviews. Neuroscience*, 10(5), pp.319–332.

Cornish-Bowden, A., 1974. A simple graphical method for determining the inhibition constants of mixed, uncompetitive and non-competitive inhibitors. *The Biochemical Journal*, 137(1), pp.143–144.

Cruz-Monserrate, Z. et al., 2003. Dolastatin 15 binds in the vinca domain of tubulin as demonstrated by Hummel-Dreyer chromatography. *European Journal of Biochemistry*, 270(18), pp.3822–3828.

Cutts, J.H., Beer, C.T. & Noble, R.L., 1960. Biological Properties of Vincaleukoblastine, an Alkaloid in *Vinca rosea* Linn , with Reference to Its Antitumor Action. *Cancer Research*, 20, pp.1023–1031.

D'Amato, R.J. et al., 1994. 2-Methoxyestradiol, an endogenous mammalian metabolite, inhibits tubulin polymerization by interacting at the colchicine site. *Proceedings of the National Academy of Sciences of the United States of America*, 91, pp.3964–3968.

Dariolli, R. et al., 2013. Porcine adipose tissue-derived mesenchymal stem cells retain their proliferative characteristics, senescence, karyotype and plasticity after long-term cryopreservation. *PLOS ONE*, 8, p.e67939.

Davis, L.J. et al., 2002. The importance of lattice defects in katanin-mediated microtubule severing in vitro. *Biophysical Journal*, 82, pp.2916–2927.

Desbène, S. & Giorgi-Renault, S., 2002. Drugs that inhibit tubulin polymerization: the particular case of podophyllotoxin and analogues. *Current Medicinal Chemistry. Anti-cancer Agents*, 2, pp.71–90.

Deschênes, A. & Sourial, E., 2007. Ligand scaffold replacement using MOE pharmacophore tools. *Methodology*, pp.1–14.

DiPaola, R., 2002. To Arrest or Not To G 2 -M Cell-Cycle Arrest. *Clinical Cancer Research*, 8(November), pp.3311–3314.

Downing, K.H. & Nogales, E., 1999. Crystallographic structure of tubulin: implications for dynamics and drug binding. *Cell Structure and Function*, 24, pp.269–275.

Downing, K.H. & Nogales, E., 1998. New insights into microtubule structure and function from the atomic model of tubulin. *European Biophysics Journal*, 27, pp.431–436.

Drechsel, D.N. et al., 1992. Modulation of the dynamic instability of tubulin assembly by the microtubule-associated protein tau. *Molecular Bology of the Cell*, 3, pp.1141–1154.

Ducki, S., 2007. The development of chalcones as promising anticancer agents. *IDrugs : the investigational drugs journal*, 10(2003), pp.42–46.

Dumontet, C. & Jordan, M.A., 2010. Microtubule-binding agents: a dynamic field of cancer therapeutics. *Nature Reviews. Drug Discovery*, 9(10), pp.790–803.

Edelman, M., 2003. Phase 2 study of cryptophycin 52 (LY355703) in patients previously treated with platinum based chemotherapy for advanced non-small cell lung cancer. *Lung Cancer*, 39(2), pp.197–199.

Edwards, M.L., Stemerick, D.M. & Sunkara, P.S., 1990. Chalcones: A new class of antimitotic agents. *Journal of Medicinal Chemistry*, 33(7), pp.1948–1954.

Elie-Caille, C. et al., 2007. Straight GDP-Tubulin Protofilaments Form in the Presence of Taxol. *Current Biology*, 17, pp.1765–1770.

Eskens, F.A.L.M. et al., 2014. A phase I pharmacokinetic study of the vascular disrupting agent ombrabulin (AVE8062) and docetaxel in advanced solid tumours. *British Journal of Cancer*, pp.1–8.

Farrell, K.W. et al., 1987. Phase dynamics at microtubule ends: The coexistence of microtubule length changes and treadmilling. *Journal of Cell Biology*, 104, pp.1035–1046.

Ganguly, A. et al., 2012. The role of microtubules and their dynamics in cell migration. *Journal of Biological Chemistry*, 287(52), pp.43359–43369.

Garland, D.L., 1978. Kinetics and mechanism of colchicine binding to tubulin: evidence for ligand-induced conformational change. *Biochemistry*, 17, pp.4266–4272.

Gascoigne, K.E. & Taylor, S.S., 2008. Cancer cells display profound intra- and interline variation following prolonged exposure to antimitotic drugs. *Cancer Cell*, 14(2), pp.111–122.

Gascoigne, K.E. & Taylor, S.S., 2009. How do anti-mitotic drugs kill cancer cells? *Journal of Cell Science*, 122, pp.2579–2585.

Geney, R., Chen, J. & Ojima, I., 2005. Recent advances in the new generation taxane anticancer agents. *Medicinal Chemistry*, 1, pp.125–139.

Gerth, K. et al., 1996. Epothilones A and B: antifungal and cytotoxic compounds from *Sorangium cellulosum* (Myxobacteria). Production, physico-chemical and biological properties. *The Journal of Antibiotics*, 49, pp.560–563.

Giannakakou, P. & Fojo, T., 2000. Discodermolide: Just another microtubule-stabilizing agent? No! A lesson in synergy. *Clinical Cancer Research*, 6(May), pp.1613–1615.

Gireesh, K.K. et al., 2012. CIL-102 binds to tubulin at colchicine binding site and triggers apoptosis in MCF-7 cells by inducing monopolar and multinucleated cells. *Biochemical Pharmacology*, 84(5), pp.633–645.

Glynn, S.A. et al., 2004. A new superinvasive in vitro phenotype induced by selection of human breast carcinoma cells with the chemotherapeutic drugs paclitaxel and doxorubicin. *British Journal of Cancer*, 91(10), pp.1800–1807.

Goldman, R.D., 1971. The role of three cytoplasmic fibers in BHK-21 cell motility. I. Microtubules and the effects of colchicine. *Journal of Cell Biology*, 51(3), pp.752–762.

Goldstein, L.S. & Philp, A. V, 1999. The road less traveled: emerging principles of kinesin motor utilization. *Annual Review of Cell and Developmental Biology*, 15, pp.141–183.

Goldstein, L.S. & Yang, Z., 2000. Microtubule-based transport systems in neurons: the roles of kinesins and dyneins. *Annual Review of Neuroscience*, 23, pp.39–71.

Goodin, S., Kane, M.P. & Rubin, E.H., 2004. Epothilones: Mechanism of action and biologic activity. *Journal of Clinical Oncology*, 22, pp.2015–2025.

Goto, H. et al., 2002. Activity of a new vascular targeting agent, ZD6126, in pulmonary metastases by human lung adenocarcinoma in nude mice. *Cancer Research*, 62, pp.3711–3715.

Gottesman, M.M., Fojo, T. & Bates, S.E., 2002. Multidrug resistance in cancer: role of ATP-dependent transporters. *Nature Reviews. Cancer*, 2(1), pp.48–58.

Gould, R.R. & Borisy, G.G., 1977. The pericentriolar material in Chinese hamster ovary cells nucleates microtubule formation. *Journal of Cell Biology*, 73, pp.601–615.

Greco, F. & Vicent, M.J., 2009. Combination therapy: Opportunities and challenges for polymer-drug conjugates as anticancer nanomedicines. *Advanced Drug Delivery Reviews*, 61(13), pp.1203–1213.

Guha, S. et al., 1996. Tubulin conformation and dynamics: A red edge excitation shift study. *Biochemistry*, 35(41), pp.13426–13433.

Gupta, S. & Bhattacharyya, B., 2003. Antimicrotubular drugs binding to vinca domain of tubulin. *Molecular and Cellular Biochemistry*, 253, pp.41–47.

Hamel, E., 1996. Antimitotic natural products and their interactions with tubulin. *Medicinal Research Reviews*, 16(2), pp.207–231.

Hamel, E. et al., 2006. Synergistic effects of peloruside A and laulimalide with taxoid site drugs, but not with each other, on tubulin assembly. *Molecular Pharmacology*, 70, pp.1555–1564.

Hande, K.R. et al., 2006. The pharmacokinetics and safety of ABT-751, a novel, orally bioavailable sulfonamide antimitotic agent: Results of a phase 1 study. *Clinical Cancer Research*, 12, pp.2834–2840.

Hartman, J.J. et al., 1998. Katanin, a microtubule-severing protein, is a novel AAA ATPase that targets to the centrosome using a WD40-containing subunit. *Cell*, 93, pp.277–287.

Hartman, J.J. & Vale, R.D., 1999. Microtubule disassembly by ATP-dependent oligomerization of the AAA enzyme katanin. *Science (New York, N.Y.)*, 286, pp.782–785.

Hayden, J.H., Bowser, S.S. & Rieder, C.L., 1990. Kinetochores capture astral microtubules during chromosome attachment to the mitotic spindle: Direct visualization in live newt lung cells. *Journal of Cell Biology*, 111, pp.1039–1045.

Holland, A.J. & Cleveland, D.W., 2009. Boveri revisited: chromosomal instability, aneuploidy and tumorigenesis. *Nature reviews. Molecular Cell Biology*, 10(7), pp.478–487.

Huang, H. et al., 2012. Resveratrol reverses temozolomide resistance by downregulation of MGMT in T98G glioblastoma cells by the NF-κB-dependent pathway. *Oncology Reports*, 27(6), pp.2050–2056.

Hugle, M., Belz, K. & Fulda, S., 2015. Identification of synthetic lethality of PLK1 inhibition and microtubule-destabilizing drugs. *Cell Death and Differentiation*, pp.1–11.

Iwasaki, S. et al., 1984. Studies on macrocyclic lactone antibiotics. VII. Structure of a phytotoxin “rhizoxin” produced by *Rhizopus chinensis*. *The Journal of Antibiotics*, 37, pp.354–362.

Iyer, S. V et al., 2013. Understanding the role of keratins 8 and 18 in neoplastic potential of breast cancer derived cell lines. *PloS one*, 8(1), p.e53532.

Jandial, D.D. et al., 2014. Molecular Targeted Approaches to Cancer Therapy and Prevention using Chalcones. *Current Cancer Drug Targets*, pp.181–200.

Jordan, A. et al., 1998. Tubulin as a target for anticancer drugs: Agents which interact with the mitotic spindle. *Medicinal Research Reviews*, 18(4), pp.259–296.

Jordan, M.A., Thrower, D. & Wilson, L., 1992. Effects of vinblastine, podophyllotoxin and nocodazole on mitotic spindles. Implications for the role of microtubule dynamics in mitosis. *Journal of Cell Science*, 102 (Pt 3, pp.401–416.

Jordan, M.A. & Wilson, L., 2004. Microtubules as a target for anticancer drugs. *Nature Reviews. Cancer*, 4, pp.253–265.

Jorfi, S. et al., 2015. Inhibition of microvesiculation sensitizes prostate cancer cells to chemotherapy and reduces docetaxel dose required to limit tumor growth in vivo. *Scientific Reports*, 5(August), p.13006.

Jourdain, L. et al., 1997. Stathmin: A tubulin-sequestering protein which forms a ternary T2S complex with two tubulin molecules. *Biochemistry*, 36, pp.10817–10821.

Kamei, K. et al., 2011. Microfluidic image cytometry. *Methods in Molecular Biology (Clifton, N.J.)*, 706, p.15.

Kim, B.J. & Lee, H., 2008. Lys-110 is essential for targeting PCNA to replication and repair foci, and the K110A mutant activates apoptosis. *Biology of the cell / under the auspices of the European Cell Biology Organization*, 100(12), pp.675–686.

Kitchens, C.A. et al., 2011. Identification of chemosensitivity nodes for vinblastine through small interfering RNA high-throughput screens. *The Journal of pharmacology and Experimental Therapeutics*, 339(3), pp.851–858.

Koiso, Y. et al., 1994. Ustiloxins, antimitotic cyclic peptides from false smut balls on rice panicles caused by *Ustilaginoidea virens*. *The Journal of Antibiotics*, 47, pp.765–773.

Komlodi-Pasztor, E., Sackett, D.L. & Fojo, A.T., 2012. Inhibitors targeting mitosis: Tales of how great drugs against a promising target were brought down by a flawed rationale. *Clinical Cancer Research*, 18(1), pp.51–63.

Kowalski, R.J., Giannakakou, P. & Hamel, E., 1997. Activities of the microtubule-stabilizing agents epothilones A and B with purified tubulin and in cells resistant to paclitaxel (Taxol®). *Journal of Biological Chemistry*, 272, pp.2534–2541.

Kruczynski, A. et al., 1998. Antimitotic and tubulin-interacting properties of vinflunine, a novel fluorinated Vinca alkaloid. *Biochemical Pharmacology*, 55, pp.635–648.

Kumar, N., 1981. Taxol-induced polymerization of purified tubulin. Mechanism of action. *Journal of Biological Chemistry*, 256, pp.10435–10441.

Larsson, N. et al., 1997. Control of microtubule dynamics by oncoprotein 18: dissection of the regulatory role of multisite phosphorylation during mitosis. *Molecular and Cellular biology*, 17, pp.5530–5539.

Lawrence, N.J. et al., 2006. Effects of α-substitutions on structure and biological activity of anticancer chalcones. *Bioorganic and Medicinal Chemistry Letters*, 16, pp.5844–5848.

Lee, F.Y.F. et al., 2001. BMS-247550: A novel epothilone analog with a mode of action similar to paclitaxel but possessing superior antitumor efficacy. *Clinical Cancer Research*, 7, pp.1429–1437.

Lee, J.C., Harrison, D. & Timasheff, S.N., 1975. Interaction of vinblastine with calf brain microtubule protein. *Journal of Biological Chemistry*, 250(24), pp.9276–9282.

Lehár, J. et al., 2009. Synergistic drug combinations tend to improve therapeutically relevant selectivity. *Nature Biotechnology*, 27(7), pp.659–666.

Lemos, C.L. et al., 2000. Mast, a conserved microtubule-associated protein required for bipolar mitotic spindle organization. *The EMBO journal*, 19, pp.3668–3682.

Lewis, S.A. et al., 1985. Three expressed sequences within the human beta-tubulin multigene family each define a distinct isotype. *Journal of Molecular Biology*, 182, pp.11–20.

Li, Y. et al., 1995. Ustiloxins, new antimitotic cyclic peptides: interaction with porcine brain tubulin. *Biochemical Pharmacology*, 49, pp.1367–1372.

Liang, C.-C., Park, A.Y. & Guan, J.-L., 2007. In vitro scratch assay: a convenient and inexpensive method for analysis of cell migration in vitro. *Nature Protocols*, 2(2), pp.329–333.

Limame, R. et al., 2012. Comparative analysis of dynamic cell viability, migration and invasion assessments by novel real-time technology and classic endpoint assays. *PLoS ONE*, 7(10), p.e46536.

Lippert, J.W., 2007. Vascular disrupting agents. *Bioorganic and Medicinal Chemistry*, 15, pp.605–615.

Liu, C. & Chari, R. V, 1997. The development of antibody delivery systems to target cancer with highly potent maytansinoids. *Expert Opinion on Investigational drugs*, 6, pp.169–172.

Liu, J. et al., 2007. *In vitro* and *in vivo* anticancer activities of synthetic (-)-laulimalide, a marine natural product microtubule stabilizing agent. *Anticancer Research*, 27, pp.1509–1518.

Lu, Y. et al., 2012. An overview of tubulin inhibitors that interact with the colchicine binding site. *Pharmaceutical Research*, 29, pp.2943–2971.

Ludueña, R.F. et al., 1990. Effect of phomopsin A on the alkylation of tubulin. *Biochemical Pharmacology*, 39, pp.1603–1608.

Ludueña, R.F. et al., 1992. Interaction of dolastatin 10 with bovine brain tubulin. *Biochemical Pharmacology*, 43, pp.539–543.

Mabjeesh, N.J. et al., 2003. 2ME2 inhibits tumor growth and angiogenesis by disrupting microtubules and dysregulating HIF. *Cancer Cell*, 3, pp.363–375.

Madiraju, C. et al., 2005. Tubulin assembly, taxoid site binding, and cellular effects of the microtubule-stabilizing agent dictyostatin. *Biochemistry*, 44, pp.15053–15063.

Maiato, H. et al., 2003. Human CLASP1 is an outer kinetochore component that regulates spindle microtubule dynamics. *Cell*, 113, pp.891–904.

Maiato, H., Sampaio, P. & Sunkel, C.E., 2004. Microtubule-associated proteins and their essential roles during mitosis. *International Review of Cytology*, 241, pp.53–153.

Mandelkow, E. & Mandelkow, E.M., 1995. Microtubules and microtubule-associated proteins. *Current Opinion in Cell Biology*, 7, pp.72–81.

Margolis, R.L. & Wilson, L., 1998. Microtubule treadmilling: What goes around comes around. *BioEssays*, 20, pp.830–836.

Margolis, R.L. & Wilson, L., 1978. Opposite end assembly and disassembly of microtubules at steady state in vitro. *Cell*, 13, pp.1–8.

Marklund, U. et al., 1996. Oncoprotein 18 is a phosphorylation-responsive regulator of microtubule dynamics. *The EMBO Journal*, 15, pp.5290–5298.

Matei, D. et al., 2009. Activity of 2 methoxyestradiol (Panzem® NCD) in advanced, platinum-resistant ovarian cancer and primary peritoneal carcinomatosis: A Hoosier Oncology Group trial. *Gynecologic Oncology*, 115, pp.90–96.

Matson, D.R. & Stukenberg, P.T., 2011. Spindle poisons and cell fate: a tale of two pathways. *Molecular Interventions*, 11(2), pp.141–150.

McIntosh, J.R., Grishchuk, E.L. & West, R.R., 2002. Chromosome-microtubule interactions during mitosis. *Annual Review of Cell and Developmental Biology*, 18, pp.193–219.

McKean, P.G., Vaughan, S. & Gull, K., 2001. The extended tubulin superfamily. *Journal of Cell Science*, 114, pp.2723–2733.

McLeod, H.L. et al., 1996. Multicentre phase II pharmacological evaluation of rhizoxin. Eortc early clinical studies (ECSG)/pharmacology and molecular mechanisms (PAMM) groups. *British Journal of Cancer*, 74(12), pp.1944–1948.

McNally, F.J. & Vale, R.D., 1993. Identification of katanin, an ATPase that severs and disassembles stable microtubules. *Cell*, 75, pp.419–429.

Modzelewska, A. et al., 2006. Anticancer activities of novel chalcone and bis-chalcone derivatives. *Bioorganic and Medicinal Chemistry*, 14(10), pp.3491–3495.

Molitor, T.P. & Traktman, P., 2013. Molecular genetic analysis of VRK1 in mammary epithelial cells: depletion slows proliferation in vitro and tumor growth and metastasis in vivo. *Oncogenesis*, 2, p.e48.

Mollinedo, F. & Gajate, C., 2003. Microtubules, microtubule-interfering agents and apoptosis. *Apoptosis*, 8, pp.413–450.

Montaldi, A.P. & Sakamoto-Hojo, E.T., 2013. Methoxyamine sensitizes the resistant glioblastoma T98G cell line to the alkylating agent temozolomide. *Clinical and Experimental Medicine*, 13(4), pp.279–288.

Morris, P.G. & Fornier, M.N., 2008. Microtubule active agents: Beyond the taxane frontier. *Clinical Cancer Research*, 14, pp.7167–7172.

Newton, C.N. et al., 2004. MCAK, a Kin I kinesin, increases the catastrophe frequency of steady-state HeLa cell microtubules in an ATP-dependent manner in vitro. *FEBS Letters*, 572, pp.80–84.

Nogales, E., 2000. Structural insights into microtubule function. *Annual Review of Biochemistry*, 69, pp.277–302.

Palmer, T.D. et al., 2011. Targeting tumor cell motility to prevent metastasis. *Advanced Drug Delivery Reviews*, 63(8), pp.568–581.

Panda, D. et al., 1996. Differential effects of vinblastine on polymerization and dynamics at opposite microtubule ends. *Journal of Biological Chemistry*, 271, pp.29807–29812.

Panda, D. et al., 1997. Stabilization of microtubule dynamics by estramustine by binding to a novel site in tubulin: a possible mechanistic basis for its antitumor action. *Proceedings of the National Academy of Sciences of the United States of America*, 94(20), pp.10560–10564.

Panda, D., Roy, S. & Bhattacharyya, B., 1992. Reversible dimer dissociation of tubulin S and tubulin detected by fluorescence anisotropy. *Biochemistry*, 31(40), pp.9709–9716.

Pasquier, E. et al., 2010. ENMD-1198, a new analogue of 2-methoxyestradiol, displays both antiangiogenic and vascular-disrupting properties. *Molecular Cancer Therapeutics*, 9, pp.1408–1418.

Pawlik, T.M. & Keyomarsi, K., 2004. Role of cell cycle in mediating sensitivity to radiotherapy. *International Journal of Radiation Oncology Biology Physics*, 59(4), pp.928–942.

Pearce, A.G. et al., 2001. The generation and characterization of a radiation-resistant model system to study radioresistance in human breast cancer cells. *Radiation Research*, 156(6), pp.739–750.

Peters, J.-M., 2006. The anaphase promoting complex/cyclosome: a machine designed to destroy. *Nature Reviews. Molecular Cell Biology*, 7, pp.644–656.

Peterson, J.R. & Mitchison, T.J., 2002. Small molecules, big impact: A history of chemical inhibitors and the cytoskeleton. *Chemistry and Biology*, 9, pp.1275–1285.

Peyrot, V. et al., 1989. Interaction of tubulin and cellular microtubules with the new antitumor drug MDL 27048. A powerful and reversible microtubule inhibitor. *Journal of Biological Chemistry*, 264(35), pp.21296–21301.

Peyrot, V. et al., 1992. Mechanism of binding of the new antimitotic drug MDL 27048 to the colchicine site of tubulin: equilibrium studies. *Biochemistry*, 31, pp.11125–11132.

Piehl, M. et al., 2004. Centrosome maturation: measurement of microtubule nucleation throughout the cell cycle by using GFP-tagged EB1. *Proceedings of the National Academy of Sciences of the United States of America*, 101, pp.1584–1588.

Pourroy, B. et al., 2006. Antiangiogenic concentrations of vinflunine increase the interphase microtubule dynamics and decrease the motility of endothelial cells. *Cancer Research*, 66(6), pp.3256–3263.

Prabhakar, V. et al., 2014. In vitro anticancer activity of monosubstituted chalcone derivatives. *International Journal of Tumor Therapy*, 3(1), pp.1–9.

Rahbari, R. et al., 2009. A novel L1 retrotransposon marker for HeLa cell line identification. *BioTechniques*, 46(4), pp.277–284.

Rahman, M.A., 2011. Chalcone: A Valuable Insight into the Recent Advances and Potential. *Chemical Sciences Journal*, 2011(3), p.CSJ–29.

Rai, A., Surolia, A. & Panda, D., 2012. An Antitubulin Agent BCFMT Inhibits Proliferation of Cancer Cells and Induces Cell Death by Inhibiting Microtubule Dynamics. *PLoS ONE*, 7(8), p.e44311.

Rai, S.S. & Wolff, J., 1996. Localization of the vinblastine-binding site on β-tubulin. *Journal of Biological Chemistry*, 271, pp.14707–14711.

Rao, S. et al., 1999. Characterization of the Taxol binding site on the microtubule. Identification of Arg282 in β-tubulin as the site of photoincorporation of a 7-benzophenone analogue of Taxol. *Journal of Biological Chemistry*, 274, pp.37990–37994.

Ren, Y. & Wei, D., 2004. Quantification intracellular levels of oligodeoxynucleotide-doxorubicin conjugate in human carcinoma cells in situ. *Journal of Pharmaceutical and Biomedical Analysis*, 36(2), pp.387–391.

Ricart, A.D. et al., 2011. A phase I study of MN-029 (denibulin), a novel vascular-disrupting agent, in patients with advanced solid tumors. *Cancer Chemotherapy and Pharmacology*, 68, pp.959–970.

Rickard, J.E. & Kreis, T.E., 1990. Identification of a novel nucleotide-sensitive microtubule-binding protein in HeLa cells. *Journal of Cell Biology*, 110, pp.1623–1633.

Risinger, A.L., Giles, F.J. & Mooberry, S.L., 2009. Microtubule dynamics as a target in oncology. *Cancer Treatment Reviews*, 35, pp.255–261.

Romero, J. & Lee, H., 2008. Asymmetric bidirectional replication at the human DBF4 origin. *Nature Structural & Molecular biology*, 15(7), pp.722–729.

Rowinsky, E.K. et al., 1993. Clinical toxicities encountered with paclitaxel (Taxol). *Seminars in Oncology*, 20(4 Suppl 3), pp.1–15.

Rustin, G.J. et al., 2010. A Phase Ib trial of CA4P (combretastatin A-4 phosphate), carboplatin, and paclitaxel in patients with advanced cancer. *British Journal of Cancer*, 102(9), pp.1355–1360.

Salic, A. & Mitchison, T.J., 2008. A chemical method for fast and sensitive detection of DNA synthesis in vivo. *Proceedings of the National Academy of Sciences of the United States of America*, 105(7), pp.2415–2420.

Sams-Dodd, F., 2005. Target-based drug discovery: Is something wrong? *Drug Discovery Today*, 10(2), pp.139–147.

Santi, S.A. & Lee, H., 2011. Ablation of Akt2 induces autophagy through cell cycle arrest, the downregulation of p70s6k, and the deregulation of mitochondria in MDA-MB231 cells. *PLoS ONE*, 6(1).

Santi, S.A. & Lee, H., 2010. The Akt isoforms are present at distinct subcellular locations. *American Journal of Physiology. Cell Physiology*, 298(3), pp.C580–C591.

Saxton, W.M. et al., 1984. Tubulin dynamics in cultured mammalian cells. *Journal of Cell Biology*, 99, pp.2175–2186.

Schiff, P.B., Fant, J. & Horwitz, S.B., 1979. Promotion of microtubule assembly in vitro by taxol. *Nature*, 277(5698), pp.665–667.

Schmidt, M. & Bastians, H., 2007. Mitotic drug targets and the development of novel anti-mitotic anticancer drugs. *Drug Resistance Updates*, 10, pp.162–181.

Schuyler, S.C. & Pellman, D., 2001. Microtubule “plus-end-tracking proteins”: The end is just the beginning. *Cell*, 105, pp.421–424.

Schwartz, E.L., 2009. Antivascular actions of microtubule-binding drugs. *Clinical Cancer Research*, 15(8), pp.2594–2601.

Sève, P. & Dumontet, C., 2008. Is class III beta-tubulin a predictive factor in patients receiving tubulin-binding agents? *The Lancet Oncology*, 9, pp.168–175.

Shan, B. et al., 1999. Selective, covalent modification of beta-tubulin residue Cys-239 by T138067, an antitumor agent with in vivo efficacy against multidrug-resistant tumors. *Proceedings of the National Academy of Sciences of the United States of America*, 96, pp.5686–5691.

Shi, W. & Siemann, D.W., 2005. Preclinical studies of the novel vascular disrupting agent MN-029. *Anticancer Research*, 25, pp.3899–3904.

Singh, P. et al., 2008. Microtubule assembly dynamics: An attractive target for anticancer drugs. *IUBMB Life*, 60(6), pp.368–375.

Skehan, P. et al., 1990. New colorimetric cytotoxicity assay for anticancer-drug screening. *Journal of the National Cancer Institute*, 82(13), pp.1107–1112.

Small, J.V. et al., 2002. How do microtubules guide migrating cells? *Nature reviews. Molecular cell biology*, 3(12), pp.957–964.

Smith, C.D. et al., 1994. Cryptophycin: A new antimicrotubule agent active against drug-resistant cells. *Cancer Research*, 54, pp.3779–3784.

Smith, C.D. & Zhang, X., 1996. Mechanism of action of cryptophycin: Interaction with the Vinca alkaloid domain of tubulin. *Journal of Biological Chemistry*, 271, pp.6192–6198.

Smith, D.B. et al., 1988. A phase I and pharmacokinetic study of amphethinile. *British Journal of Cancer*, 57, pp.623–627.

Solomon, V.R., Hu, C. & Lee, H., 2009. Hybrid pharmacophore design and synthesis of isatin-benzothiazole analogs for their anti-breast cancer activity. *Bioorganic and Medicinal Chemistry*, 17(21), pp.7585–7592.

Stanton, R.A. et al., 2011. Drugs that target dynamic microtubules: A new molecular perspective. *Medicinal Research Reviews*, 31, pp.443–481.

Strober, W., 2001. Trypan blue exclusion test of cell viability. *Current protocols in Immunology*, Appendix 3, p.Appendix 3B.

Sui, M. et al., 2004. Cell cycle-dependent antagonistic interactions between paclitaxel and gamma-radiation in combination therapy. *Clinical Cancer Research*, 10(14), pp.4848–4857.

Sui, M. et al., 2012. G2 checkpoint abrogator abates the antagonistic interaction between antimicrotubule drugs and radiation therapy. *Radiotherapy and Oncology*, 104(2), pp.243–248.

Sui, M. & Fan, W., 2005. Combination of γ-radiation antagonizes the cytotoxic effects of vincristine and vinblastine on both mitotic arrest and apoptosis. *International Journal of Radiation Oncology Biology Physics*, 61(4), pp.1151–1158.

Tae, J.K. et al., 2007. Antitumor and antivascular effects of AVE8062 in ovarian carcinoma. *Cancer Research*, 67, pp.9337–9345.

Takahashi, M. et al., 1987. Rhizoxin binding to tubulin at the maytansine-binding site. *Biochimica et Biophysica Acta*, 926, pp.215–223.

Takanari, H. et al., 1990. Instability of pleomorphic tubulin paracrystals artificially induced by Vinca alkaloids in tissue-cultured cells. *Biology of the cell / under the auspices of the European Cell Biology Organization*, 70, pp.83–90.

Taylor, S.S. et al., 2001. Kinetochore localisation and phosphorylation of the mitotic checkpoint components Bub1 and BubR1 are differentially regulated by spindle events in human cells. *Journal of Cell Science*, 114(Pt 24), pp.4385–4395.

Thomas, J.P. et al., 2002. A phase II study of CI-980 in previously untreated extensive small cell lung cancer: an Ohio State University phase II research consortium study. *Cancer Investigation*, 20(2), pp.192–198.

Thomas, N.E. et al., 2014. Reversible action of diaminothiazoles in cancer cells is implicated by the induction of a fast conformational change of tubulin and suppression of microtubule dynamics. *Molecular Cancer Therapeutics*, 13(1), pp.179–89.

Thompson, W.C., Wilson, L. & Purich, D.L., 1981. Taxol induces microtubule assembly at low temperature. *Cell Motility*, 1, pp.445–454.

Tokési, N. et al., 2010. TPPP/p25 promotes tubulin acetylation by inhibiting histone deacetylase 6. *Journal of Biological Chemistry*, 285(23), pp.17896–17906.

Tombes, R.M., Peloquin, J.G. & Borisy, G.G., 1991. Specific association of an M-phase kinase with isolated mitotic spindles and identification of two of its substrates as MAP4 and MAP1B. *Cell Regulation*, 2, pp.861–874.

Toppmeyer, D.L. et al., 1994. Role of P-glycoprotein in dolastatin 10 resistance. *Biochemical Pharmacology*, 48, pp.609–612.

Uzbekov, R., Kireyev, I. & Prigent, C., 2002. Centrosome separation: Respective role of microtubules and actin filaments. *Biology of the Cell*, 94(4-5), pp.275–288.

Vale, R.D., 1991. Severing of stable microtubules by a mitotically activated protein in Xenopus egg extracts. *Cell*, 64, pp.827–839.

Valiron, O., Caudron, N. & Job, D., 2001. Microtubule dynamics. *Cell Molecular Life Sciences*, 58, pp.2069–2084.

Vandré, D.D. et al., 1991. Proteins of the mammalian mitotic spindle: phosphorylation/dephosphorylation of MAP-4 during mitosis. *Journal of Cell Science*, 98 (Pt 4), pp.577–588.

Vasiliev, J.M. et al., 1970. Effect of colcemid on the locomotory behaviour of fibroblasts. *Journal of Embryology and Experimental Morphology*, 24(3), pp.625–640.

Vaughan, K.T., 2005. TIP maker and TIP marker; EB1 as a master controller of microtubule plus ends. *Journal of Cell Biology*, 171, pp.197–200.

Venghateri, J.B. et al., 2013. Ansamitocin P3 depolymerizes microtubules and Induces apoptosis by binding to tubulin at the vinblastine site. *PLoS ONE*, 8(10), p.e75182.

Vichai, V. & Kirtikara, K., 2006. Sulforhodamine B colorimetric assay for cytotoxicity screening. *Nature Protocols*, 1(3), pp.1112–1116.

Villasante, A. et al., 1986. Six mouse alpha-tubulin mRNAs encode five distinct isotypes: testis-specific expression of two sister genes. *Molecular and Cellular Biology*, 6, pp.2409–2419.

Walczak, C.E., Cai, S. & Khodjakov, A., 2010. Mechanisms of chromosome behaviour during mitosis. *Nature Reviews. Molecular Cell Biology*, 11(2), pp.91–102.

Walker, R.A. et al., 1988. Dynamic instability of individual microtubules analyzed by video light microscopy: rate constants and transition frequencies. *Journal of Cell Biology*, 107, pp.1437–1448.

Warfield, R.K. & Bouck, G.B., 1974. Microtubule-macrotubule transitions: intermediates after exposure to the mitotic inhibitor vinblastine. *Science (New York, N.Y.)*, 186, pp.1219–1221.

Warner, F.D. & Satir, P., 1973. The substructure of ciliary microtubules. *Journal of Cell Science*, 12, pp.313–326.

Weisenberg, R.C., Borisy, G.G. & Taylor, E.W., 1968. The colchicine-binding protein of mammalian brain and its relation to microtubules. *Biochemistry*, 7, pp.4466–4479.

Whitehurst, A.W. et al., 2007. Synthetic lethal screen identification of chemosensitizer loci in cancer cells. *Nature*, 446(7137), pp.815–819.

Wilmes, A. et al., 2007. Peloruside A synergizes with other microtubule stabilizing agents in cultured cancer cell lines. *Molecular Pharmaceutics*, 4, pp.269–280.

Wilson, L. et al., 1982. Interaction of vinblastine with steady-state microtubules in vitro. *Journal of Molecular Biology*, 159, pp.125–149.

Yang, H., Ganguly, A. & Cabral, F., 2010. Inhibition of cell migration and cell division correlates with distinct effects of microtubule inhibiting drugs. *Journal of Biological Chemistry*, 285(42), pp.32242–32250.

You, Y., 2005. Podophyllotoxin derivatives: current synthetic approaches for new anticancer agents. *Current Pharmaceutical Design*, 11(13), pp.1695–1717.

Yvon, A.M., Wadsworth, P. & Jordan, M.A., 1999. Taxol suppresses dynamics of individual microtubules in living human tumor cells. *Molecular Biology of the Cell*, 10, pp.947–959.

Zajchowski, D.A., Sager, R. & Webster, L., 1993. Estrogen inhibits the growth of estrogen receptor-negative, but not estrogen receptor-positive, human mammary epithelial cells expressing a recombinant estrogen receptor. *Cancer Research*, 53(20), pp.5004–5011.

Zeng, X. et al., 2010. Pharmacologic inhibition of the anaphase-promoting complex induces a spindle checkpoint-dependent mitotic arrest in the absence of spindle damage. *Cancer Cell*, 18(4), pp.382–395.

Zhang, C. et al., 2009. S9, a novel anticancer agent, exerts its anti-proliferative activity by interfering with both PI3K-Akt-mTOR signaling and microtubule cytoskeleton. *PLoS ONE*, 4(3).

Zhang, C. et al., 2014. Synergistic action by multi-targeting compounds produces a potent compound combination for human NSCLC both in vitro and in vivo. *Cell Death and Disease*, 5(3), p.e1138.

Zhou, J. & Giannakakou, P., 2005. Targeting microtubules for cancer chemotherapy. *Current Medicinal Chemistry. Anti-cancer Agents*, 5, pp.65–71.

6.0 Appendix

Table A1: List of antibodies used

Primary Antibody	Company	Cat Number	Dilution	Application
α-Tubulin	Santa Cruz	sc-8035	1:200	Western blotting
α-Tubulin	Santa Cruz	sc-53030	1:500	Immunofluorescence
β-Actin	Santa Cruz	sc-47778	1:200	Western blotting
γ-Tubulin	Santa Cruz	sc-7396	1:500	Immunofluorescence
γ-H2AX	Abcam	ab 11174	1:500	Immunofluorescence
BubR1	Abcam	ab 4637	1:50, 3µg/1mg protein, 1:1000	Immunofluorescence, Immunoprecipitation & Western
Cdc20	Abcam	ab 18217	1:200	Western blotting
Cdc25C	Santa Cruz	sc-327	1:200	Western blotting
Cdk1	Santa Cruz	sc-137034	1:200	Western blotting
Cenp-B	Abcam	ab 25734	1:50	Immunofluorescence
Cleaved PARP	Santa Cruz	sc-56196	1:200	Western blotting
Cyclin A	Santa Cruz	sc-271682	1:200	Western blotting
Cyclin B	Santa Cruz	sc-245	1:200	Western blotting
Cyclin E	Santa Cruz	sc-198	1:200	Western blotting
Gapdh	Santa Cruz	sc-47724	1:200	Western blotting
Histone H3	Santa Cruz	sc-10809	1:200	Western blotting
Normal IgG	Santa Cruz	sc-2027	3µg/1mg protein	Immunoprecipitation
PARP	Santa Cruz	sc-8007	1:200	Western blotting
p-Cdc25C,T48	Cell Signalling	9527	1:1000	Western blotting
p-Cdc25C,S216	Abcam	ab 32051	1:1000	Western blotting
p-Cdk1,T161	Santa Cruz	sc-12341	1:200	Western blotting
p-Cdk1,Y15	Santa Cruz	sc-7989	1:200	Western blotting
p-Histone H3, S10	Santa Cruz	sc-8656	1:200	Western blotting
MDR1	Santa Cruz	sc-1517	1:200	Western blotting
MRP1	Santa Cruz	sc-18835	1:200	Western blotting
Securin	Abcam	ab-3305	1:1000	Western blotting
Wee1	Santa Cruz	sc-5285	1:200	Western blotting